Cyclone impacts on sea ice in the Atlantic Arctic Ocean

publikationsbasierte Dissertation

vorgelegt von:

Lars Aue

zur Erlangung des akademischen Grades
„doctor rerum naturalium"
(Dr. rer. nat.)
in der Wissenschaftsdisziplin „Klimaphysik"

eingereicht an der
Mathematisch-Naturwissenschaftlichen Fakultät
Institut für Physik und Astronomie
der Universität Potsdam
und
dem Alfred-Wegener-Institut
Helmholtz Zentrum für Polar- und Meeresforschung
Forschungsstelle Potsdam

Potsdam, den 23.10.2023

Abstract

The Arctic is the hot spot of the ongoing, global climate change. Over the last decades, near-surface temperatures in the Arctic have been rising almost four times faster than on global average. This amplified warming of the Arctic and the associated rapid changes of its environment are largely influenced by interactions between individual components of the Arctic climate system. On daily to weekly time scales, storms can have major impacts on the Arctic sea-ice cover and are thus an important part of these interactions within the Arctic climate. The sea-ice impacts of storms are related to high wind speeds, which enhance the drift and deformation of sea ice, as well as to changes in the surface energy budget in association with air mass advection, which impact the seasonal sea-ice growth and melt.

The occurrence of storms in the Arctic is typically associated with the passage of transient cyclones. Even though the above described mechanisms how storms/cyclones impact the Arctic sea ice are in principal known, there is a lack of statistical quantification of these effects. In accordance with that, the overarching objective of this thesis is to statistically quantify cyclone impacts on sea-ice concentration (SIC) in the Atlantic Arctic Ocean over the last four decades. In order to further advance the understanding of the related mechanisms, an additional objective is to separate dynamic and thermodynamic cyclone impacts on sea ice and assess their relative importance. Finally, this thesis aims to quantify recent changes in cyclone impacts on SIC. These research objectives are tackled utilizing various data sets, including atmospheric and oceanic reanalysis data as well as a coupled model simulation and a cyclone tracking algorithm.

Results from this thesis demonstrate that cyclones are significantly impacting SIC in the Atlantic Arctic Ocean from autumn to spring, while there are mostly no significant impacts in summer. The strength and the sign (SIC decreasing or SIC increasing) of the cyclone impacts strongly depends on the considered daily time scale and the region of the Atlantic Arctic Ocean. Specifically, an initial decrease in SIC (day -3 to day 0 relative to the cyclone) is found in the Greenland, Barents and Kara Seas, while SIC increases following cyclones (day 0 to day 5 relative to the cyclone) are mostly limited to the Barents and Kara Seas.

For the cold season, this results in a pronounced regional difference between overall (day -3 to day 5 relative to the cyclone) SIC-decreasing cyclone impacts in the Greenland Sea and overall SIC-increasing cyclone impacts in the Barents and Kara Seas. A cyclone case study based on a coupled model simulation indicates that both dynamic and thermodynamic mechanisms contribute to cyclone impacts on sea ice in winter. A typical pattern consisting of an initial dominance of dynamic sea-ice changes followed by enhanced thermodynamic

ice growth after the cyclone passage was found. This enhanced ice growth after the cyclone passage most likely also explains the (statistical) overall SIC-increasing effects of cyclones in the Barents and Kara Seas in the cold season.

Significant changes in cyclone impacts on SIC over the last four decades have emerged throughout the year. These recent changes are strongly varying from region to region and month to month. The strongest trends in cyclone impacts on SIC are found in autumn in the Barents and Kara Seas. Here, the magnitude of destructive cyclone impacts on SIC has approximately doubled over the last four decades. The SIC-increasing effects following the cyclone passage have particularly weakened in the Barents Sea in autumn. As a consequence, previously existing overall SIC-increasing cyclone impacts in this region in autumn have recently disappeared. Generally, results from this thesis show that changes in the state of the sea-ice cover (decrease in mean sea-ice concentration and thickness) and near-surface air temperature are most important for changed cyclone impacts on SIC, while changes in cyclone properties (i.e. intensity) do not play a significant role.

Kurzfassung

Die Arktis ist der Hotspot des globalen Klimawandels. In den letzten Jahrzehnten sind die oberflächennahen Temperaturen in der Arktis fast viermal so schnell gestiegen wie im globalen Durchschnitt. Diese verstärkte Erwärmung der Arktis und die damit verbundenen raschen Umweltveränderungen werden u.a. durch Wechselwirkungen zwischen den einzelnen Komponenten des arktischen Klimasystems angetrieben. Auf täglichen bis wöchentlichen Zeitskalen können Stürme große Einflüsse auf das arktische Meereis haben und sind somit ein wichtiger Teil dieser Wechselwirkungen innerhalb des arktischen Klimas. Der Einfluss der Stürme auf das Meereis resultiert aus den hohen Windgeschwindigkeiten, welche die Drift und Verformung des Meereises verstärken, sowie aus Änderungen in der Oberflächenenergiebilanz im Zusammenhang mit der Avektion von Luftmassen, was das Wachstum und Schmelzen des Meereises beeinflusst.

Das Auftreten von Stürmen in der Arktis ist oft mit dem Durchzug von Zyklonen verbunden. Obwohl die oben beschriebenen Mechanismen, wie sich Stürme/Zyklone auf das arktische Meereis auswirken, im Prinzip bekannt sind, fehlt es an einer statistischen Quantifizierung dieser Effekte. Dementsprechend ist das übergeordnete Ziel dieser Arbeit eine statistische Quantifizierung der Auswirkungen von Zyklonen auf die Meereiskonzentration (engl. Sea Ice Concentration, SIC) im atlantischen Arktischen Ozeans über die letzten vier Jahrzehnte. Um ein Verständnis für die zugrunde liegenden Mechanismen zu erlangen, besteht ein weiteres Ziel darin, die dynamischen und thermodynamischen Auswirkungen von Zyklonen auf das Meereis zu trennen und ihre relative Bedeutung zu analysieren. Zuletzt zielt diese Arbeit darauf ab, aktuelle Veränderungen der Zykloneneinflüsse auf das Meereis zu quantifizieren. Zum Erreichen dieser Forschungsziele werden verschiedene Datensätze genutzt, darunter atmosphärische und ozeanische Reanalysedaten sowie eine gekoppelte Modellsimulation und ein Algorithmus zur automatischen Identifikation von Zyklonen.

Die Ergebnisse dieser Arbeit zeigen, dass Zyklone die SIC im atlantischen Arktischen Ozean von Herbst bis Frühjahr signifikant beeinflussen, während es im Sommer meist keine signifikanten Auswirkungen gibt. Die Stärke und das Vorzeichen (abnehmende oder zunehmende SIC) der Auswirkungen der Zyklone hängt stark von der betrachteten täglichen Zeitskala und der Region des Arktischen Ozeans ab. So ist ein anfänglicher Rückgang der SIC (Tag -3 bis Tag 0 relativ zum Zyklonendurchgang) in der Grönland-, der Barents- und der Karasee festzustellen, während ein SIC-Anstieg nach dem Zyklonendurchgang (Tag 0 bis Tag 5 relativ zum Zyklonendurchgang) hauptsächlich auf die Barents- und die Karasee beschränkt ist.

Für die kalte Jahreszeit ergibt sich daraus ein ausgeprägter regionaler Unterschied zwischen insgesamt (Tag -3 bis Tag 5 relativ zum Zyklon) SIC-verringernden Zyklonenauswirkungen in der Grönlandsee und insgesamt SIC-erhöhenden Zyklonenauswirkungen in der Barents- und Karasee. Die Analyse spezifischer Zyklonenfälle basierend auf einer gekoppelten Modellsimulation zeigt, dass sowohl dynamische als auch thermodynamische Mechanismen zu den Auswirkungen von Zyklonen auf das Meereis im Winter beitragen. Hierbei wurde ein typisches Muster bestehend aus einer anfänglichen Dominanz dynamischer Meereisveränderungen gefolgt von verstärktem thermodynamischem Eiswachstum nach der Zyklonenpassage gefunden. Dieses verstärkte Eiswachstum nach der Zyklonenpassage erklärt u.a. auch die (statistischen) insgesamt SIC-erhöhenden Effekte von Zyklonen in der Barents- und Karasee im Winter.

Signifikante Änderungen in den Auswirkungen von Zyklonen auf die SIC über die letzten vier Dekaden sind das ganze Jahr über zu finden. Diese Veränderungen variieren stark von Region zu Region und von Monat zu Monat. Die stärksten Trends in den Auswirkungen von Zyklonen auf die SIC sind im Herbst in der Barents- und Karasee zu beobachten. Hier hat sich die Stärke der zerstörerischen Auswirkungen von Zyklonen auf die SIC in den letzten vier Jahrzehnten ungefähr verdoppelt. Die SIC-erhöhenden Effekte nach der Zyklonenpassage haben sich in der Barentssee im Herbst besonders abgeschwächt. Dadurch sind zuvor existierende, insgesamt SIC-erhöhende Zyklonenauswirkungen in dieser Region und Jahreszeit zuletzt verschwunden. Generell zeigen die Ergebnisse dieser Arbeit, dass Änderungen im Zustand des Meereises (Abnahme der mittleren Meereiskonzentration und -dicke) sowie in der Lufttemperatur die veränderten Auswirkungen der Zyklonen auf die SIC antreiben, während Veränderungen in den Eigenschaften der Zyklonen (z.B. ihre Intensität) keine wesentliche Rolle spielen.

Contents

1   Introduction

"Polar exploration is at once the cleanest and most isolated way of having a bad time which has yet been devised" (Cherry-Garrard, 1922).

In the year 1863, way before computers, numerical models or weather apps had been invented, a british marine officer named Robert Fitzroy published a book called "The Weather Book: A Manual of Practical Meteorology" (Fitzroy, 1863). This moment is often perceived as the origin of the concept of weather forecasting (Bott, 2016). Amongst others, Fitzroys work contained descriptions of cyclonal rotating vortices originating at the interface between cold-polar and warm-subtropic air masses, shaping the weather in the mid-latitudes. This demonstrates that cyclones have been substantial for weather forecasting in the mid-latitudes from the very beginning of this scientific discipline and thus highlights their importance within the field of meteorology.

A further pioneering discipline of natural science is polar exploration. As indicated above by the quote of Apsley Cherry-Garrard, the fascination for the polar regions started driving people into these harsh and hostile environments a long time ago, despite the associated risks and discomforts. With respect to the Arctic, one of its most fundamental and at the same time most fascinating aspects is its ice-covered ocean. Theories of a frozen ocean, a *Mare Glaciale*, reach back into the 16th century, when Arctic geography was mostly a mixture of myth and hypothesis (Serreze and Barry, 2005). It took a few more centuries until Nansens Fram expedition from 1893–1896 verified the theory of the transpolar drift (Nansen, 1897) and thereby conclusively proofed that the north pole was indeed neither located on land nor on a solid ice sheet, but on movable sea ice.

Nowadays, more than 100 years later, both meteorology and polar exploration have fundamentally changed. Polar research is not conducted by a handful of pioneers on dog sleds anymore, but by large teams of scientists on research vessels, backed up by satellites and numerical climate models. In meteorology, such numerical models are deployed on super computers to produce hourly weather forecasts on horizontal scales of down to a few kilometres. These technological advances enable scientists around the world to tackle a variety of new, increasingly complex problems.

One such problem is to understand the fundamental changes currently going on in the Arctic at a rapid pace (IPCC, 2021). Over the last decades, near-surface temperatures in the Arctic have been rising nearly four times faster than on global average (Rantanen et al., 2022),

a phenomenon referred to as *Arctic amplification*. This amplified climate change in the Arctic is to a large degree driven by feedback mechanisms between individual components of the climate system (e.g., Pithan and Mauritsen, 2014; Stuecker et al., 2018; Block et al., 2020; Previdi et al., 2021; Wendisch et al., 2023). This demonstrates that - in order to predict the future evolution of the Arctic environment - a detailed understanding of the complex interaction processes within the coupled Arctic climate system is of fundamental importance. In that sense, also the two initially mentioned parts of the climate system, namely cyclones and the Arctic sea ice, can be brought together. This can be illustrated with a concrete example:

In late January 2022, a storm in the Barents and Kara Seas associated with the strongest cyclone ever detected north of 70° (based on ERA5 reanalysis data from 1979 to 2022) led to a regional loss of sea-ice area of more than 400.000 km² in only 6 days (Blanchard-Wrigglesworth et al., 2022, visualized in Figure 1.1). This is a regional record sea-ice loss in the whole satellite era (since 1979) and corresponds to a larger area than the total size of Germany. These impressive numbers emphasize the importance of the topic of this thesis: The analysis of the impact of cyclones on the Arctic sea-ice cover.

As will be outlined in the following section 1.1, the Arctic sea ice plays a crucial role within the global climate system. Consequently, research on the Arctic sea-ice cover, its future changes and its interactions with the remaining parts of the climate system is of high scientific relevance. Recent statistical studies covering a multitude of cyclone events indicate that cyclones are a significant driver of the overall Arctic sea-ice variability (e.g., Schreiber and Serreze, 2020). However, this overall impact of cyclones on sea ice, extending beyond individual examples such as the record Arctic cyclone from January 2022, is not yet fully understood. This thesis builds-up on the recent advances in this field in order to arrive at a more complete understanding of cyclone impacts on the Arctic sea ice. Hereby, a regional focus on the Atlantic Arctic Ocean (Figure 1.1) is chosen, because this region is characterized by a particularly strong near surface warming and sea-ice decline over the last decades (Isaksen et al., 2022; Rieke et al., 2023).

1.1 The Arctic sea-ice cover

1.1.1 Sea ice in the coupled Arctic climate system

The importance of the Arctic sea-ice cover for the climate system originates to a large degree from its role as an insulator between atmosphere and ocean, limiting the exchange of heat and moisture. In winter, this insulation of the relatively warm ocean from the colder
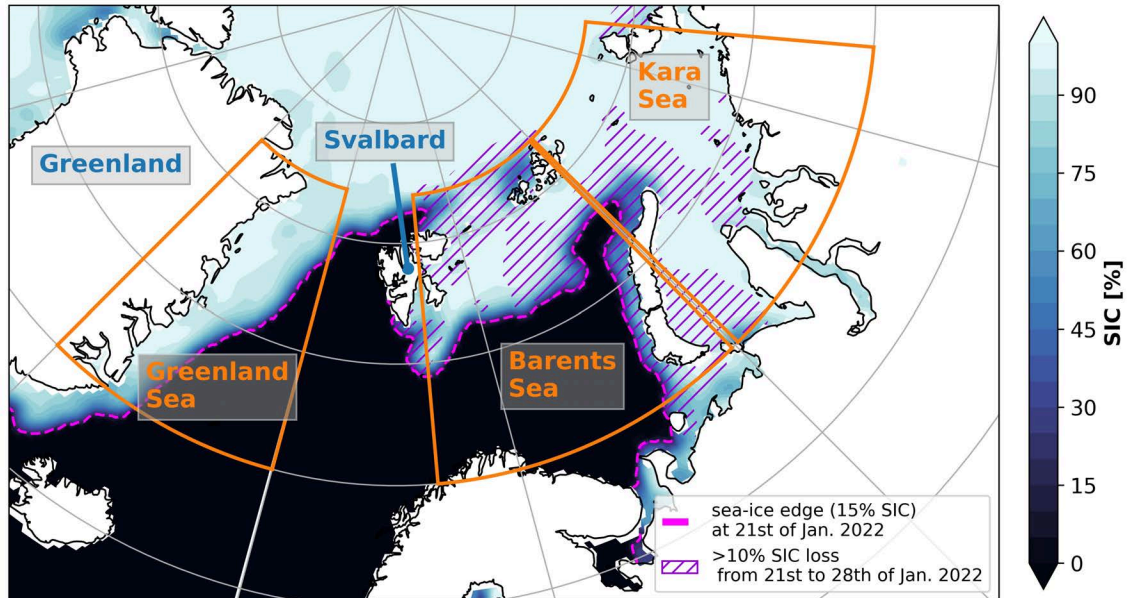
Figure 1.1: Overview on the study domain of the Greenland, Barents and Kara Seas as well as sea-ice concentration (SIC) before and SIC loss during the record Arctic cyclone from January 2022, following Blanchard-Wrigglesworth et al. (2022).

atmosphere has a cooling effect on atmospheric near-surfaces temperatures (McPhee, 2017). Importantly, the sea-ice cover also impacts the radiation balance at the surface, since it reflects a comparatively high amount of the incoming solar radiation due to its high albedo (Maykut, 1986). The sea ice thus has a surface cooling effect, because the surface absorbs less radiation than it would in absence of the sea ice. The associated ice-albedo feedback (simplified summarized as: Warming $\rightarrow$ ice retreat $\rightarrow$ further warming) is one of the main drivers of Arctic amplification (e.g., Pithan and Mauritsen, 2014). If related changes in the snow on top of the ice and melt ponds are included, this positive ice-albedo feedback is further enhanced (Curry et al., 1995).

On the other hand, clouds are known to dampen the ice-albedo feedback by reflecting parts of the incoming solar radiation before it reaches the surface (e.g., Choi et al., 2020). Additionally, there is scientific debate whether (and how) clouds itself might respond to the Arctic sea-ice loss and related enhanced fluxes of heat and moisture to the atmosphere, and if related cloud-sea ice feedbacks exist (Kay and Gettelman, 2009; Morrison et al., 2019). All of this illustrates the complexity of the interactions between the sea-ice cover and the remaining parts of the Arctic climate system.

These interactions also include the polar oceans: For example, during the formation of sea ice in high latitudes, brine is released into comparatively cold surface waters, creating a water mass of high density. As a consequence, the water sinks down and surrounding

surface water is pulled in to replace the sinking water (e.g., Rudels and Quadfasel, 1991). The newly formed deep water afterwards becomes part of the meridional overturning circulation extending through the global oceans. This convection in high latitudes is thus an important part of the network of global ocean currents and particularly impacts the characteristics of deep water masses in the oceans (Olbers et al., 2012).

The considerations in the previous paragraph already indicate that the sea-ice cover is not only important for the Arctic itself, but also for the global climate. This also applies from an atmospheric point of view: In general, the polar regions are a radiation sink (e.g., Trenberth and Caron, 2001), which results in an atmospheric temperature decline from the comparatively warm tropics towards the comparatively cold polar regions. The related pronounced meridional temperature gradient in the mid-latitudes is the primary driver of the (polar) jet streams in both hemispheres (e.g., Kraus, 2004). The retreat of the Arctic sea ice contributes to an amplified warming of the Arctic compared to the mid-latitudes and thus reduces this meridional temperature gradient. In accordance with that, there is scientific debate whether and how the Arctic sea-ice retreat can remotely impact the weather in the mid-latitudes via changes in atmospheric dynamics (recently, Riebold et al., 2023).

1.1.2 Recent changes of the Arctic sea ice

In view of the various interaction processes involving the sea-ice cover, it becomes evident that sea ice plays a significant role in the climate system of the Arctic and the whole planet. At the same time, though, it is undergoing rapid changes due to ongoing global warming: The ice-covered area is declining almost everywhere in the Arctic, strongest in summer on the Pacific side of the Arctic in the Beaufort, Chukchi, East Siberian and Laptev Seas, and in winter on the Atlantic side in the Barents Sea (Meier and Stroeve, 2022). Comparing the September Arctic sea-ice extent for the most recent and the earliest decade of the satellite era reveals a decline from $7.06 \times 10^6 \, \text{km}^2$ (1981–1990) to $4.57 \times 10^6 \, \text{km}^2$ (2011–2020) (Meier and Stroeve, 2022). This corresponds roughly to a loss of a third of the 1981–1990 sea-ice extent.

In addition to the spatial extent of the sea-ice cover, also its thickness (and thus the overall ice volume) is decreasing (Kwok, 2018; Meier and Stroeve, 2022). Particularly pronounced is the ongoing loss of the comparatively thick multiyear ice, which decreased by more than 50 % between 1999 and 2017 (Kwok, 2018). This observed thinning of the sea-ice cover can impact its ability to resist atmospheric and oceanic forcing (e.g., Rheinlænder et al., 2022), which can potentially contribute to enhanced ice loss in the future. A recent study by Kim et al. (2023) combined climate model projections with recent observational trends and predicts the first ice-free month in the Arctic (defined as a monthly sea-ice area below

$1 \times 10^6 \, \mathrm{km}^2$) for September between 2030 and 2050. The exact timing depends largely on the greenhouse gas emission scenario. Notably, their results suggest that there is not a single scenario, including the SSP1-2.6 low emission scenario, where an ice-free Arctic in September within the next decades can be avoided. Whether an ice-free Arctic will also occur in the remaining (summer) months, though, depends on the particular emission scenario.

In summary, the Arctic sea ice is of fundamental importance for the climate system and its fate within a warming Arctic remains to some degree uncertain. As indicated before, the atmosphere including cyclones is an important factor that shapes this future of the Arctic sea ice. The following part of this introduction will provide an overview on the main atmospheric drivers of Arctic sea-ice variability and illustrate the role of cyclones within this field.

1.2 The atmosphere as driver of sea-ice variability

Generally, both the atmosphere and the ocean drive the interannual to decadal variability of the Arctic sea ice. Hereby, oceanic forcing of sea-ice variability is mainly related to variations in ocean heat transport into the Arctic through the Bering Strait (e.g., Woodgate et al., 2010), on the one hand, and the Fram Strait and Barents Sea Opening (e.g., Årthun et al., 2012; Muilwijk et al., 2019), on the other hand. For the strong, recent retreat of the winter sea ice in the Barents and Kara Seas, a close link to atmospheric forcing was revealed recently (Liu et al., 2022), emphasizing the high importance of atmosphere-sea ice interactions for the changing Arctic climate.

1.2.1 Large-scale circulation patterns

As summarized by Serreze and Meier (2019), the variability in the extent of the sea-ice cover, both on regional and Arctic-wide scales, is in general strongly shaped by the occurrence of atmospheric circulation patterns, which influence near-surface wind speeds and temperatures. Of particular importance are the Arctic Oscillation (AO) and the closely related North Atlantic Oscillation (NAO). These are the dominant modes of atmospheric circulation variability in the mid- and high-latitudes in the northern hemisphere (e.g., Thompson and Wallace, 1998).

Hereby, the NAO primarily drives a dipole in winter sea ice between the Greenland Sea and the Labrador Sea (Deser et al., 2000), related to the advection of heat and moisture and the drift of sea ice associated with the Icelandic Low. A positive AO phase is characterized

by decreased SLP in the Arctic and a subsequent (i) weakening of the Beaufort gyre, (ii) a westward shift of the Transpolar Drift and (iii) a stronger cyclonic sea-ice motion to the north of the Kara and Laptev Seas (Rigor et al., 2002). Points (ii) and (iii) favor a thinner sea-ice cover in winter by creating a more divergent sea-ice motion pattern in the Arctic (Rigor et al., 2002). This results in enhanced growth of new ice in leads and in coastal areas, where ice advection away from the coast is increased. Furthermore, ridging of sea ice in the Beaufort gyre is an important process increasing ice thickness, thus, the (i) weakening of the Beaufort gyre additionally contributes to a thinner sea-ice cover. Rigor et al. (2002) found that this AO related thinning of the sea ice in winter significantly impacts sea-ice anomalies in the following summer, but this link has weakened since the 2000s due to a shift in the centers of action of the AO (e.g., Stroeve et al., 2011).

Another relevant circulation pattern is the so called Arctic Dipole Anomaly, which contributed significantly to the pronounced minimum in September sea-ice extent in the year 2007 (Wang et al., 2009). Hereby, an anticyclonic structure over Greenland and the central Arctic in combination with prevailing cyclonic conditions over northeastern Europe resulted in strong meridional winds that pushed sea ice out of the Arctic Ocean into the North Atlantic during large parts of the summer. This example highlights the importance of the occurrence of cyclones and anticyclones, which add-up to seasonal circulation anomalies, for the interannual variability of the Arctic sea-ice cover (e.g., Screen et al., 2011; Wernli and Papritz, 2018).

1.2.2 Role of cyclones

Focusing on shorter, sub-seasonal time scales, particularly the occurrence of synoptic cyclones is of importance for the Arctic sea ice. This is because cyclone passages are frequently associated with strong wind speeds and abrupt wind direction changes (e.g., Graham et al., 2019). The resulting impacts on the sea-ice cover consist of (i) increased ice drift speed and potentially increased ice deformation (Itkin et al., 2017; Graham et al., 2019). Additionally, cyclones frequently advect moist and warm (cold and dry) air masses along with the southerly (northerly) winds on their eastern (western) flank (e.g., Boisvert et al., 2016; Graham et al., 2019). This can impact the sea-ice cover via (ii) stalling or enhancing the seasonal sea-ice growth in autumn–winter and melt in spring–summer.

Both these processes (i–ii) could be observed during the previously mentioned, record Arctic cyclone from 2022: Temperatures in the Barents Sea increased by about 10 K during the cyclone passage and peaked to just below freezing on the 23th of January (Blanchard-Wrigglesworth et al., 2022). At the same time, surface wind speeds of more than 12 m/s occurred throughout the area, including a maximum 1-hourly wind speed over the Barents

Sea of 28 m/s (ca. 100 km/h) on 24th of January. This is a record maximum for this region for the complete 1979–2022 coverage of the utilized ERA5 data. Another notable cyclone case is given by the strong summer cyclone in August 2012 in the central Arctic: This event caused a strong local ice volume decrease due to (iii) enhanced bottom melt caused by up-mixing of relatively warm ocean water under the influence of high wind speeds (Zhang et al., 2013; Stern et al., 2020).

To summarize, the analysis of specific (extreme) cyclone events reveals different mechanisms of cyclone-related sea-ice changes (i–iii). First statistical studies further indicate that cyclones are significantly impacting the overall variability of the Arctic sea ice (e.g., Schreiber and Serreze, 2020). An improved quantification and understanding of these cyclone impacts can thus result in more accurate predictions on the state of the sea-ice cover (Capute and Torn, 2021). On shorter time scales of days to weeks, improved forecasts of sea-ice changes during cyclone events are important for socio-economic activities in the Arctic, such as Arctic navigation or aviation (Gultepe et al., 2019; Inoue, 2021). Given the expected further warming of the Arctic and a related retreat and thinning of the sea-ice cover, such activities are expected to be increasing in the future (Cao et al., 2022). On longer time scales, advanced understanding of cyclone impacts on sea ice and their changes with the ongoing warming of the Arctic can improve the representation of cyclone-sea ice interactions in climate models. This can contribute to more accurate model predictions on the future of the Arctic sea-ice cover. The importance of the Arctic sea ice for our climate and ecosystem has been discussed before and thus, such improved model predictions are of high relevance for our society.

1.3   Thesis structure and research questions

This thesis is based on three separate, peer-reviewed publications, and aims to close knowledge gaps with respect to cyclone impacts on the Arctic sea ice. In the following paragraphs, a set of three research questions (RQs) is established as a framework in which the individual publications are synthesized within this thesis. The contribution of the publications to the RQs of this thesis as well as the context to existing literature in the field is discussed after the presentation of each RQ. Before the results (publications) are presented in chapters 3–5, an overview on the theoretical background and the methodological basis of this thesis is provided in chapter 2. In the sixth and final chapter, the main findings of the individual publications 1–3 (chapters 3–5) are synthesized in order to answer the three raised RQs. In the following, the individual publications 1–3 will solely be referred to as chapters 3–5 according to their placement in this thesis.

RQ1: What is the statistical impact of cyclone passages on sea-ice concentration (SIC) in the Atlantic Arctic Ocean?

The overarching objective of this thesis is to statistically quantify the impact of cyclone passages on SIC in the Atlantic Arctic Ocean over the last decades. For this purpose, a cyclone tracking algorithm is applied to the ERA5 reanalysis (Hersbach et al., 2020) to create a cyclone occurrence data set (details in section 2.2). This cyclone occurrence data set is utilized to compare daily SIC changes for cyclone and non-cyclone conditions.

RQ1 is mainly tackled in the chapters 3 and 5 of this thesis. In chapter 3, cyclone impacts on SIC are quantified for the winter months (December to February) and for the two most recent decades (2000–2020). The main focus of chapter 3 is to establish a robust method to quantify cyclone-related SIC changes including specific novel aspects compared to the existing literature in the field. Specifically, a recent study by Schreiber and Serreze (2020) provided a quantification of seasonally averaged cyclone impacts on SIC in the Arctic Ocean. Their analysis, however, is limited to a specific time period of four days following each cyclone passage. In direct comparison, chapter 3 of this thesis provides the following novel aspects: I) a detailed analysis of the temporal variability of cyclone-related SIC changes on time scales of up to a week before/after each cyclone, and II) the dependency of cyclone impacts on the intensity of the cyclones and on the local sea-ice conditions during the cyclone passage. Other statistical studies that address cyclone impacts on Arctic SIC are either limited to the summer months (Finocchio et al., 2020, 2022), focus on different regions of the Arctic (Finocchio and Doyle, 2021) or tackle this problem on a cyclone-centered grid (Clancy et al., 2022).

Further novel aspects related to RQ1 are contained in chapter 5 of this thesis: Here, the analysis of cyclone impacts on SIC (based on the method established in chapter 3) is extended beyond winter to cover the whole year on a monthly basis. Such a monthly quantification of cyclone impacts on SIC throughout the year has not been provided before. Recently, such a monthly analysis was tackled by Finocchio et al. (2022), but limited to the summer months. The annual cycle of cyclone impacts on SIC obtained in chapter 5 is again discussed in the context of variations in cyclone intensity and sea-ice conditions during the cyclone passage.

RQ2: What are the individual contributions of dynamic and thermodynamic processes to sea-ice changes related to cyclones?

As was already discussed and will be further elaborated in section 2.3, cyclones can impact the sea ice through both dynamically and thermodynamically driven processes. However, the interplay of these dynamic and thermodynamic mechanisms and their relative

importance for cyclone impacts on SIC is not yet quantitatively well known. Thus, a separate quantification of dynamic and thermodynamic cyclone-related SIC changes is another objective of this thesis.

First insights with respect to the related RQ2 of this thesis are provided in chapter 3. Here, cyclone anomalies in wind speed and direction as well as in the surface energy budget (at the interface between the atmosphere and the ocean including sea ice) are calculated. These provide an initial assessment on the impact of cyclones on the conditions that control dynamic and thermodynamic sea-ice changes.

In chapter 4 of this thesis, these cyclone-related dynamic and thermodynamic sea-ice changes are directly quantified based on a nudged simulation of the coupled atmosphere-ocean-sea ice model HIRHAM-NAOSIM 2.2 (model description in section 4.6). Hereby, both SIC and sea-ice thickness (SIT) changes are analyzed. The framework of a case study from the time period of the Multidisciplinary drifting Observatory for the Study of Arctic Climate (MOSAiC) expedition (Shupe et al., 2020) was chosen for the analysis. That way, the suitability of the model simulation for the analysis can be evaluated utilizing field observations. The case study covers three consecutive intense cyclones that traversed the Barents Sea within two weeks in February 2020. However, results from these cases are also set into the context of cyclones during the whole MOSAiC winter (January–March 2020).

Similar cyclone case studies addressing the contribution of dynamics and thermodynamics to sea-ice changes were conducted by Boisvert et al. (2016) and Blanchard-Wrigglesworth et al. (2022). However, these studies rely on a scaling approach to derive the contribution of thermodynamics to sea-ice changes out of anomalies in the surface energy budget. In comparison, the explicit analysis of coupled model tendencies for both dynamic and thermodynamic sea-ice changes is a novel aspect of chapter 4. Coupled model data, namely a subset of CMIP5 models, is also utilized by Cai et al. (2020) to analyze sea-ice growth rates in the Arctic in response to cyclones. Their study focuses solely on changes in SIT, however, and does not include dynamic and thermodynamic SIC changes. Furthermore, the higher horizontal resolution of the HIRHAM-NAOSIM model compared to the CMIP5 models allows a more regional focus on sea-ice changes in the Barents and Kara Seas in the analysis contained in this thesis.

Another recent study by Clancy et al. (2022) utilizes a sea-ice model forced with atmospheric reanalysis data to analyze cyclone-related dynamic and thermodynamic changes in both SIC and SIT. In contrast to chapter 4 of this thesis, they focus on a cyclone-centered grid in their study. Nonetheless, their results provide an important reference to the here presented findings. A new aspect of chapter 4 compared to the study by Clancy et al. (2022)

is the coupled model set-up compared to the analysis of an atmospherically-forced sea-ice model. A further novelty is the focus on a series of multiple consecutive cyclone events with high intensity and similar tracks (in the following also referred to as a *cyclone cluster*).

RQ3: Do the SIC impacts of cyclones change in a warming Arctic and what are the related mechanisms?

As previously outlined, one of the most urgent research questions with respect to cyclone impacts on sea ice is to assess, whether (and how) these cyclone impacts will change in a warming Arctic with a thinner and less compact sea-ice cover. Thus, this topic is the focus of RQ3 of this thesis.

First insights into recent changes in cyclone impacts on SIC averaged for the winter months (December to February) are provided in chapter 3. Here, cyclone impacts on SIC in winter are compared for the two most recent decades (2000–2020) and the two earliest decades (1979–1999) of the satellite era.

Apart from that, RQ3 is mainly tackled in chapter 5. For the analysis in chapter 5, atmospheric (ERA5, Hersbach et al., 2020) and oceanic (ORAS5, Zuo et al., 2019) reanalysis data sets are exploited for the last decades (specifically for 1979–2018). These data sets are utilized to I) analyze monthly trends in cyclone impacts on SIC for different regions of the Atlantic Arctic Ocean and II) compare cyclone impacts on SIC between the two time periods 1979–1999 and 2000–2018. The recent changes in cyclone impacts on SIC are interpreted in the context of changes in cyclone intensity, sea-ice properties (including SIC and SIT) and two meter air temperature.

Both the statistical cyclone impacts on SIC (see RQ1) and their recent changes have not yet been analyzed on a monthly basis throughout the whole year. Schreiber and Serreze (2020) analyze such changes on a seasonally averaged basis, and Finocchio et al. (2022) provide a monthly analysis but limited to the summer months June to August. Thus, results from chapter 5 of this thesis add novel findings to the existing literature in the field. A further novel aspect of chapter 5 of this thesis is a detailed analysis of the relation between changed cyclone impacts on SIC and preceding changes in local sea-ice conditions, exemplary for the months October and November.

2 Theory and methods

This section aims to lay the theoretical foundations for the following analysis of the impact of synoptic cyclones on the Arctic sea-ice cover. In a first step, the phenomenon of a cyclone will be defined and the related theoretical concepts of atmospheric dynamics will be introduced. Afterwards, the concept of cyclone tracking, which is the methodological backbone of this thesis, will be presented. Finally, the fundamentals of Arctic sea-ice variability will be discussed. The particular focus is to provide the theoretical background necessary to understand how atmospheric forcing related to cyclones can impact the sea ice both dynamically and thermodynamically.

2.1 Synoptic cyclones

2.1.1 Related fundamentals of atmospheric dynamics

Detailed descriptions of the theoretical concepts of atmospheric dynamics and synoptic meteorology, which are the foundations for this section, can be found e.g. in Kraus (2004), Etling (2008), Bott (2016) or Achatz (2022). To start generally, cyclones are usually defined as flow areas with low air pressure and cyclonic vorticity (Bott, 2016). In this thesis, the term cyclone will refer to cyclones at surface level only, which are characterized by a local minimum in sea level pressure (SLP) surrounded by closed isobars. Cyclones are associated with anti-clockwise winds in the northern hemisphere and are important drivers of the weather in the mid-latitudes.

In order to theoretically describe the motion of air associated with cyclones, one needs to go back to the fundamental equation of motion for fluids and gases, also referred to as Navier-Stokes equation:

$$\frac{\partial \vec{v}}{\partial t} = -\frac{1}{\rho} \nabla p + \vec{g} - 2\vec{\Omega} \times \vec{v} + \vec{F_R} \tag{2.1}$$

where $\vec{v}$ is the wind vector, ρ is the density of the fluid/gas, p is the pressure, $\vec{g}$ is the gravitational acceleration, $\vec{\Omega}$ is the angular velocity of the earth and $\vec{F_R}$ represents friction.

For an idealized fluid, the friction can be neglected, and thus the term $\vec{F_R}$ vanishes from equation 2.1. For synoptic phenomena with scales of about $1000\,\mathrm{km}$, the temporal change

of the zonal and meridional wind components as well as the part of the Coriolis force associated with the vertical wind speed in equation 2.1 remain at least one order of magnitude smaller than the other parts of the equation (Kraus, 2004). Thus, the Coriolis force ($\vec{F_C}$) and the pressure gradient force ($\vec{F_P}$) are the dominating terms for the (horizontal) motion of an idealized fluid on synoptic scales. This approximation is known as the *geostrophic approximation*, and the equation for the resulting geostrophic wind $\vec{v}_g$ is:

$$\vec{v}_g = \frac{1}{\rho f}\vec{k} \times \nabla_H p \tag{2.2}$$

where $\vec{v}_g$ is the geostrophic wind vector, ρ is the density of air, f is the Coriolis parameter, $\vec{k}$ is a unit vector normal to the surface and p is the air pressure.

For the practical example of a cyclone, the geostrophic balance consists of the pressure gradient force driving winds towards the core of the low pressure system, which are then deflected to the right on the northern hemisphere by the Coriolis force (Figure 2.1 A). This results in the above-mentioned, anti-clockwise rotational winds around the core of the cyclone (Figure 2.1 B).

On larger scales, the concept of the geostrophic wind also explains the existence of the westerly base flow in the mid-latitudes. Due to the higher solar irradiation in lower latitudes than in higher latitudes (e.g., Trenberth and Caron, 2001), meridional temperature gradients exist in the atmosphere. Furthermore, the density of air depends on its temperature. This
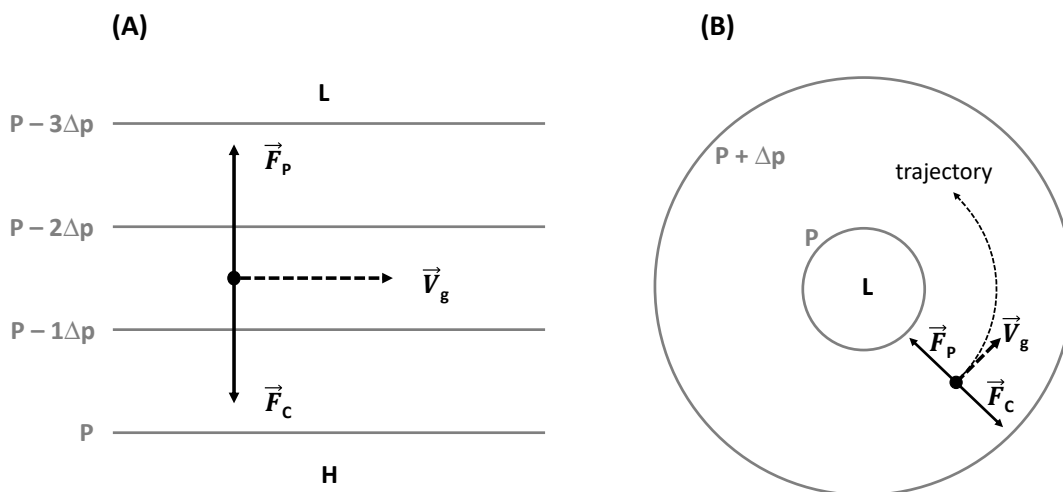

Figure 2.1: Visualization of the geostrophic flow in general (A) and specifically around a cyclone (B) adapted from Kraus (2004).

is expressed in the ideal gas law, which can be formulated in its general form and in a way directly including the density:

$$pV = nRT \tag{2.3}$$

$$p = \rho R_M T \tag{2.4}$$

where p is the air pressure, V is the volume, n is the amount of substance of gas (number of moles), R is the general gas constant, T is the temperature, ρ is the density and R_M is the specific gas constant (defined as general gas constant divided by the molar mass of a specific gas).

From equation 2.4 it follows that for a constant pressure, the density of air increases with decreasing temperature. An increase in density (of a body with constant mass) is accompanied by a reduction in volume, thus, a cold air column has a lower vertical extent than a warm air column. Consequently, at a specific height above the ground, the air pressure is lower in a cold air column than in a warm air column, as their is less mass situated above the specific height. This is also quantified in the barometric height formula, linking the pressure decrease with height to the temperature of the air column:

$$\frac{\partial p}{\partial z} = -\frac{p}{R_L T} g \tag{2.5}$$

where p is the air pressure, z is the height above ground, R_L is the specific gas constant of dry air, T is the temperature of the air column and g is the gravitational acceleration.

These considerations eventually explain the westerly base flow in the mid-latitudes as visualized in Figure 2.2: In accordance with the geostrophic approximation, the air is flowing from high pressure (warm air in the south) towards low pressure (cold air in the north) and is thereby deflected to the right by the Coriolis force, resulting in a westerly flow at boundaries between warm and cold air masses.

In Figure 2.2 (A), the surfaces of constant pressure (isobaric surfaces) and constant temperature are parallel. Due to the ideal gas law, this applies also to the surfaces of constant pressure and constant density. This case is referred to as a barotropic atmosphere. The opposite case is referred to as baroclinicity. In this case, the geostrophic wind is increasing with height (Figure 2.2 B) due to the presence of horizontal temperature gradients on isobaric surfaces. This vertical shear of the geostrophic wind is referred to as thermal wind and is described by the related thermal wind equation:
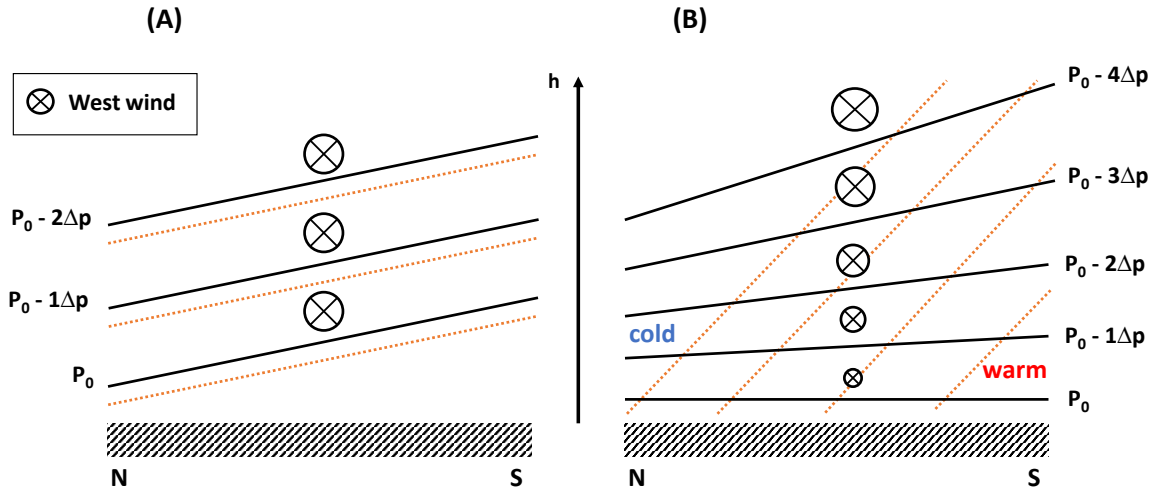
Figure 2.2: Visualization of the geostrophic flow in a barotropic (A) and baroclinic (B) atmosphere adapted from Kraus (2004). Black lines indicate isobars, dashed orange lines indicate isotherms.

$$\vec{v}_T = \frac{\partial \vec{v}_g}{\partial z} = \frac{g}{fT}\vec{k} \times \nabla_H T \tag{2.6}$$

where $\vec{v}_T$ is the thermal wind vector, $\vec{v}_g$ is the geostrophic wind vector, z is the height above ground, g is the gravitational acceleration, f is the Coriolis parameter, T is the air temperature and $\vec{k}$ is a unit vector normal to the surface.

The increase of the geostrophic wind with height under baroclinic conditions is the reason for the existence of the wind speed maxima in the upper atmosphere of the mid-latitudes, which are commonly referred to as jet streams. The concept of baroclincity is, however, also important for the formation of cyclones: As already indicated in section 1.1, the formation of cyclones is often taking place at boundaries between cold-polar and warm-subtropic air masses. This is because such conditions favor the growth of baroclinic instabilities.

2.1.2 Cyclone activity in the Arctic

A detailed description of the theory of cyclogenesis (the formation of cyclones) requires a significant number of further theoretical concepts, including the quasi-geostrophic theory, and is thus beyond the scope of this thesis. Instead, the focus of this subsection is to explain, which atmospheric conditions are favoring cyclogenesis and to give an overview on cyclone activity in the Arctic. Detailed theoretical descriptions of cyclogenesis can e.g. be found in Etling (2008), Bott (2016) or Achatz (2022).

In general, cyclones form out of initial baroclinic pertubations, mostly at frontal zones between cold and warm air masses. A few factors determine, whether an initial baroclinic pertubation will decay or whether it will grow and can eventually result in the formation of a cyclone. Two important factors are I) the static stability, determined by the vertical potential temperature gradient and II) the vertical wind shear (e.g., Etling, 2008). Both these factors are combined in a parameter called maximum Eady growth rate (EGR). The EGR is based on the Eady atmospheric model (Eady, 1949) and was shown to be a suitable estimate of growth rates of lower-tropospheric baroclinic instabilities (Lindzen and Farrell, 1980). It is defined as:

$$EGR = 0.31 \frac{f}{N} \left| \frac{\partial \vec{v}}{\partial z} \right| \tag{2.7}$$

$$N = \sqrt{\frac{g}{\theta} \frac{\partial \theta}{\partial z}} \tag{2.8}$$

where f is the Coriolis parameter, N the Brunt-Väisälä frequency, $\vec{v}$ the horizontal wind vector, z the vertical height, g the gravitational acceleration and θ the potential temperature.

The dependence of the EGR on the vertical wind shear, which is related to horizontal temperature gradients via the thermal wind equation (equation 2.6), explains why cyclogenesis is frequently taking place at boundaries between cold and warm air masses. To provide an overview on the seasonally varying cyclone activity in the Arctic, Figure 2.3 displays seasonal means of the EGR and the cyclone frequency for winter (DJF) and summer (JJA) for 2000–2020 based on ERA5 data and a cyclone tracking algorithm (description of the latter in the following section 2.2). Following Madonna et al. (2020), the calculation of the EGR is based on the potential temperature at 700 hPa, while the vertical gradients in equations 2.7 and 2.8 are obtained using wind, geopotential height and potential temperature at 850 hPa and 500 hPa.

In winter, regions with a comparatively high cyclone frequency extend from the south coast of Greenland towards Iceland and further north into the Barents and Kara Seas (Figure 2.3). Maxima in the EGR are particularly found around Iceland and at the southeast coast of Greenland. This indicates that cyclones mostly form in this region and afterwards travel into the Barents and Kara Seas, where they decay. The existence of this winter storm track in the Atlantic Arctic Ocean is a well known feature (e.g., Serreze, 1995).

Cyclone activity in the Arctic is less regionally constraint in summer than in winter. Comparatively high cyclone frequencies are found over large parts of the Eurasian continent, and a pronounced maximum is located in the central Arctic (Figure 2.3). Compared to winter,
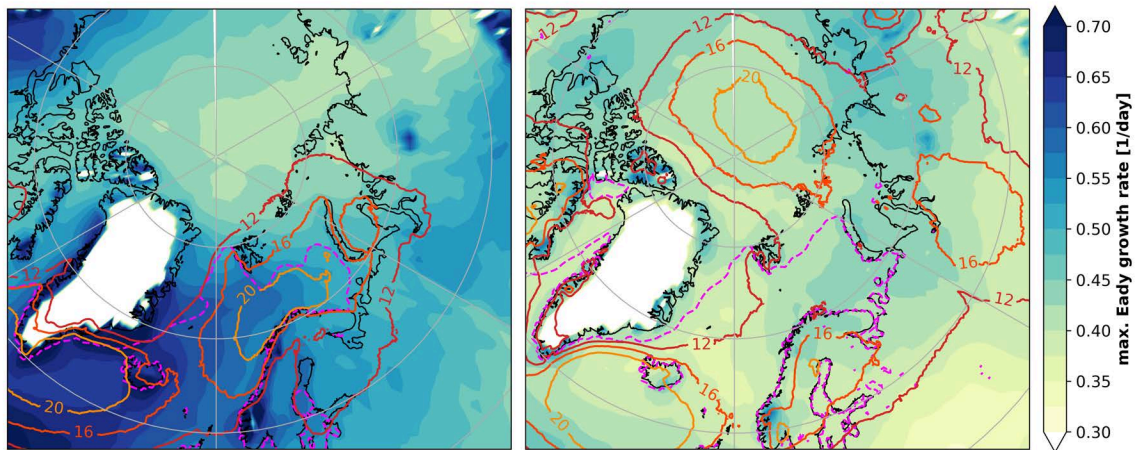
Figure 2.3: Mean Eady growth rate (blue colors) and cyclone frequency (percentage of days with cyclone occurrence, solid contourlines) for winter (DJF, left) and summer (JJA, right) for 2000–2020 based on ERA5 and a cyclone tracking algorithm. Dashed pink line indicates the position of the 15 % SIC contour (ice edge) for 2000–2020.

cyclone counts are decreased in the Norwegian and Barents Seas. This shift in cyclone activity is in accordance with differences in the regional distribution of the EGR. The EGR in summer is lower than in winter for most regions, particularly along the North Atlantic winter storm track. A maximum of the EGR in summer is found over northeastern parts of the Eurasian continent. This regional increase in baroclinicity is related to the formation of a frontal zone over Eurasia, frequently located along the boreal forest/tundra boundary (Serreze, 1995). The high cyclone counts in the central Arctic in summer are mostly related to cyclones that form at this frontal zone, enter the Arctic Ocean from central to eastern Eurasia and eventually decay while travelling northwards (Serreze and Barrett, 2008).

2.2 Cyclone tracking and cyclone occurrence mask

The specific data sets and methods utilized in each result chapter 3–5 are presented in place, in accordance with the publication-based structure of this thesis. However, since the method of cyclone tracking and a derived cyclone occurrence data set is the common ground for most parts of this thesis, an overview on this particular methodological aspect is provided in this section.

Cyclone tracking tools allow a statistical analysis of a large number of cyclone cases without the need to manually review meteorological weather maps for each individual event. They are thus a powerful tool for the climatological analysis of synoptic events. A variety of cyclone tracking tools is available, of which most are either based on SLP or vorticity. A

comparison of up to fifteen different cyclone detection and tracking methods applied to the same input data set by Neu et al. (2013) revealed a generally robust agreement between different tracking methods.

In this thesis, a SLP based algorithm is applied to 6-hourly ERA5 data (Hersbach et al., 2020). The algorithm is a modified version of the one initially presented by Bardin and Polonsky (2005) and Akperov et al. (2007), containing some adaptions for the Arctic region (Akperov et al., 2015). The basic principle of this algorithm is to search for local SLP minima, which are surrounded by closed isobars. More details are provided in the following paragraph and can also be found in Akperov et al. (2020):

The first step is to search for grid-points where the SLP is lower than in the eight surrounding grid-points. These grid-points are identified as candidates for a cyclone center. To locate the outermost closed isobar of a cyclone, the pressure from the previous grid point is gradually increased and compared to the SLP of the surrounding grid points to identify the locations where the pressure no longer increases. That way, cyclone center positions and cyclone areas are determined for each time step. Cyclones from different time steps are connected to cyclone tracks based on maximum allowed differences in geographic cyclone positions and SLP. In addition to the cyclone center position and the cyclone area, cyclone depth is provided as a measure of cyclone intensity. The cyclone depth is determined as SLP difference between the outermost closed isobar of a cyclone and its center.

Based on the geographic coordinates of the outermost closed isobar of each cyclone, a binary cyclone occurrence mask was created as data base for this thesis (Figure 2.4). Specifically, all grid-points within an outermost closed isobar of a cyclone are defined as *within cyclone influence* for the corresponding 6-hourly time-step. The 6-hourly cyclone occurrence data was then aggregated to a daily time scale. Hereby, all grid-points which are within cyclone influence for at least one out of four 6-hourly time steps are considered as within cyclone influence on the daily time scale.

In chapters 3 and 5, the daily cyclone occurrence data is used to calculate composites of changes in SIC over different daily time scales associated with cyclone passages. Such daily changes in SIC can be attributed to the cyclone passages more robustly than absolute SIC values, which are strongly affected by the inter-annual variability of the Arctic sea-ice cover. To further account for the fact that the SIC in the Arctic also changes regularly over a few days/a week (in accordance with the seasonal cycle of SIC), cyclone-related SIC changes are always compared to a non-cyclone reference. More details can be found in chapters 3 and 5.
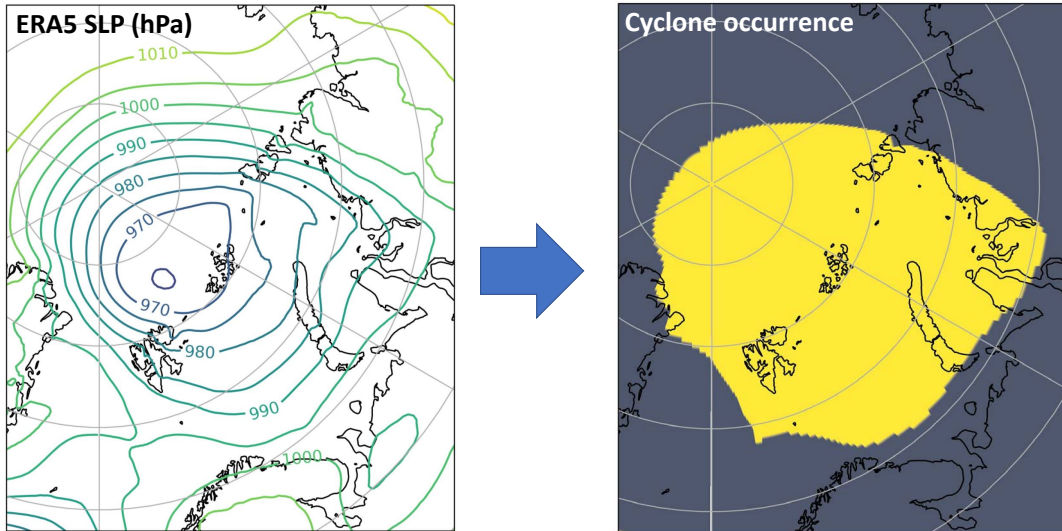
Figure 2.4: ERA5 SLP (left) and cyclone area (right, yellow grid-cells) as classified by a cyclone tracking algorithm, for the 20th of February 2020 (0 UTC).

2.3 Dynamic and thermodynamic sea-ice variability related to cyclones

The focus of the following section is to discuss, how the atmosphere (and specifically cyclones) can drive dynamic and thermodynamic sea-ice variability. A more general description of the Arctic sea ice including its physical and chemical properties can be found e.g. in Petrich and Eicken (2017) or Weeks and Ackley (1986).

Sea ice forms thermodynamically via freezing of sea water. After its initial formation, thermodynamic mechanisms further control the growth and melt of the sea ice, which is expressed in its energy balance. At the atmosphere-sea ice boundary, this balance is given e.g. by Maykut (1986) for the assumption of thermal equilibrium as:

$$(1 - \alpha)F_{SW} - I_o + F_{LW\downarrow} - F_{LW\uparrow} + F_S + F_L + F_C + F_M = 0 \qquad (2.9)$$

where α is the surface albedo, F_{SW} is the shortwave downward radiation, I_o represents the transmission of shortwave radiation through the ice, $F_{LW\downarrow}$ ($F_{LW\uparrow}$) is the longwave downward (upward) radiation absorbed (emitted) by the ice, F_S (F_L) is the turbulent sensible (latent) heat flux between ice and atmosphere, F_C is the conductive heat flux through the ice and F_M is the heat loss due to melting of ice.

The surface energy balance at the top of the sea ice is coupled to the balance at the ice-ocean boundary at the bottom via the conductive heat flux through the ice (F_C). The ice-ocean surface energy balance is not directly impacted by the atmosphere and is therefore not presented here, details can be found in Maykut (1986).

The terms representing radiation and heat fluxes in equation 2.9 directly depend on atmospheric quantities, which can be impacted by cyclone passages. For example, according to Maykut (1986), the turbulent fluxes of sensible (F_S) and latent (F_L) heat can be parameterized as:

$$F_S = \rho c_p C_S u (T_a - T_0) \tag{2.10}$$

$$F_L = \rho L C_L u (q_a - q_o) \tag{2.11}$$

where ρ is the density of the air, c_p is the specific heat of air, T_a is the air temperature at a reference height (usually 10 m), T_0 is the temperature of the surface, u is the wind speed at the reference height, L is the latent heat of vaporization, q_0 and q_a are specific humidities at the surface and reference level, and C_S and C_L are bulk transfer coefficients for sensible and latent heat (Deardorff, 1968).

Cyclones frequently cause high wind speeds and often advect warm/moist (cold/dry) air masses on their eastern (western) flank. In accordance with equations 2.10 and 2.11, this combination can lead to strong changes in turbulent heat fluxes at the ice-atmosphere interface. The cyclone-related advection of air masses can further impact the radiative fluxes at the ice-atmosphere interface. Increased cloudiness within warm-moist air masses increases $F_{LW\downarrow}$, because more longwave radiation is emitted back to the surface. In the absence of the polar night, this increased cloudiness obviously also reduces the amount of incoming shortwave radiation (F_{SW}). Within cold-dry air masses, reduced cloudiness can have the opposite effect, namely reduced longwave downward radiation and (in the absence of the polar night) increased shortwave downward radiation. Cyclone-related air mass advection can additionally alter the longwave downward radiation by impacting the amount of atmospheric water vapour. Altogether, it becomes evident that cyclone passages can alter the surface energy balance at the ice-atmosphere boundary via many different mechanisms, of which some can cancel each other out, while others can amplify each other. That way, cyclones can directly impact sea-ice melt and growth.

Once the sea ice has formed thermodynamically, also dynamic processes contribute to its variability. This is summarized in the momentum equation of sea ice (e.g., Serreze and Barry, 2005):

$$\frac{m\partial \vec{U_{ice}}}{\partial t} = \vec{\tau_a} + \vec{\tau_w} + mf\vec{k} \times \vec{U_{ice}} + \vec{F} - mg\nabla H \tag{2.12}$$

where m is the ice mass per unit area, $\vec{U_{ice}}$ is the ice velocity, f is the Coriolis parameter, $\vec{k}$ is a unit vector normal to the surface, $\vec{\tau_a}$ ($\vec{\tau_w}$) is the air (water) stress, $\vec{F}$ is the internal ice stress, H is the dynamic height of the sea surface and g is the gravitational acceleration.

The first two terms in equation 2.12 are usually dominant by more than an order of magnitude (Haas, 2017), even though ice interactions can also be large in winter and near coasts. The atmospheric influence on sea-ice motion, summarized in the term τ_a, is thus one of the dominant elements. This was also quantified by Thorndike and Colony (1982), who revealed that away from coasts about 70 % of the variance in ice motion is explained by the local surface geostrophic wind. More specifically, Nansen (1902) was the first to observe that the daily movement of the pack ice occurs at about 2 % of the wind speed and 30° to the right of the wind velocity vector. Colony and Thorndike (1984) arrived at slightly different numbers utilizing data from drifting buoys deployed on ice floes, namely a drift speed of 1 % of the mean wind speed and an angle of 18° to the right. In general, these findings emphasize the high potential of cyclones to impact sea-ice dynamics, since cyclone passages frequently lead to abrupt changes in wind direction (and thus the direction of the ice drift) and to high wind speed conditions (thus enhancing the sea-ice drift speed).

Of particular importance for the sea-ice impact of cyclones is the interplay of the dynamic and thermodynamic mechanisms described in equations 2.9 and 2.12. Two such processes are highlighted here in the following:

The first one consists of divergence-induced new ice formation, which is described more generally, e.g., by von Albedyll (2022). During this process, divergent ice drift results in the formation of leads and openings in the sea-ice cover, which provide room for the growth of new ice, because the ocean surface is exposed to cold Arctic air temperatures (in autumn and winter). This mechanism gains sea-ice area at cost of sea-ice thickness. However, it is also an effective way to increase overall ice volume, because thin ice (in leads) grows faster than thick ice (e.g., Haas, 2017; Petty et al., 2018). In the context of cyclone events, this process is an example for dynamic cyclone impacts (high wind speed and abrupt changes in wind direction resulting in enhanced lead formation) potentially enabling thermodynamic

follow-up impacts (advection of cold-dry air on a cyclones' western flank favoring new ice growth in leads). Such enhanced new ice formation in leads was previously observed for cyclone cases during the N-ICE2015 campaign by Graham et al. (2019).

The second process is an example for thermodynamic cyclone impacts that potentially influence subsequent dynamic sea-ice changes: As previously discussed, potential changes in the surface energy budget due to the advection of warm-moist air masses on a cyclones eastern flank can hamper the growth of sea ice. At the same time, the internal ice-strength is depending on the SIT, as expressed e.g. in the parametrization for the ice-strength P as suggested by Hibler (1979):

$$P = P^* A h e^{-C^*(1-A)} \tag{2.13}$$

where A (h) is the average ice concentration (thickness) per grid cell, P^* is the compressive ice strength parameter and C^* is the ice concentration parameter.

From equation 2.13 it follows that a cyclone-related stalling of ice growth can weaken the ice-strength and thus facilitate (dynamic) ice deformation, when the ice drift converges. Both these concepts can help to interpret sea-ice changes in relation to cyclone passages in the following results chapters 3–5.

3   New insights into cyclone impacts on sea ice in the Atlantic sector of the Arctic Ocean in winter

Summary of the publication:

Objectives	• Quantify sea-ice concentration (SIC) changes related to cyclones in Arctic winter considering: Their temporal variability, regional differences between the Greenland, Barents and Kara Seas, the case conditions, i.e. cyclone intensity and state of the sea-ice cover. • Analyze changes in SIC impacts of winter cyclones between „old Arctic" (1979-1999) and „new Arctic" (2000-2020).
Contributions to RQs	• This study contributes to **RQ1** and **RQ3** of this thesis by quantifying cyclone impacts on SIC and their recent changes in winter.
Key points	• Cyclones cause an anomalous SIC decrease in the Greenland Sea and an anomalous increase in the Barents Sea in winter. • Intense cyclones combined with locally low to medium SIC leads to the strongest impacts on sea ice. • Cyclone impacts on sea ice have intensified under "New Arctic" conditions, particularly during the last decade in the Barents Sea.
Own Share	• I processed the utilized data sets, carried out the scientific analysis and designed all figures contained in the manuscript. • I wrote the first draft of the manuscript and was in charge of leading the manuscript revision and managing the submission and peer-review process.

3.1 Abstract

Based on the ERA5 reanalysis, we report on statistically significant impacts of transient cyclones on sea-ice concentration (SIC) in the Atlantic sector of the Arctic Ocean in winter under 'New Arctic' conditions (2000–2020). This includes a pattern of reduced SIC prior to and during cyclones for the whole study domain, while a regional difference between increased SIC in the Barents Sea and reduced SIC in the Greenland Sea is found as the net effect from 3 days prior to 5 days after the cyclone passage. Generally, locally low to medium SIC conditions combined with intense cyclones drive highest SIC changes. There are indications that both thermodynamic and dynamic effects contribute to the SIC changes, but a detailed quantification is required in future research. We provide evidence that cyclone impacts on SIC have amplified compared to the 'Old Arctic' (1979–1999), particularly in the Barents Sea.

3.2 Introduction

Cyclones are important drivers of heat and moisture transport from lower latitudes into the polar regions; they account for nearly three-quarters of the average annual moisture transport into the Arctic (Fearon et al., 2021). The direct thermodynamic impacts of intrusions of warm and moist air in winter are increased downward fluxes of longwave radiation and sensible heat at the snow/ice surface, accompanied by a reduction in sea-ice concentration (SIC) (Woods and Caballero, 2016). It has been shown that anomalous warming and moistening triggered by extreme cyclone events can result in near-melting conditions in winter in the Arctic, turn the normally negative surface energy budget into a positive one, and thus promote ice melt or reduced ice growth (Boisvert et al., 2016; Moore, 2016; Rinke et al., 2017). But cyclone impacts on Arctic sea ice in winter are not limited to thermodynamics. Cyclone-related wind anomalies lead to a shift of the ice edge position and thus locally reduce or increase the sea-ice extent dynamically (Boisvert et al., 2016; Schreiber and Serreze, 2020). Furthermore, ice deformation during storms can promote ice drift divergence and subsequent lead formation and new ice growth as well as ice drift convergence, closing of leads, and formation of pressure ridges (Itkin et al., 2017).

Due to these various dynamic and thermodynamic impacts, cyclones are an important driver of Arctic sea-ice variability, which plays a key role in the Arctic climate system. Apart from that, the ice edge position and the local SIC are important factors for the marine ecosystem and short-term predictions of both are also crucial for navigation in the Arctic Ocean and its marginal seas. With the climate warming and associated reductions

in sea-ice thickness and concentration (IPCC, 2021), Arctic navigation is hereby expected to increase in the future (Cao et al., 2022). All this makes it important to understand the impact of cyclones on sea ice. Thereby, the focus of our study is on the Atlantic sector of the Arctic Ocean in winter. This is motivated by (i) the dominance of the North Atlantic storm track, in particular in winter, and (ii) the strong SIC variability and sea-ice decline over the last winters in the Atlantic sector.

Cyclone impacts on Arctic sea ice in winter are rarely studied in a statistical manner. Recently, Schreiber and Serreze (2020) analyzed the temporal change in local SIC 4 days after cyclone events (compared to a non-cyclone reference) and found an overall increase in SIC. Their results are to some extent in contradiction with previous findings from case studies (Graham et al., 2019; Boisvert et al., 2016), which reported about cyclones' destructive effects on the sea-ice cover in winter. Another recent study emphasized that the SIC change depends on whether considering the warm sector to the east of the cyclone or the cold sector to the west (Clancy et al., 2022). Additionally, these few existing statistical studies are limited to the day of the cyclone event itself or to a fixed time frame of a few days following the cyclone. However, this approach bears the risk that the results are influenced by the choice of the specific time frame. Accordingly, Schreiber and Serreze (2020) pointed out that analyzing short-term cyclone impacts on sea ice on varying time scales (of i.e. different number of days before/after each cyclone) is a possible path to more robust results.

The first objective of our study is to quantify the cyclone impacts on SIC in the Arctic in winter, considering the following new aspects: (i) temporal variability on time scales up to a week before/after the occurrence of each cyclone, (ii) detailed regional differences between the Greenland, Barents and Kara Seas, and (iii) the case conditions, i.e. dependency on cyclone intensity and state of the local ice cover. The second objective is to explore if the impacts have changed over the past four decades and if a signature of the 'New Arctic' conditions has emerged.

3.3 Data and methods

3.3.1 Database and cyclone identification

The analysis is based on the ERA5 reanalysis (Hersbach et al., 2020), with a $0.25°$ horizontal resolution, and focused on winter (December to February) of the last two decades from 2000 to 2020. We have chosen this comparatively short investigation period to focus our analysis on cyclone impacts on SIC under the 'New Arctic' conditions. Those are

characterized by a strong sea-ice decline and increased cyclone intensity over the last 20 years (Valkonen et al., 2021). However, we also compare our findings to results from 1979 to 1999, the first two decades of the ERA5 coverage, representing the 'Old Arctic'.

The 6-hourly ERA5 data of mean sea level pressure (MSLP) are used as input for a cyclone detection and tracking algorithm (Akperov et al., 2020). The algorithm determines cyclones by identifying local minima in MSLP, that are surrounded by closed isobars. In addition to the cyclone position and pressure, the tracking algorithm provides the geographical coordinates of the outermost closed isobar for each 6-hourly time step in the lifetime of a cyclone. We define all grid-cells that are enclosed by this outermost isobar as being located within the cyclone area and thus create a binary cyclone occurrence data set matching the spatial resolution of the ERA5 horizontal grid. We use the cyclone depth as a measure of cyclone intensity. Hereby, the cyclone depth is determined as the difference between the pressure in the cyclone geometric center and the outermost closed isobar. Following (Akperov et al., 2020), we define intense cyclones as those with a cyclone depth of more than 20 hPa, a threshold roughly corresponding to the 90th percentile of cyclone depth distribution. The results are insensitive to the choice of this threshold.

3.3.2 Quantification of cyclone impacts on SIC

We use SIC data from ERA5, which is based on satellite data (HadISST2 and OSI SAF; Hersbach et al., 2020). Our basic concept to quantify cyclone impacts on sea ice follows Schreiber and Serreze (2020) and is based on statistics of SIC on grid-cell level for two groups of samples: days with cyclone presence at a grid-cell for at least one out of four 6-hourly time steps, and days without any cyclone presence at the grid-cell. To capture all short-term impacts on sea ice that are associated with a cyclone travelling across a certain location, we do not limit our analysis to the day of the cyclone event itself, but evaluate the temporal evolution of SIC prior to, during and following each cyclone passage. For this purpose, each cyclone sample consists of a SIC time series of several days, starting from three days prior to the day of the first arrival of the cyclone at a grid-cell and extending to seven days after the cyclone passage. Corresponding SIC time series for the non-cyclone samples are calculated. Averaging all non-cyclone samples at a grid-cell results in a non-cyclone reference that we subtract from the cyclone samples at the same grid-cell. Hereby, we calculate the non-cyclone reference separately for December, January and February, and choose the appropriate reference for each cyclone sample, since the temporal evolution of SIC due to the seasonal cycle can change significantly between the individual months. Eventually, we obtain a multi-day time series at each grid-cell that represents the difference in temporal evolution of SIC between cyclone and non-cyclone samples.

To evaluate both the temporal and spatial variability of cyclone impacts on SIC, we analyze (i) time series of spatial averages over the Greenland Sea ($70° - 82°$N, $30°$W$- 00°$E), Barents Sea ($70° - 82°$N, $20° - 60°$E) and Kara Sea ($70° - 82°$N, $60° - 100°$E; Figure 3.1d) as well as (ii) composites on grid-cell level for different time frames. Statistical significance (reported at 95% level) is calculated using the Students t-test.

To initially discuss thermodynamic and dynamic aspects of SIC changes, we calculate the surface energy budget (SEB, positive values indicate energy gain of surface) as the sum of net radiation and turbulent heat fluxes and apply a metric called cross-ice-edge wind, similar to the one recently introduced by Finocchio et al. (2020). Hereby we calculate the angle between the local ice edge (defined as grid-cells with SIC between 15% and 40%) and a zonally oriented line, and apply a coordinate transformation to the zonal and meridional wind speed. The SEB and wind analyses are again based on the 6-hourly ERA5 data.

3.4 Cyclone impacts on SIC

3.4.1 Effects of different time scales and regions

Our analysis reveals that the impact of cyclones on SIC strongly depends on the analyzed time scale and selected sub-region of the Arctic Ocean (Figure 3.1a). Generally, at the day of the first arrival of a cyclone at a location (day 0), SIC is lower than in the non-cyclone reference for all regions due to the dominant eastern flank effects (warm sector, southern wind pushes the ice edge northwards). This decrease of SIC in the cyclone samples starts already up to two days prior to the cyclone arrival, which fits to findings of Woods and Caballero (2016). Starting with day 3 after the cyclone event, an increase in SIC is found for the Barents and the Kara Seas, with the increase being more pronounced in the Barents Sea. This post-cyclone response agrees with the increase in SIC after four days as discussed by Schreiber and Serreze (2020), which they explain primarily due to thermodynamic effects (stronger ice growth during cyclone conditions).

In contrast, no such increase in SIC appears in the Greenland Sea, where the cyclone related decrease in SIC lasts consistently for a week. This results in an interesting pattern with respect to the overall impact of cyclones on SIC one week after the cyclone passage. On this time scale, the strongest changes in SIC occur in the Greenland and Barents Seas, but are of opposing sign. The magnitude of the overall SIC change at days 5–7 is about 2.5% for both marginal seas, increasing in the Barents Sea and decreasing in the Greenland Sea. This also means that the changes in SIC from day 0 to days 5–7 are small in the Greenland Sea, while they are large (5%) averaged over the Barents Sea. These results suggest that cyclones make
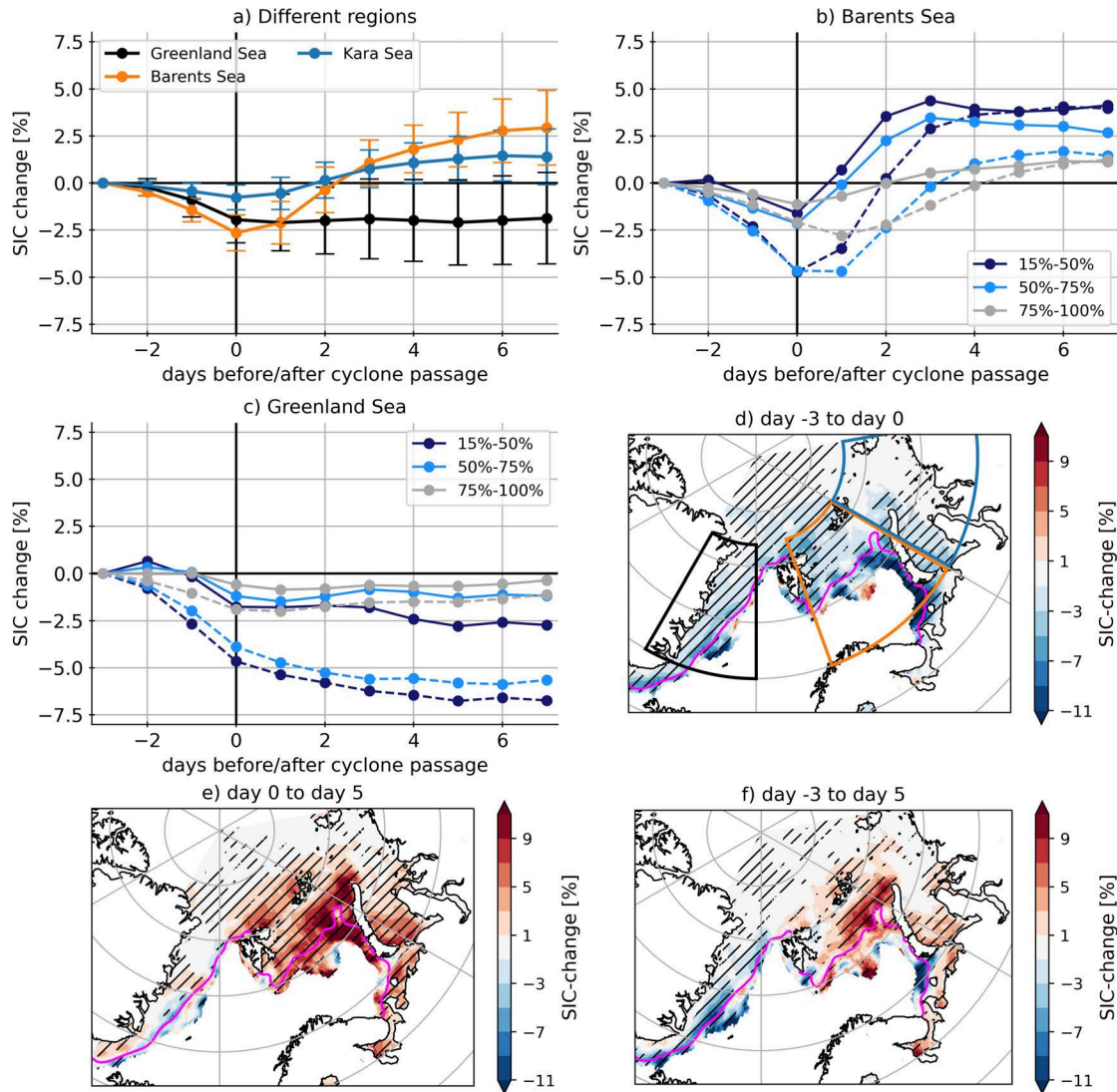
Figure 3.1: Difference in SIC change [%] over a few days between the cyclone samples and the non-cyclone reference, averaged for different sub-domains of the Arctic Ocean (a) and for different classes of SIC and cyclone depth (dashed/solid lines represent intense/non-intense cyclones) in the Barents Sea (b) and Greenland Sea (c). Error bars in (a) indicate standard deviation of cyclone impacts for individual years in 2000-2020. (d–f): SIC change at grid-cell level averaged over three different time periods. Shading indicates significance at 95% level and pink line shows the position of the ice edge. The sub-domains used in (a–c) are displayed in (d).

an impact on SIC via different mechanisms in both regions (section 3.4.4). SIC changes are generally less pronounced in the Kara Sea, indicating that cyclones are not an important source of SIC variability in this part of the Arctic Ocean. This is understandable because winter SIC is generally higher in the Kara Sea than in the Barents and Greenland Seas (e.g. Dörr et al., 2021), making the ice cover less susceptible to the impact of cyclones, in addition to the constraint by the Novaya Zemlya island and the coast. Figure 3.1a further

shows that generally the SIC reduction prior and during the cyclone covers only 2 days, while the change in SIC after the cyclone passage persists longer. This indicates that the processes acting to restore the SIC changes are slower than those driving the SIC reduction during the arrival of the cyclone, and was previously discussed for the impact of moisture intrusions in the Barents Sea in winter (Woods and Caballero, 2016).

3.4.2 Effects of SIC conditions and cyclone depth

The impact of an individual cyclone can vary from event to event, depending on the local sea-ice conditions at the time of the passage. Therefore, we investigated the sensitivity of the cyclone impact on SIC to the local SIC at the grid-cell that was passed over (Figure 3.1b–c, solid lines). For this purpose, we created three subsets of grid-cells within the cyclone area for each cyclone case containing grid-cells with SIC from $15\,\% - 50\,\%$ (low SIC), $50\,\% - 75\,\%$ (medium SIC) and $75\,\% - 100\,\%$ (high SIC).

Our analysis indicates that the strongest overall cyclone impacts on SIC (after 1 week) occur close to the ice edge at grid-cells with comparatively low SIC in both the Greenland and Barents Seas. This supports the hypothesis raised earlier (for example by Schreiber and Serreze, 2020) that regions with high SIC are more resistant to cyclone related changes in winter. Partly, this might also be related to the fact that cyclones likely weaken as they move into the denser pack ice and get cut off from their open ocean energy source. To further follow-up on the importance of cyclone intensity, we analyze cyclone impacts separately for intense and non-intense cyclones over all three types of SIC conditions.

Generally, the SIC decrease during the cyclone (day 0) is amplified for intense cyclones compared to non-intense cyclones (Figure 3.1b–c, dashed vs. solid lines). Furthermore, this amplification is considerably stronger for low and medium SIC conditions than for high SIC conditions, indicating that especially the combination of low to medium SIC and intense cyclones leads to the highest SIC changes during a cyclone passage. For the Greenland Sea, this is also found 7 days after the cyclone passage. In contrast, no difference with respect to cyclone depth is found at day 7 in the Barents Sea, at least for low and high SIC conditions. Surprisingly however, for medium SIC conditions, the SIC increase is weaker for intense cyclones. The reason for this could be that such conditions, including the upper ocean stratification, provide enough air-to-sea momentum to drive oceanic upwelling and associated upward heat fluxes (Manucharyan and Thompson, 2017).

To our knowledge, the effects of different cyclone strength on SIC in winter have not been studied before, but it was recently hypothesized that the effects of intense cyclones are more rapid (Schreiber and Serreze, 2020). Our results partly verify this. Intense cyclones show

a stronger rate of decrease in SIC prior to and during the cyclone passage, compared to non-intense cyclone effects, but after the cyclone, changes are similar.

3.4.3   Spatial variability of SIC response to cyclones

To investigate the spatial variability of cyclone impacts on SIC in more detail, Figure 3.1d–f shows the analysis for three time periods, which are chosen based on results of Figure 3.1a. These capture the SIC decrease taking place prior to and during the cyclone, the SIC increase after the cyclone passage as well as the overall effect on the local sea-ice cover.

For our entire study domain it becomes clear that the cyclone-related decrease and increase in SIC can be separated by the chosen timescales. In other words, SIC generally decreases prior to and during the arrival of the cyclone (day -3 to day 0; Figure 3.1d) and increases after the cyclone passage (day 0 to day 5; Figure 3.1e) in all grid-cells. Both the obtained spatial pattern and the magnitude of the post-cyclone increase in SIC for day 0 to day 5 supports the finding of the 4-day changes of Schreiber and Serreze (2020). Additionally, the spatial patterns confirm that the results for the sub-regions (Figure 3.1a–c) are robust and not a consequence of inappropriate spatial averaging.

For both the pre-cyclone decrease and post-cyclone increase of SIC, the strongest changes are of the order of approximately $10\,\%$ and are found in the Barents Sea, west of Novaja Zemlya. With respect to the overall impact of cyclones on SIC (day -3 to day 5), a significant decrease in SIC occurs in the Greenland Sea and in the southeastern Barents Sea, while a significant increase in SIC appears in the northern Barents Sea (Figure 3.1f).

3.4.4   Relation to near-surface wind and surface energy budget

To investigate the physical processes responsible for the detected cyclone impact on SIC, we compare the surface energy budget (SEB) and wind conditions for the cyclone samples to the non-cyclone reference (Figure 3.2). For the wind conditions, we calculate the cross-ice-edge-windspeed (section 3.3.2) to evaluate how the position of the ice edge might change during the cyclone passage, following Finocchio et al. (2020).

Generally, the spatial patterns of SEB and wind speed agree with the spatial changes in SIC (Figure 3.1d–f). Prior to and during the cyclone arrival (Figure 3.2a–b) an increase in SEB (i.e. less net energy loss from the surface) in combination with increased on-ice wind speed is found close to the ice edge in the Greenland Sea and southeastern Barents Sea, as well as (south)west of Svalbard. This can contribute to a decreased SIC (Figure 3.1d), because (i) the ice edge gets pushed towards the coast, resulting in more ice-free grid-cells,
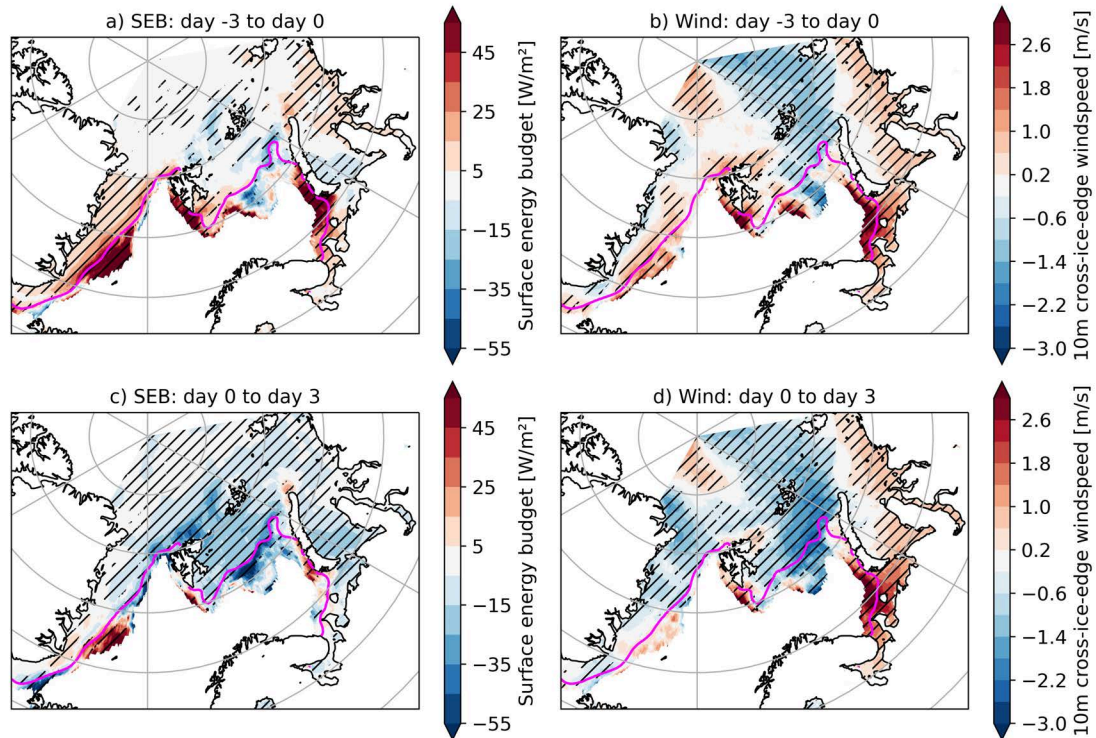
Figure 3.2: Difference in SEB (left) and cross-ice-edge wind speed (right) between the cyclone samples and the non-cyclone reference, averaged for 3 days before the cyclone (a-b) and 3 days after the cyclone (c-d). Shading indicates significance at $95\,\%$ level. Pink line indicates the position of the ice edge.

and (ii) although leads formed by the ice drift divergence rapidly refreeze in winter, the SEB change related to the advection of warm, moist air on the front side of the cyclone slows down the growth of this new thin ice, making it more liable to deformation when the ice drift converges.

After the cyclone passage (Figure 3.2c–d), increased off-ice wind speed in combination with cold, dry air on the backside of the cyclone and a more negative SEB contribute to an increased SIC in the northern Barents Sea (Figure 3.1e). In the southern Barents and Greenland Seas, however, no such signal is detected. The combination of these dynamic and thermodynamic mechanisms, previously discussed for sea-ice growth and variability in winter (Park et al., 2015; Boisvert et al., 2016; Hegyi and Taylor, 2017; Graham et al., 2019; Schreiber and Serreze, 2020; Cai et al., 2020), results in the clear regional difference with respect to the overall time scale (Figure 3.1f; Supplementary Figure S3.1).

The changes in SEB and wind speed fit to the front (warm sector) and back side (cold sector) effects of cyclones travelling along the main winter cyclone track from the North Atlantic into the Barents Sea towards the Kara Sea (Supplementary Figure S3.2). For those,

increased on-ice airflow is expected for the Greenland Sea, because the grid-cells are affected by (south)westward winds, before the cyclone leaves the Greenland Sea to enter the Barents Sea. The latter region is, however, affected by both the (northward) on-ice winds located in front (east) of the cyclone and the (southward) off-ice winds located behind (west of) the cyclone.

Statistical differences in regional cyclone properties – another possible explanation for our findings – cannot explain the regionally different sea-ice impact in the Greenland and the Barents Seas. The number of cyclone passages and the mean cyclone intensity are similar for both regions (Supplementary Figure S3.2). However, variations in cyclone properties likely contribute to the interannual variability of cyclone impacts on sea ice (error bars in Figure 3.1a). In this regard, also variations in large-scale atmospheric circulation and sea-ice cover might play an important role.

3.5   Signature of 'New Arctic' conditions

The 'New Arctic' conditions, here represented by the period 2000-2020, are characterized by a reduced and thinner sea-ice cover. In winter, the Barents Sea is the region with the largest ice retreat; it contributes to about one quarter of the observed Arctic sea-ice loss in winter (Docquier et al., 2020). The northward shifted ice edge compared to the 'Old Arctic' (here represented by the period 1979–1999) is shown in Figure 3.3a–b.

Recently, the question has emerged if cyclone effects on SIC in winter have changed under these changing ice state conditions (Schreiber and Serreze, 2020; Valkonen et al., 2021). Indeed, we find significant differences in the overall cyclone impact (day -3 to day 5) between both periods (Figure 3.3a). The cyclone related increase in SIC in the northeastern Barents Sea is significantly stronger (up to 5 %) for the recent two decades than in the past. Also, the cyclone related decrease in SIC in the southeastern Barents Sea is amplified. These intensified effects in the Barents Sea are associated with a decrease in mean SIC and an associated shift of the mean position of the ice edge (Figure 3.3b).This indicates that local SIC conditions are a key factor for the changed impact of cyclones on sea ice and is in accordance with our previous findings (section 3.4.2; Figure 3.1b–c). In addition, it can be assumed that also the decreasing ice thickness promotes increased cyclone impacts because a thinner ice cover is more susceptible to atmospheric and oceanic forcings (Rampal et al., 2009; Zhang et al., 2012; Rheinlænder et al., 2022).

Potentially, and as we have discussed in section 3.4.2, changes in cyclone characteristics might have contributed to the intensified effect on SIC. However, estimates of trends in
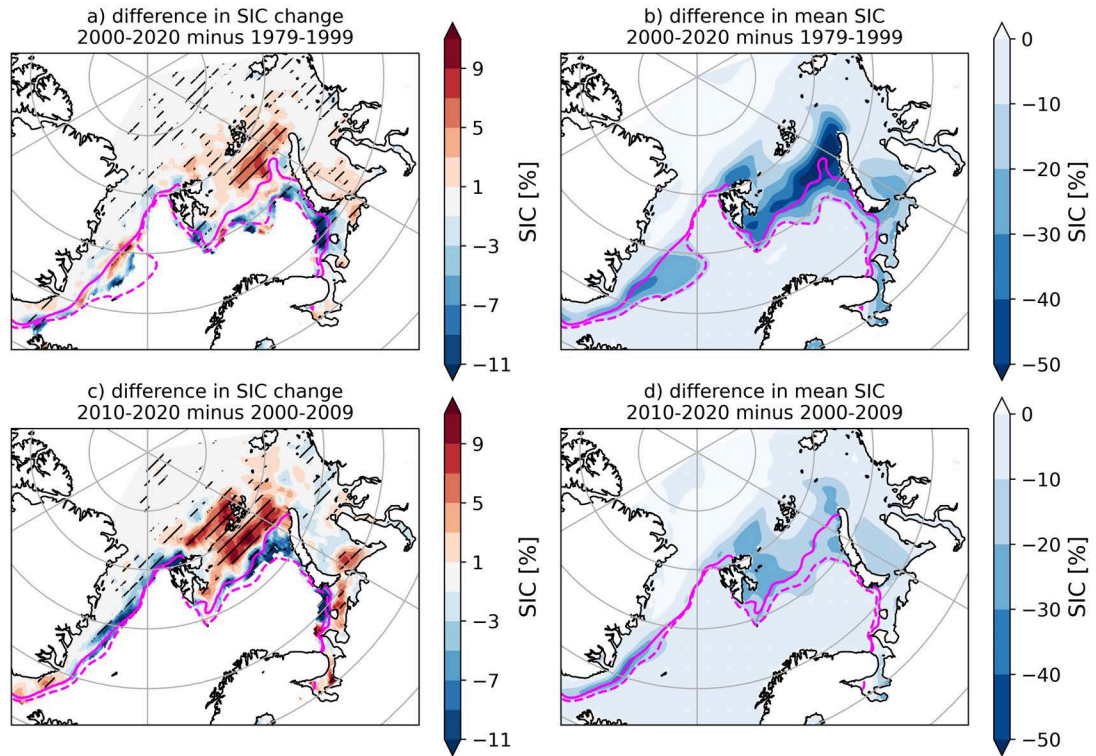
Figure 3.3: Difference in cyclone impact on sea-ice concentration (SIC) (left), defined as 8-day SIC change (day -3 to day 5) between the cyclone samples and the non-cyclone reference, and difference in mean SIC (right) between 'Old Arctic' and 'New Arctic' conditions (a, b) as well as between the two decades within the 'New Arctic' period (2000-2009 vs. 2010-2020, c, d). Shading indicates significance at 95 % level, whereas changes in mean SIC (b, d) are significant at all grid points and therefore not shaded. Solid (dashed) pink line shows the position of the ice edge for the newer (older) time period.

(deep) cyclone occurrence and intensity over the past four decades are uncertain. While some studies discuss an increase of cyclone depth and the occurrence of deep cyclones in winter (Zahn et al., 2018), others do not find significant changes (Vessey et al., 2020) or report on positive and negative trends depending on the period (Valkonen et al., 2021). Based on our calculations using the ERA5 reanalysis, we find a slight but non-significant decrease in the occurrence of intense cyclones in the study domain (not shown). This indicates that changes in sea-ice conditions are a more likely explanation for the amplified cyclone impacts than changes in cyclone characteristics.

Still, the 'New Arctic' undergoes a rapid climate change, including an accelerated warming in the most recent decade (IPCC, 2021). Hence, we compare the cyclone impact on SIC between 2010–2020 with that during 2000–2009 (Figure 3.3c–d; Supplementary Figure S3.3). Our results show a further significant intensification of the cyclone-related impact on SIC in the Barents Sea in the most recent decade. This change is even stronger than the

difference between the 'Old Arctic' and 'New Arctic' (1979–1999 vs. 2000–2020; Figure 3.3a). At the same time, the recent decrease in mean SIC is less strong than for 1979–1999 compared to 2000–2020, which could be expected because of the shorter period. Nevertheless, the fact that a stronger intensification of the cyclone impact on SIC is found for a smaller difference in mean SIC might indicate that the SIC in the Barents Sea has reached a critically low value during the last decade, making the ice cover significantly more susceptible to the passage of cyclones than in previous times. This hypothesis is supported by the strong intensification of cyclone impacts on the sea-ice cover which we found when grid-cells' SIC transfers from the $75 - 100\,\%$ category to the lower categories (Figure 3.1b).

3.6   Conclusions

We provide new insights into the cyclone impacts on SIC in the Atlantic sector of the Arctic Ocean in winter. Overall, we show that this impact strongly depends on the considered time scale, region, cyclone intensity and local sea-ice conditions, and we provide a quantitative assessment of those effects.

In conclusion, a cyclone related SIC increase in the Barents Sea and a SIC decrease in the Greenland Sea were found, both reaching values of up to $10\,\%$ one week after the cyclone for individual grid-cells. The regionally averaged impact varies between $1 - 6\,\%$ for both regions, depending on cyclone intensity and local sea-ice conditions. This seems to be a rather small effect on first glance, however, given the fact that the sea ice in, e.g., the northern Barents Sea is affected by approximately 15–20 cyclones each winter (Supplementary Figure S3.2), these SIC impacts easily sum up and form a significant contribution to the overall SIC variability in this region. This effect obviously depends to some extent on the number, timing and properties of cyclones when they approach and move over a certain location. Further, in winter even a change in SIC by a few percent generates a large impact on SEB, and subsequently on near-surface air temperatures (Lüpkes et al., 2008). In the course of our analysis we further point out that the cyclone impacts have amplified recently, associated with the declining SIC in the Arctic. However, the quantification and detailed understanding of the thermodynamic and dynamic processes that drive the cyclone-induced regional and temporal SIC changes is a remaining research task, which is further complicated by feedbacks from SIC to the atmosphere, including the wind speed (Jakobson et al., 2019). Regional coupled model experiments should be beneficial in this regard with the approach to first study individual winter events before starting a statistical analysis.

3.7 Supplementary material

1. Figure S3.1: Difference in surface energy budget and cross-ice-edge wind speed between cyclone samples and non-cyclone reference.

2. Figure S3.2: Climatology of cyclone count and cyclone properties in winter.

3. Figure S3.3: Difference in SIC change between cyclone samples and non-cyclone reference for different time periods.
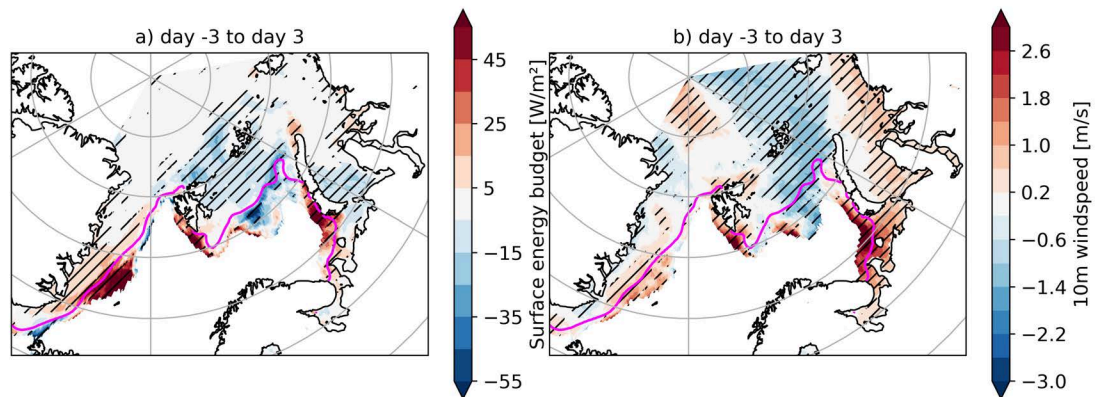

Figure S3.1: Difference in surface energy budget (SEB; left) and cross-ice-edge wind speed (right) between cyclone samples and non-cyclone reference, averaged from 3 days before to 3 days after cyclone. Shading indicates significance at 95 % level. Pink line indicates the position of the ice edge. All results are based on ERA5, December to February 2000 to 2020.
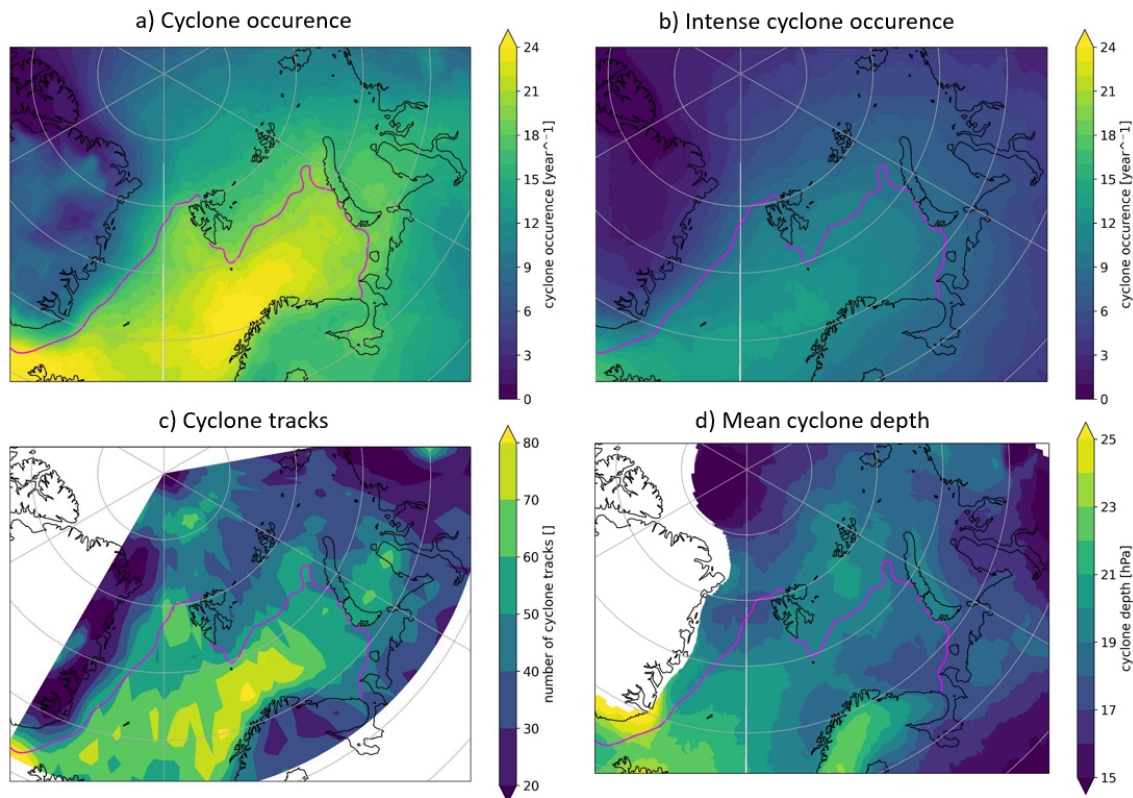
Figure S3.2: Number of all (a) and intense (b) cyclones per winter (December to February), whose area reaches a certain grid-cell. Intense cyclones are defined as cyclones that reach a cyclone depth of at least 20hPa. (c) indicates the number of cyclone tracks in each grid-cell on a 2-degree horizontal grid, whereas cyclone tracks are defined as the position of the geometric centers of the cyclones (in contrast to (a-b) that consider the whole cyclone area). (d) indicates the mean cyclone depth of all cyclones, whose area reaches a certain grid-cell. All results are based on ERA5 and Akperov et al. (2020) tracking algorithm, averaged for 2000 to 2020. Pink line shows the position of the ice edge.
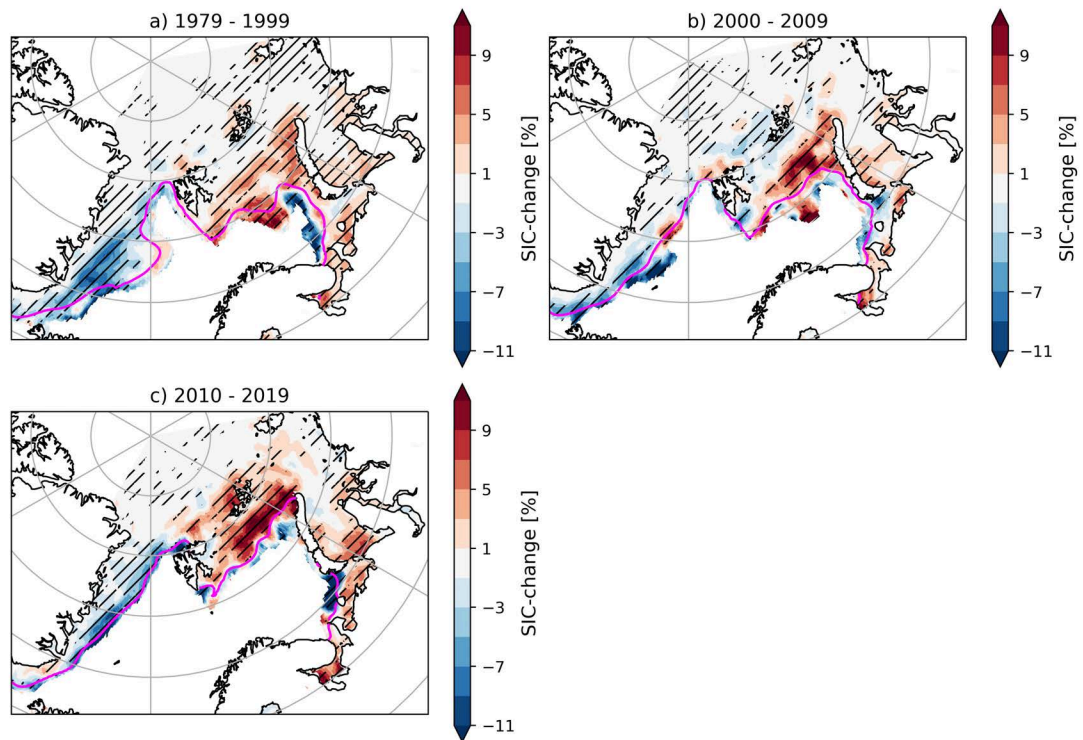
Figure S3.3: Difference in 8-day SIC change (day -3 to day 5) between cyclone samples and non-cyclone reference, averaged over different time periods. Shading indicates significance at 95 % level, pink line shows the position of the ice edge. All results are based on ERA5, December to February.

4 Impact of three intense winter cyclones on the sea ice cover in the Barents Sea: A case study with a coupled regional climate model

Summary of the publication:

Objectives	• Quantify dynamic and thermodynamic changes in sea-ice concentration (SIC) and thickness (SIT) in response to a series of three winter cyclones. • Determine whether preceding cyclone passages influence the response of the sea ice to following cyclones.
Contributions to RQs	• This study contributes to **RQ2** by separately quantifying dynamic and thermodynamic sea-ice changes for a number of particular cyclone cases.
Key points	• Dynamic processes dominate changes in SIC and SIT during the passage of the three presented winter cyclones. • Thermodynamics processes drive increases in SIC and SIT after the passage of the three presented winter cyclones. • The pattern of dynamic SIC changes followed by thermodynamic SIC changes seems to be typical of winter cyclones.
Own Share	• I processed the utilized data sets, carried out the scientific analysis and designed all figures contained in the manuscript. • I wrote the first draft of the manuscript and was in charge of leading the manuscript revision and managing the submission and peer-review process.

4.1 Abstract

We utilize a nudged simulation with the coupled regional atmosphere-ocean-sea-ice model
HIRHAM–NAOSIM over the Arctic to conduct an in-depth analysis of the impact of a
sequence of three intense cyclones on the sea-ice cover in the Barents and Kara Seas in
February 2020. To clarify the underlying mechanisms we decompose changes in sea-ice
concentration (SIC) and thickness (SIT) into their dynamic and thermodynamic contri-
butions and analyze them in concert with simulated changes in the wind forcing and the
surface energy budget. Our findings reveal that changes in SIT during and after the cyclone
passages are mostly driven by dynamic processes such as increased ice drift and deforma-
tion. With respect to SIC, the relative importance of dynamics and thermodynamics de-
pends on the considered time scale and on the general conditions of the cyclone passages. If
cyclones follow on each other in rapid succession, dynamic mechanisms dominate the SIC
response for time scales of more than two weeks and thermodynamic effects via advection
of warm-moist/cold-dry air masses on the cyclone's front/back side only play a secondary
role. However, if sufficiently long time elapses until the arrival of the next storm, ther-
modynamic SIC increase due to refreezing under the influence of cold and dry air at the
backside of the cyclone becomes the dominating mechanism during the days following the
cyclone passage.

4.2 Introduction

In winter, the North Atlantic storm track has a large influence on the climate conditions
in the Atlantic sector of the Arctic Ocean. Particularly the interannual variability of the
Barents-Kara Sea (BKS) sea ice in winter is primarily driven by atmospheric processes
(Liu et al., 2022). Mechanisms include changes in the atmospheric circulation patterns,
wind field, and longwave downward radiation (LWD), e.g. due to inflow of warm-moist
air (Park et al., 2015; Woods and Caballero, 2016; Zhang et al., 2023). Synoptic cyclones
play an important role here (Sorteberg and Kvingedal, 2006; Rinke et al., 2017; Graham
et al., 2019) and exert significant impacts on sea-ice concentration (SIC) (Kriegsmann and
Brümmer, 2014; Schreiber and Serreze, 2020; Valkonen et al., 2021; Clancy et al., 2022;
Aue et al., 2022) and sea-ice thickness (SIT) (Boisvert et al., 2016; Ricker et al., 2017a)
in winter. Generally, the impacts on sea ice are related to both dynamic and thermody-
namic atmospheric forcing. For the former, strong surface winds and rapid changes in
wind direction related to cyclone passages can trigger divergent/convergent sea-ice motion
with impact on SIC through opening/closing of leads and on SIT through ice compres-
sion and possible formation of pressure ridges as well as through enhanced ice growth in

case of increasing lead fraction (Itkin et al., 2017). Thermodynamically, the advection of warm-moist/cold-dry air at the cyclones front/back side favors positive/negative anomalies in LWD and sensible heat fluxes. The resulting reduced/increased energy loss at the surface finally leads to lower/higher sea-ice growth rates (SGR) in winter (Cai et al., 2020).

The understanding of these mechanisms is important for sea-ice forecasts (Serreze and Stroeve, 2015; Wayand et al., 2019), particularly during hazardous weather systems such as storms, typically associated with strong cyclones. Such conditions are challenging for Arctic navigation (Inoue, 2021), aviation (Gultepe et al., 2019), and other human activities. Furthermore, understanding of the mechanisms helps to improve weather and climate models with respect to the simulations of storm interactions with the underlying ocean, including sea ice. This is important for a better understanding of how cyclone impacts might evolve under diminishing and thinner sea-ice conditions in the future (Cai et al., 2020). Considering the accelerated winter sea-ice retreat in BKS (Liu et al., 2022), such research is of primary importance.

Over the last decades, a decrease in sea-ice extent and thickness has been observed over the Arctic Ocean (e.g., Kwok, 2018; Meier and Stroeve, 2022). Particularly a thinning of the sea-ice cover is relevant for its response to cyclones, because thinner ice is more sensitive to atmospheric forcing. Evidence for this is given by an observed increase in ice deformation and drift speed under thinner ice conditions (e.g., Rampal et al., 2009; Spreen et al., 2011). There is also indication that thinner sea ice is more vulnerable to break-up events under strong winds (Rheinlænder et al., 2022), which are often associated with cyclone passages. Additionally, cyclones can have stronger thermodynamic impacts on a thinner ice cover, because thinner ice grows faster than thicker ice (e.g., Haas, 2017; Petty et al., 2018).

However, the relative contributions of the dynamic and thermodynamic processes to the cyclone's impacts on winter sea ice are still not well known. The few existing studies arrive at mixed results. Based on an analysis of daily SGR under the impact of winter cyclones in the Nordic Seas in CMIP5 models, Cai et al. (2020) found that the absolute value of the thermodynamic SGR change exceeds the dynamic contribution in response to strong cyclonic circulation. In observation-based studies, Schreiber and Serreze (2020) came to the same conclusion for SIC response to cyclones, while Clancy et al. (2022) argued that both processes are important and comparable in magnitude. Further, Clancy et al. (2022) stressed that dynamic processes are the primary reason for the front/back side difference in the sea-ice response to cyclones and particularly dominate the response of SIT to cyclones. The dominance of dynamics with respect to SIT changes is supported by a recent case study of the record Arctic cyclone in January 2022 by Blanchard-Wrigglesworth et al. (2022). Apart from that, Cai et al. (2020) found that the dynamic and thermodynamic

responses of SGR to strong cyclones have a similar spatial pattern across different models, but there is no clear agreement on the sign. One model simulates anomalies of dynamic and thermodynamic SGRs with same sign, while the dynamic and thermodynamic SGRs offset each other in two other models. For Arctic moisture intrusion events, Park et al. (2015) showed that the LWD-related thermodynamic processes are dominant (and last as long as 1-2 weeks) for sea-ice reductions after the first couple of days, which are characterised mostly by sea-ice changes due to dynamics.

More generally, Koo et al. (2021) discussed that dynamic contributions may account for about 35 % of the total increase of the mean SIT during the ice-growing season in the central Arctic Ocean. Moreover, von Albedyll et al. (2022) emphasized a possible large dynamic thickening via rafting and ridging under conditions of mobile, unconsolidated sea-ice pack. However, the inclusion of SIT in the analysis of cyclone-related sea-ice changes is challenging. It is reasonable to assume that a smaller SIT promotes stronger cyclone impacts because a thinner sea ice is more susceptible to atmospheric and oceanic forcings (Zhang et al., 2012; Rheinlænder et al., 2022). Limited daily SIT data hamper a systematic analysis and thus the few results rely on case studies and/or modeling (Boisvert et al., 2016; Cai et al., 2020). In conclusion, the relative importance of dynamic and thermodynamic mechanisms for cyclone impacts on the sea-ice cover in winter remains a topic of research interest.

The objective of this study is to quantify the dynamic and thermodynamic contributions to changes in SIC and SIT in response to a sequence of cyclones in the BKS in winter and to explore the related mechanisms in detail, utilizing a coupled regional climate model. The presented sequence of cyclones consists of three intense storms that passed through the BKS in mid-February 2020. Using these cyclone cases as an example, we evaluate the spatial patterns of cyclone-induced sea-ice changes in winter and discuss their dependencies on the state of the sea-ice cover. An additional objective is to determine whether the sea ice has a memory of preceding cyclone passages that might influence its response to cyclones that follow.

4.3   Data and methods

4.3.1   HIRHAM–NAOSIM simulation

In our analysis of cyclone impacts on the Arctic sea-ice cover we rely on a coupled model simulation, which enables us to decompose the sea-ice changes into dynamic and thermodynamic contributions. The simulation was performed applying version 2.2 of the coupled

regional climate model HIRHAM–NAOSIM. This version represents a further development of the base version 2.0, which is described and evaluated by Dorn et al. (2019). Version 2.2 includes new parameterizations and changed parameter settings. The differences between the two versions are listed in the Supplementary Material.

HIRHAM–NAOSIM is applied over a circum-Arctic domain using rotated latitude-longitude grids with horizontal resolution of $1/4°$ ($\sim 27\,\text{km}$) in the atmosphere component HIRHAM and $1/12°$ ($\sim 9\,\text{km}$) in the ocean–sea ice component NAOSIM. More detailed information on the model components and their coupling are given by Dorn et al. (2019).

The simulation was initialized on 1st of January 2019 and run through 31th of December 2020, driven by ERA5 reanalysis data (Hersbach et al., 2020) at HIRHAM's lateral boundaries as well as HIRHAM's lower and NAOSIM's upper boundaries, which lie outside the coupling domain (defined as the overlap area of the components' model domains). For NAOSIM's open lateral boundaries, ORAS5 reanalysis data (Zuo et al., 2019) were used. HIRHAM was initialized with the corresponding ERA5 fields, while NAOSIM was started from rest with temperature, salinity, ice thickness, and ice concentration fields from ORAS5. HIRHAM's prognostic fields were nudged to the corresponding ERA5 fields with a uniform nudging time scale of $16.67\,\text{h}$ (which corresponds to a nudging of $1\,\%$ per time step).

4.3.2 Supplementary evaluation data

We complement the HIRHAM–NAOSIM simulation with in-situ observations obtained during the Multidisciplinary drifting Observatory for the Study of Arctic Climate (MOSAiC) expedition (Shupe et al., 2020) and ERA5 reanalysis data to demonstrate that the model is able to (i) capture the synoptic situation (Supplementary Figures S4.1, S4.2) and (ii) produce a realistic spatial pattern of SIC changes (Supplementary Figure S4.3) during the cyclone passages. It should be noted that the ERA5 SIC field is highly smoothed and has limitations to represent the observed strong gradient in SIC across the MIZ (Renfrew et al., 2021). However, for this cyclone case, the spatial patterns of SIC changes based on ERA5 are in strong agreement with high-resolution satellite derived SIC data based on AMSR (not shown). To further evaluate the simulated sea-ice thickness (SIT) with remote sensing observations (Supplementary Figure S4.3), we utilize merged CryoSat-2 and SMOS satellite data (Ricker et al., 2017b).

During February 2020, RV Polarstern was located close to the North Pole in the central Arctic (Figure 4.1). The supplementary model evaluation is based on data from the 10-meter meteorological flux tower installed at the meteorological observatory (Met-City)

(Cox et al., 2021a) located in approximately 500 m distance to the RV Polarstern, three autonomous Atmospheric Surface Flux Stations (ASFS) (Cox et al., 2021b,c,d) situated in the Distributed Network in a distance of approximately 25 km to RV Polarstern (Shupe et al., 2022), and a microwave radiometer HATPRO (Humidity and Temperature Profiler) (Walbröl et al., 2022). We use data averaged to 3-hourly resolution of 2-m air temperature, vertically integrated water vapour (IWV; 0-10 km height), mean sea level pressure (SLP) and 10-m wind speed. For the comparisons with the simulation, we use the nearest model grid-cell. IWV in the model simulation is the integrated specific humidity over all vertical levels from the surface up to the top (10 hPa, approx. 35 km height). To further evaluate the simulated spatial patterns of meteorological variables, we use 3-hourly ERA5 gridded data of 2-m air temperature, IWV, and SLP. We also use daily SIC data from ERA5, which are based on satellite data (HadISST2 and OSI SAF; see Hersbach et al., 2020).

4.3.3 Dynamic and thermodynamic contributions to sea-ice changes

The main objective of this study is to separately quantify dynamic and thermodynamic sea-ice changes during and after the cyclone passages to gain insights into the underlying mechanisms. We approach this by temporally integrating HIRHAM–NAOSIM's dynamic and thermodynamic SIT and SIC tendencies for specific time periods in order to decompose the overall sea-ice changes in its respective components.

The overall sea-ice changes are given by the model's continuity equations for SIT (h) and SIC (A) as

$$\frac{\partial h}{\partial t} = -\nabla \cdot (h\vec{v}) + S_h^{\text{ice}} + S_h^{\text{ow}} \, , \tag{4.1}$$

$$\frac{\partial A}{\partial t} = -\nabla \cdot (A\vec{v}) + S_A^{\text{ice}} + S_A^{\text{ow}} + D_A \, , \tag{4.2}$$

where $\vec{v}$ is the ice velocity and S_h^{ice}, S_h^{ow}, S_A^{ice}, and S_A^{ow} are the thermodynamic growth rates, which are separately calculated for the ice-covered (superscript 'ice') and the open water part (superscript 'ow') of the grid cell. A detailed description of the thermodynamic growth rates is given by Dorn et al. (2009). The term D_A represents the formation rate of open water due to shearing deformation (ridging) and is given as

$$D_A = 0.5 \left(\Delta - |\nabla \cdot \vec{v}| \right) \exp(-K(1-A)) \, , \tag{4.3}$$

where Δ represents the total deformation, determined by the strain rate tensor $\dot{\epsilon}_{ij}$ (see Hibler, 1979), and $K = 20$ is an empirical constant.

Consequently, the dynamic SIT and SIC tendencies are defined as

$$\left(\frac{\partial h}{\partial t}\right)_{\text{dyn}} = -\nabla \cdot (h\vec{v}) \; , \tag{4.4}$$

$$\left(\frac{\partial A}{\partial t}\right)_{\text{dyn}} = -\nabla \cdot (A\vec{v}) + D_A \; , \tag{4.5}$$

and the thermodynamic SIT and SIC tendencies are

$$\left(\frac{\partial h}{\partial t}\right)_{\text{thdyn}} = S_h^{\text{ice}} + S_h^{\text{ow}} \; , \tag{4.6}$$

$$\left(\frac{\partial A}{\partial t}\right)_{\text{thdyn}} = S_A^{\text{ice}} + S_A^{\text{ow}} \; . \tag{4.7}$$

Generally, we analyze these sea-ice tendencies in concert with simulated changes in sea-ice drift and surface energy budget (SEB). Since we focus on the impact of atmospheric variability on the sea ice-ocean system, we define the SEB as the sum of atmospheric net radiative, sensible, and latent heat fluxes at the surface, with positive values corresponding to a surface energy gain. To cover the importance of the ocean for (thermodynamic) sea-ice processes, we additionally provide information on upward oceanic heat fluxes when discussing thermodynamic sea-ice changes in section 4.4.3.

4.4 Results

4.4.1 Cyclone cases

From February 9 to 25, 2020, a sequence of three cyclones travelled through the BKS (Figure 4.1), shaped the local weather conditions, and led to shifts in the position of the sea-ice edge (15% SIC contour). The minimum SLP in the core of the cyclones was below 970 hPa (when crossing the sea-ice edge) for all events, which is an extremely low value compared to climatological SLP conditions in the BKS region. Consequently, all three events can be classified as intense, stronger than normal cyclones (following Rinke et al., 2017). This classification is supported by a comparison of the intensity of cyclones during the MOSAiC expedition (and particularly in February 2020) with climatological cyclone conditions along the MOSAiC drift track (Rinke et al., 2021).

The strongest cyclone event (in the following referred to as cyclone 2) occurred during February 16–20 (Figure 4.1) with a minimum pressure of less than 960 hPa. The cyclone travelled through the southern Barents Sea, crossed the ice edge near Novaya Zemlya, and
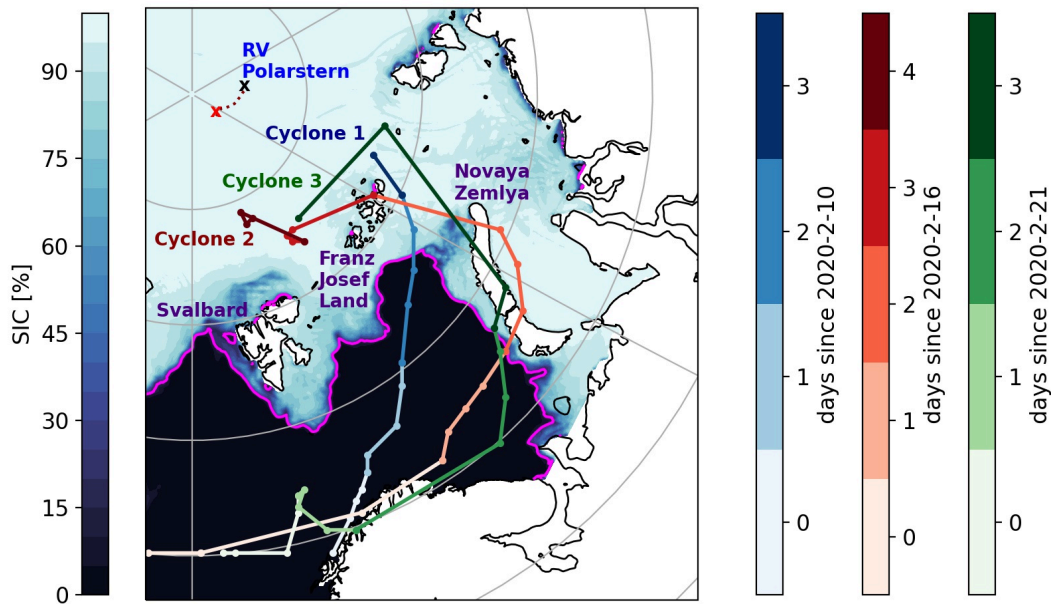
Figure 4.1: Track of cyclones 1, 2, and 3 (based on 6-hourly SLP minima in the study domain), indicated as blue, orange, and green lines, where the line color changes from bright to dark from the start to the end of the respective track. The position of the RV Polarstern at the start of the first (end of the third) cyclone event is marked as black (red) cross. Daily mean SIC and the 15 % SIC contour (pink line) are shown for the day before the start of the first of the three cyclone passages (February 9, 2020). SIC and cyclone tracks are based on the HIRHAM–NAOSIM simulation.

entered the central Arctic through the western Kara Sea. The associated advection of a comparatively warm and moist air mass on the eastern flank of the cyclone into the Arctic impacted the eastern Barents Sea, the Kara Sea, and eventually the central Arctic north of Franz Josef Land and Svalbard (Figure 4.2). On February 19, the 2-m air temperature in large parts of the central Arctic reached values slightly below the freezing point, which corresponds to an increase of approximately 20 K in only two days compared to February 17 (Figure 4.2A–C). Close to the North Pole, a rise in 2-m air temperature from -30 °C to -10 °C as well as high IWV of up to 6 kg/m² was observed when the cyclone hit RV Polarstern (Supplementary Figure S4.2). Both conditions were extremely anomalous and near-record breaking (Rinke et al., 2021).

Both before and after this particular cyclone event, the BKS region was affected by another cyclone with comparatively similar intensity and track (Figure 4.1, Supplementary Figures S4.5, S4.6). The first of the three cyclones occurred during February 10–13 (in the following referred to as cyclone 1), crossed the central Barents Sea between February 11–12, and entered the central Arctic close to Franz Josef Land. The last of the three consecutive cyclones (in the following referred to as cyclone 3) occurred during February 21–25, entered the Barents Sea on February 22, and followed almost the same path
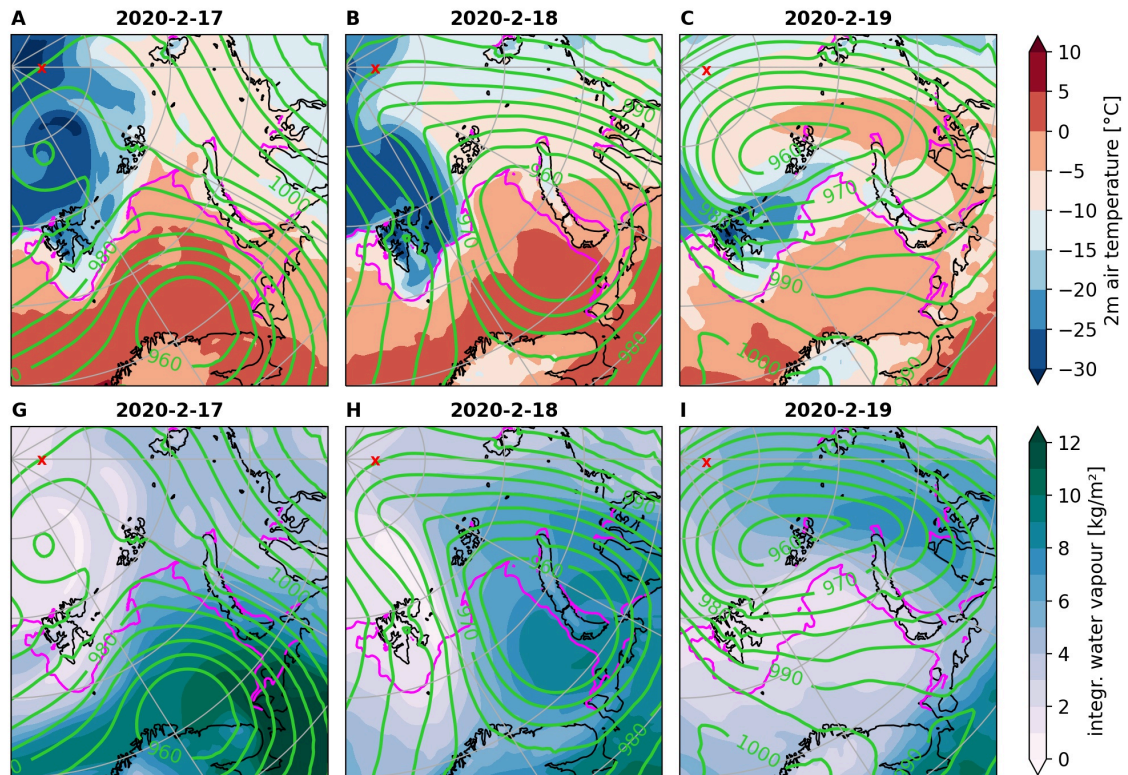
Figure 4.2: Daily means of 2-m air temperature (A–C) and integrated water vapour (IWV) (D–F) during cyclone 2 (17.2.2020 – 19.2.2020) based on the HIRHAM–NAOSIM simulation. Green contour lines represent daily mean sea level pressure (in steps of 5 hPa); pink lines indicate the position of the ice edge (15 % SIC). The position of the RV Polarstern at the corresponding days is marked as red cross.

as the second cyclone for most of its lifetime. However, in contrast to cyclone 2, it decayed quicker, i.e. one day earlier than cyclone 2, after reaching the central Arctic between Svalbard and Franz Josef Land.

The comparison of the nudged coupled model simulation with MOSAiC data demonstrates that the observed atmospheric variability in the central Arctic during this series of cyclones is captured well by the model (Supplementary Figure S4.2). With respect to larger spatial scales, the simulated patterns of 2-m air temperature and IWV over the BKS region agree with those of ERA5 (Supplementary Figure S4.1). This confirms the validity of the atmospheric forcing in the simulation.

4.4.2   Cyclone impacts on SEB

Analyzing the SEB for cyclone 2 (Figure 4.3A–C) reveals that starting with February 18, the advection of cold and dry air at the back side of the cyclone leads to a strong energy transfer from the ocean to the atmosphere in the Barents Sea. Over the open ocean, but
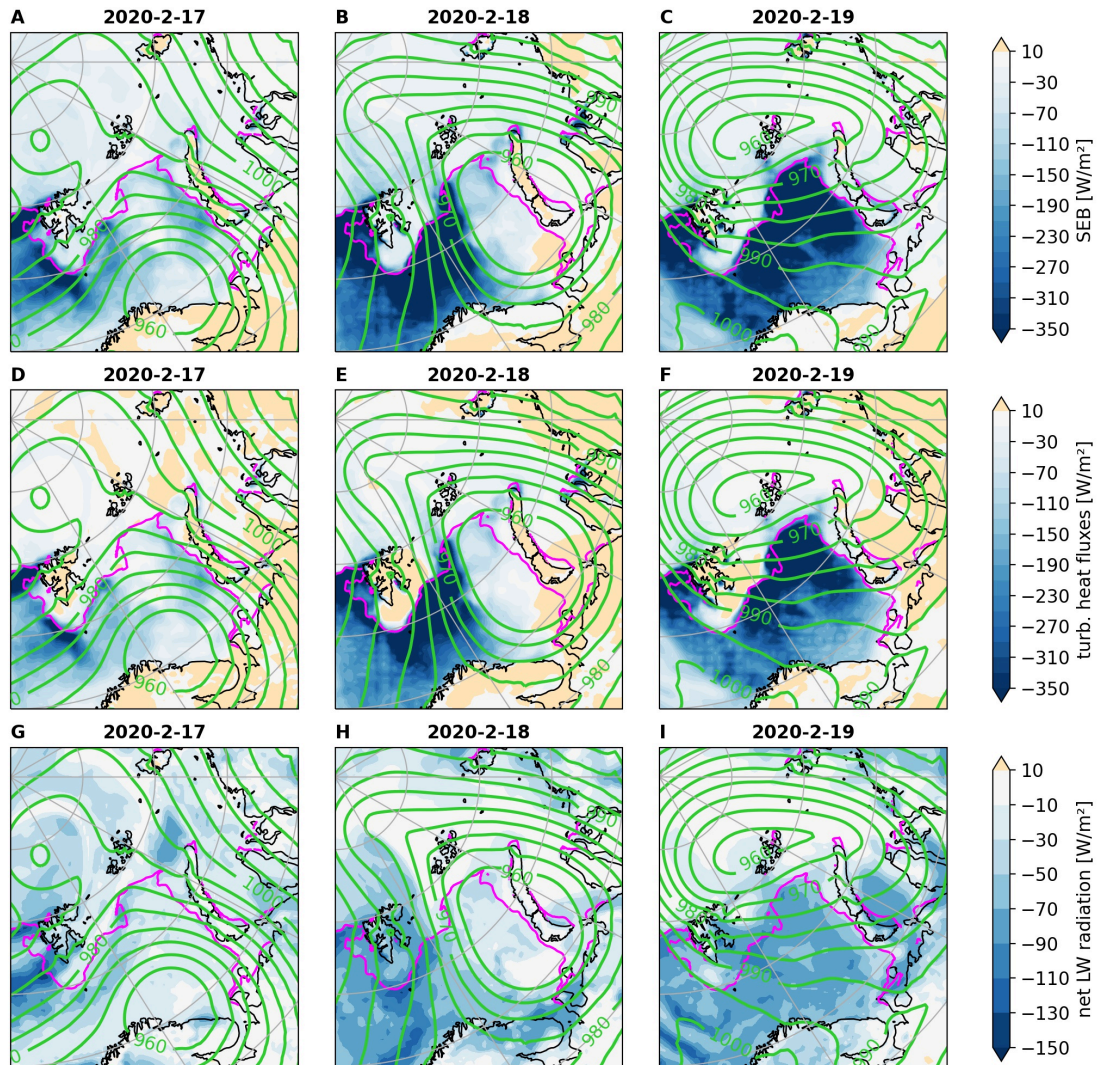
Figure 4.3: Daily means of atmospheric surface energy budget (SEB) (A–C), sum of atmospheric turbulent surface heat fluxes (D–F) and net longwave radiation (G–I) during cyclone 2 (17.2.20 – 19.2.20) based on the HIRHAM–NAOSIM simulation. Positive (negative) values indicate downward (upward) fluxes. Green contour lines represent daily mean sea level pressure (in steps of 5 hPa); pink lines indicate the position of the ice edge (15 % SIC).

also in parts of the marginal ice zone (MIZ), i.e. in the central Barents Sea and west of Svalbard, the SEB reaches values below -350 Wm^{-2}. On February 19, this advection of cold dry air further extends to the eastern Barents Sea. Comparing individual components of the SEB indicates that this intensification of the usually slightly negative wintertime SEB is almost exclusively driven by turbulent heat fluxes (Figure 4.3D–F). Changes in net longwave radiation associated with the cyclone passage (determined by an increase in longwave downward radiation) lead to a slightly less negative SEB in the Kara Sea and

central Arctic (Figure 4.3G–I), but this signal does not reach the same order of magnitude as the negative SEB change due to turbulent heat fluxes.

The SEB change during all three cyclone cases (Figure 4.3, Supplementary Figures S4.5, S4.6) is in contrast to reports on strong positive SEB changes (energy gain of the surface) in ice-covered grid-cells during an extreme cyclone in December 2015/January 2016 (Boisvert et al., 2016) and during the record Arctic cyclone in January 2022 (Blanchard-Wrigglesworth et al., 2022). For our presented mid-February 2020 case, only small patches of slightly positive SEB are found during a very few days, i.e. during cyclone 2 on February 18 southwest of Novaya Zemlya (Figure 4.3B) and during cyclone 1 on February 12 over the Barents Sea (Supplementary Figure S4.5). Apart from that, the SEB remains negative in ice-free grid-cells and is close to zero in ice-covered grid-cells. Since both the December 2015/January 2016 cyclone and the January 2022 cyclone entered the BKS close to Svalbard on a more northerly route than the Mid-February 2020 cyclones, it can be supposed that there is a strong variability in the surface impacts of individual cyclones depending on their track and presumably also on further cyclone properties.

4.4.3 Cyclone impacts on sea-ice concentration (SIC)

As a next step, we analyze changes in SIC from directly before the start of the first cyclone passage to the end of the third one (from February 9 to February 25). Figure 4.4A shows that the sequence of cyclones causes a strong decrease (increase) in SIC in the eastern (western) part of the study domain, particularly in the MIZ. Strongest changes exceeding values of 50% are found in the vicinity of Novaya Zemlya and Svalbard. The simulated spatial pattern of SIC changes shows strong similarities to satellite observations of SIC contained in the ERA5 reanalysis (Supplementary Figure S4.3), which confirms the suitability of the coupled model simulation for our study.

Dynamic and thermodynamic contributions

Figure 4.4B–D shows that dynamic mechanisms dominate the response of the sea-ice cover to the sequence of cyclones. The above-mentioned decrease in SIC east of Novaya Zemlya is caused by northeastward ice drift towards the central Kara Sea (Figure 4.4B), triggered by the cyclone passages. At the same time, the increase in SIC in the western part of the study domain is related to a strong intensification of an existing southwesterly drift of sea ice around Svalbard towards the Fram Strait. In the MIZ as well as in the consolidated ice pack, the thermodynamic SIC response (Figure 4.4C) is widely anti-correlated to the dynamic SIC changes and thus partly compensates for the dynamic decrease of SIC.
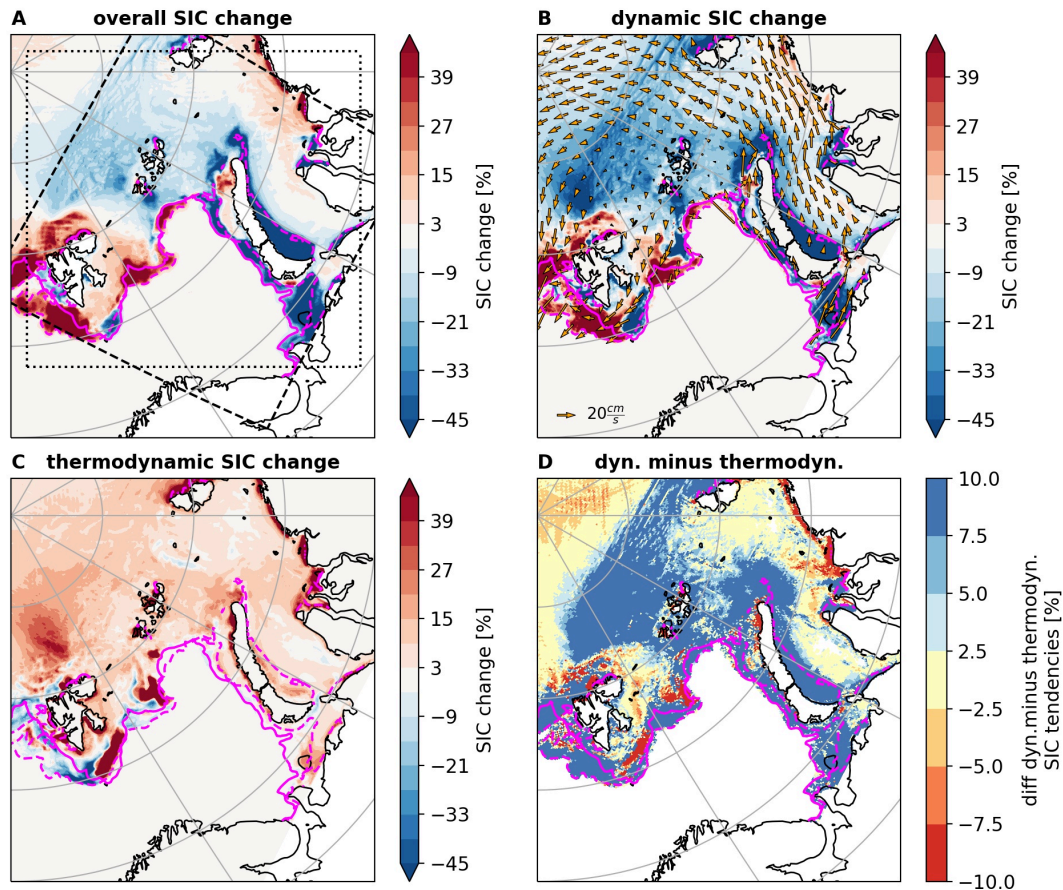
Figure 4.4: Overall SIC change during the whole sequence of cyclones (9.2.20-25.2.2020) (A), temporally integrated dynamic (advective plus rafting and ridging) SIC change as well as mean sea-ice drift vectors (B), temporally integrated thermodynamic SIC change (C), and difference between absolute values of temporally integrated dynamic and thermodynamic SIC change (D) based on the HIRHAM–NAOSIM simulation. Solid (dashed) pink lines indicate the position of the ice edge (15 % SIC) on 9.2.2020 (25.2.2020). Dashed (dotted) box in (A) indicates domain of spatially averaged SIC (SLP) changes in section 4.4.5

The thermodynamic decrease in SIC south and (north)west of Svalbard is notable, since this region is affected by the advection of cold, dry air west of the cyclone centers (Figure 4.2, Supplementary Figures S4.5, S4.6). Such atmospheric conditions tend to promote increased ice growth, which does not fit to the simulated thermodynamic SIC decrease. A possible explanation is given by the enhanced southwestward advection of sea ice during the cyclone passages into regions with comparatively warm ocean water, with the thermodynamic SIC decrease being related to basal melting of sea ice rather than to atmospheric influence. This hypothesis is supported by a spatial pattern of comparatively strong upward oceanic surface heat fluxes in the presence of sea ice (Supplementary Figure S4.7), which shows similarities to the spatial pattern of thermodynamic SIC decrease (Figure 4.4C). This

hypothesis is further backed up by recent findings of Duarte et al. (2020), who report on the importance of oceanic heat content for the melting of sea ice near Svalbard, particularly in combination with storms.

The difference between integrated dynamic and thermodynamic SIC changes (Figure 4.4D) confirms that dynamic SIC changes dominate (difference > 0) the response of the sea-ice cover to the analyzed series of cyclones not only close to the ice edge, but also in large parts of the consolidated ice pack. The clear dominance of dynamic mechanisms south and east of Novaya Zemlya indicates that the cyclone-related advection of warm and moist air into this region does not play a substantial role for SIC. For our cyclone case, only in the western Barents Sea, particularly south(east) of Svalbard, thermodynamics are (partly) of high importance for the SIC changes. There, northerly winds at the western flank of the cyclones push the ice edge southward and, at the same time, cold and dry air is advected from the central Arctic (Figures 4.1, 4.2; Supplementary Figures S4.5, S4.6). This leads to refreezing of leads and openings in the sea-ice cover that are caused by the southward drift of ice due to the cyclonic wind anomalies. In general, the role of thermodynamics during the cyclone passages seems to be limited to this refreezing in regions that have experienced dynamic decrease of SIC. Hereby, the advection of warm and moist air east of the cyclone tracks might explain why such refreezing is occurring only to a very limited extent south and east of Novaya Zemlya, while it is stronger close to the ice edge in the central Barents Sea and north of Svalbard (Figure 4.4C).

Further it should be mentioned that to some degree, thermodynamic SIC increases due to refreezing are not a direct consequence of the cyclone passages only, but would happen anyway in Arctic winter due to the seasonal sea-ice growth. A rough estimate of this effect can be obtained from the study of Aue et al. (2022), who compared cyclone related SIC changes on daily to weekly timescales with a non-cyclone reference obtained from ERA5 data for the period 2000–2020 for Arctic winter (December to February). For this, weekly SIC changes ranged from 1 to 10 % in the BKS in the non-cyclone reference. Consequently, the strong thermodynamic SIC increases in the western part of the study domain (around Svalbard) are larger than usually in winter, and the non-existing SIC growth south and east of Novaya Zemlya is unusual compared to non-cyclone conditions.

To gain further insights into the variability of the cyclone impacts on sea ice, we quantify the contributions of the individual cyclones 1–3 to the accumulated signal in the change of SIC. Accordingly, Figure 4.5 shows the SIC change simulated during each of the three cyclone passages. In order to analyze whether the apparent impacts of a cyclone may include contribution by the preceding cyclone, we make use of the fact that three cyclones with a similar track travelled across the BKS in a comparatively short time period.
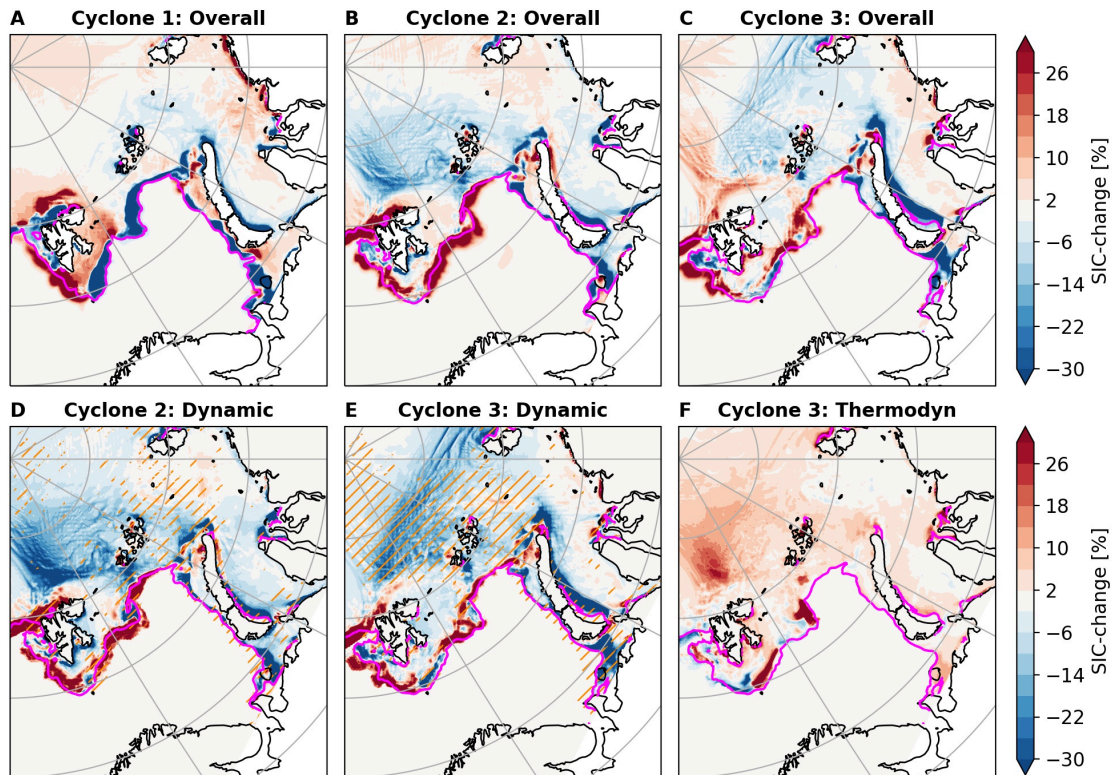
Figure 4.5: SIC change during cyclone 1 (9.2. – 13.2.2020) (A), cyclone 2 (15.2. –
20.2.2020) (B) and cyclone 3 (20.2. – 25.2.2020) (C) as well as temporally integrated
dynamic SIC changes for cyclone 2 (D) and cyclone 3 (E) and temporally integrated ther-
modynamic SIC changes during cyclone 3 (F). Orange hatching indicates grid-cells that
have lost at least 5 cm of SIT during the previous cyclone passage(s). All based on the
HIRHAM–NAOSIM simulation. Pink lines indicate the position of the ice edge (15 %
SIC) at the start of each cyclone passage.

While the SIC impacts of cyclones 2 and 3 are similar, there are differences to the SIC
change during the first of the three cyclones (Figure 4.5A–C). For the latter two cyclones,
a SIC decrease south and east of Novaya Zemlya is accompanied by a SIC increase extend-
ing along the ice edge from the central Barents Sea to the west of Svalbard. While the SIC
decrease is slightly stronger for cyclone 3, the SIC increase is slightly stronger for cyclone
2. Nonetheless, the patterns are similar. In contrast, cyclone 1 shows a strong SIC decrease
of more than 30 % not only in the eastern Barents Sea and Kara Sea but also in the central
Barents Sea and southeast of Svalbard. In addition, cyclones 2 and 3 have an almost identi-
cal track for large parts of their lifetime, while the track of cyclone 1 is somewhat different
(Figure 4.1). This suggests that the exact location of a cyclone's track and its orientation
relative to the ice edge is crucial for the resulting impact on SIC. This hypothesis is sup-
ported when comparing our findings with the winter cyclone cases analyzed by Boisvert
et al. (2016) and Blanchard-Wrigglesworth et al. (2022). In fact, the track of their cyclones

resembles that of cyclone 1 more than those of cyclone 2 and 3, and the same is true with respect to the SIC changes in the BKS, which mostly consist of a SIC decrease.

Preconditioning and time scale

It has been shown that cyclone impacts on SIC are amplified when preconditioned by locally low to medium SIC (Aue et al., 2022). Additionally, it can be assumed that also SIT plays a role for the susceptibility of the sea-ice cover to atmospheric forcing during cyclone passages (Zhang et al., 2012; Rheinlænder et al., 2022). To account for both of these effects while investigating a possible relevance of previous cyclone passages for the impact of the current cyclone on SIC, we analyze the role of grid-cell mean sea-ice thickness (SIT), also referred to as sea-ice volume per unit area.

Based on the spatial patterns of SIT decrease during previous cyclone passages, it seems that this preconditioning of the ice cover during cyclone 2 influenced the SIC changes during cyclone 3. Particularly in the consolidated ice pack, regions with dynamically-driven decrease of SIC during cyclone 3 (Figure 4.5E) widely correspond to regions that have experienced SIT decrease during the previous cyclones. In contrast, the spatial patterns of dynamic SIC changes during cyclone 2 (Figure 4.5D) do not fit to those of SIT decrease during cyclone 1.

A possible explanation is that cyclone 1 did not stay as long over the consolidated ice pack as the more intense cyclone 2, which remained north of Svalbard and Franz Josef Land for around two days before decaying (Figure 4.1). The matching patterns of SIC changes during cyclone 3 and preconditioning during cyclone 2 might as well just be a coincidence or related to the fact that both cyclones had a very similar track and presumably exerted a similar wind forcing on the sea-ice cover. Consequently, detailed future research is needed to more convincingly conclude about the effect of preconditioning of the sea ice for following cyclone passages.

North of Svalbard, the SIC was (temporary) decreased by up to 20% during cyclone 2 (Figure 4.5B), which was the most intense of the three cyclones. At the same grid-cells, thermodynamic SIC increase occurred during cyclone 3 due to refreezing (Figure 4.5F). This increase in SIC during cyclone 3 would not have been possible without the preceding cyclone 2, because SIC would have presumably been close to 100% in that part of the Arctic Ocean in February. This constraint of typically high SIC values in Arctic winter might help to explain why dynamic SIC changes are more pronounced than their thermodynamic counterparts during this series of cyclone events for large parts of the study domain.

Another factor that might dampen the thermodynamic SIC changes during the presented series of cyclones is time. Thermodynamic surface impacts via LWD can last 1–2 weeks (Park et al., 2015). Specifically, Aue et al. (2022) showed that the SIC increase following cyclone passages in the Barents Sea in winter lasts up to 5–7 days. For cyclones 1 and 2, this amount of time was not available until the next cyclone passage started. For cyclone 3 – which was not immediately followed by another cyclone – it is clearly visible that the magnitude of the thermodynamic SIC changes as well as their relative importance compared to the dynamic SIC changes increase with time (Figure 4.6). During the passage of cyclone 3, thermodynamic SIC changes are limited to only a few locations in the study domain (Figure 4.6A) and are mostly less pronounced than their dynamic counterparts (Figure 4.6D). The only exception is found north of Svalbard, but the comparatively strong refreezing in this region is related to the preceding cyclone passage as discussed earlier.

During the four days that immediately follow the cyclone passage, a broader region, which includes areas north of Svalbard and Franz Josef Land, shows an accumulated thermodynamic SIC increase of 10–20 % (Figure 4.6B). Consequently, thermodynamics also become slightly more important for the overall SIC change on that time scale (Figure 4.6E). If the time period is further extended to 8 days following the cyclone passage, a strong thermodynamic SIC increase is found in the central Arctic, in the northern Kara Sea as well as south and east of Novaya Zemlya (Figure 4.6C). On this time scale, thermodynamic SIC changes even outweigh their dynamic counterparts for large parts of the study domain (Figure 4.6F). To some degree, this thermodynamic SIC increase with time is just a consequence of seasonal sea-ice growth in winter. This effect can be roughly estimated to 1 to 10 % SIC increase in one week in the BKS for non-cyclone conditions (see section 4.4.3). This indicates that especially the strong (accumulated) thermodynamic SIC increases of more than 20 % in 8 days north of Franz Josef Land, in the northern Kara Sea and around Novaya Zemlya following cyclone 3 (Figure 4.6C) are much larger than usually for Arctic winter and thus can be partly attributed to the cyclone passage.

In conclusion, our analysis of SIC changes on different time scales suggests that during the cyclone passage dynamics clearly outweigh thermodynamics, while it is partly the other way around for the days following the cyclone, provided that there is not another cyclone passage taking place in quick succession. For cyclone 3, this results in a regional difference of SIC increase (decrease) west (east) of the cyclone track during the cyclone passage, as well as in strong increases in SIC in the whole MIZ after the cyclone passage (Supplementary Figure S4.8).
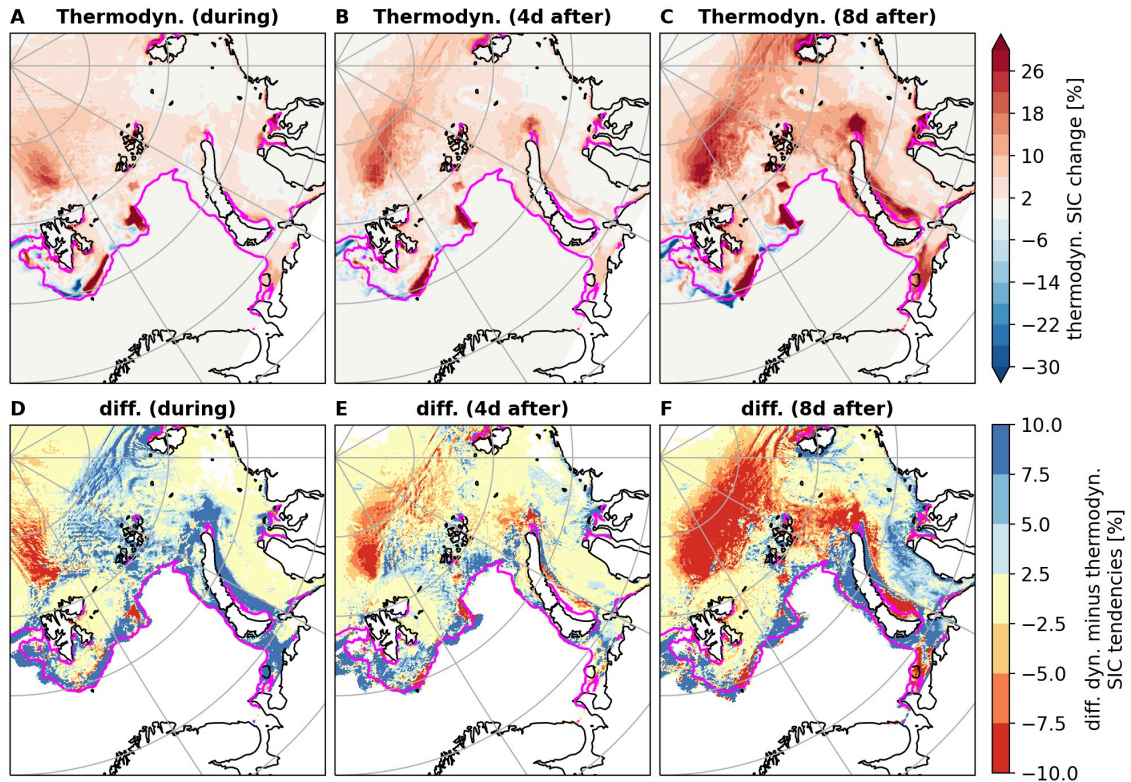
Figure 4.6: Temporally integrated thermodynamic SIC change (A–C) and difference between absolute values of temporally integrated dynamic and thermodynamic SIC change (D–F) during (20.2. – 24.2.2020), shortly after (24.2.20 – 28.2.2020) and for a longer period after (24.2. – 3.3.2020) cyclone 3 based on the HIRHAM–NAOSIM simulation. Pink lines indicate the position of the ice edge (15 % SIC) at the start of the cyclone passage.

4.4.4 Cyclone impacts on sea-ice thickness (SIT)

In this section, we extend our analysis of cyclone impacts to dynamic and thermodynamic changes in SIT, which have been rarely studied. A comparison of the simulated mean SIT from February 9 to February 22, 2020 with observations based on CryoSat-2 and SMOS satellite data (Ricker et al., 2017b) demonstrates that the spatial distribution of regions with relatively thin ice and relatively thick ice is captured by the model (Figure S4.4A–B). However, it should be noted that the simulated SIT field is generally too smooth, leading to an underestimation of SIT in the central Arctic and to an overestimation of SIT in the Kara Sea and some parts of the marginal ice zone.

Simulated SIT changes during the cyclone passages mainly consist of a decrease in SIT east of Novaya Zemlya and an increase in SIT northwest of Svalbard (Figure 4.7A). Generally, there are some differences between the simulated and observed SIT response to the cyclone passages (Figure S4.4C–D), which should be kept in mind when interpreting the results.
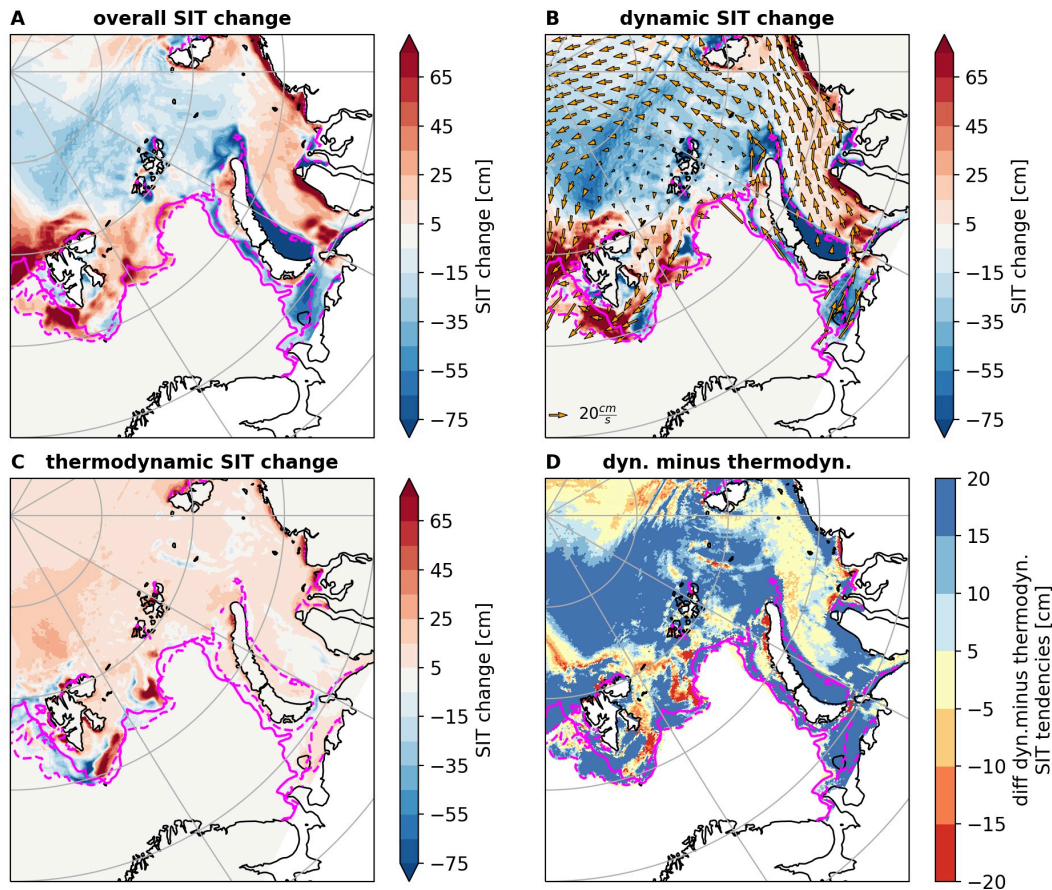
Figure 4.7: Overall SIT change during the whole sequence of cyclones (9.2.20-25.2.2020) (A), temporally integrated dynamic SIT change as well as mean sea-ice drift vectors (B), temporally integrated thermodynamic SIT change (C), and difference between absolute values of temporally integrated dynamic and thermodynamic SIT change (D) based on the HIRHAM–NAOSIM simulation. Solid (dashed) pink lines indicate the position of the ice edge (15 % SIC) on 9.2.2020 (25.2.2020).

However, the previously described main features around Novaya Zemlya and Svalbard are consistent in both datasets, which confirms the applicability of the simulation for this case study.

Dynamic and thermodynamic contributions

The results show that changes in SIT during the series of the three cyclone passages are – similarly to changes in SIC – dominated by dynamic mechanisms (Figure 4.7). Sea ice is mainly moved from the eastern coast of Novaya Zemlya towards the central Kara Sea as well as from the central Arctic (north of Franz Josef Land) towards Svalbard during the cyclone events (Figure 4.7B). This is consistent with the cyclonic wind anomalies that can be expected based on the cyclone tracks. The dominance of dynamics for SIT changes (Figure 4.7D) is even more pronounced than for SIC changes. This is in agreement with

results by Clancy et al. (2022), who analyzed cyclone-related changes in ice thickness on a cyclone-centered grid in winter utilizing model simulations.

With respect to thermodynamic changes in SIT, comparatively strong increases can be found north (up to 20 cm) as well as south and east (up to 50 cm) of Svalbard, while a decrease occurs southwest of Svalbard (Figure 4.7C). This pattern closely resembles the thermodynamic SIC changes presented in Figure 4.4. South and east of Novaya Zemlya, no thermodynamic increases in SIT are found during the cyclone passages, and at a very few locations even a minor thermodynamic decrease in SIT is visible (Figure 4.7C). This is presumably related to a stalling of ice growth caused by the advection of warm and moist air masses at the eastern flank of the cyclones and subsequent impacts on SEB. However, the overall magnitude of this stalling in sea-ice growth is rather small, as estimated by comparing the growth rates in the eastern and western part of the study domain (differences between 0 cm and 20 cm over more than two weeks). Consequently, thermodynamics do not play a large role for the overall changes in SIT during this sequence of cyclones, which are clearly dominated by dynamics (Figure 4.7D).

Preconditioning and time scale

Since our analysis of changes in SIC demonstrated a large sensitivity of the thermodynamic effect to the time scale (section 4.4.3), we further analyze this for changes in SIT (Figure 4.8).

Similarly to SIC (Figure 4.6), the thermodynamic SIT change gets stronger with time (Figure 4.8A–C) and simultaneously becomes more important relative to its dynamic counterpart (Figure 4.8D–F). This is because the thermodynamic ice growth is relatively slow compared to the dynamic SIT change. Particularly north of Svalbard and Franz Josef Land as well as close to Novaya Zemlya, thermodynamic SIT increase is enhanced during the 8 days that follow cyclone 3 (Figure 4.8C), because the now thinner ice (due to dynamics) freezes faster and produces more ice than it would have been without the cyclone passage. Nonetheless, thermodynamics do not reach a comparatively strong importance for SIT as for SIC (Figure 4.8F vs. Figure 4.6F). For large parts of the Barents and Kara Seas, dynamics remain the dominating factor also on longer time scales following the cyclone passage. A notable result is that in the southern Kara Sea along the coast of Siberia almost no ice thickness growth occurs during the 8 days following the last cyclone passage (Figure 4.8C). In contrast to SIC, this cannot be explained by the constraining boundary condition that the SIC at these grid-cells is almost 100 %. At the same time, this region was also most strongly affected by the advection of warm and moist air masses in the cyclone's eastern sector. This leaves the open question how long the cyclone-induced stalling of ice growth is actually lasting.
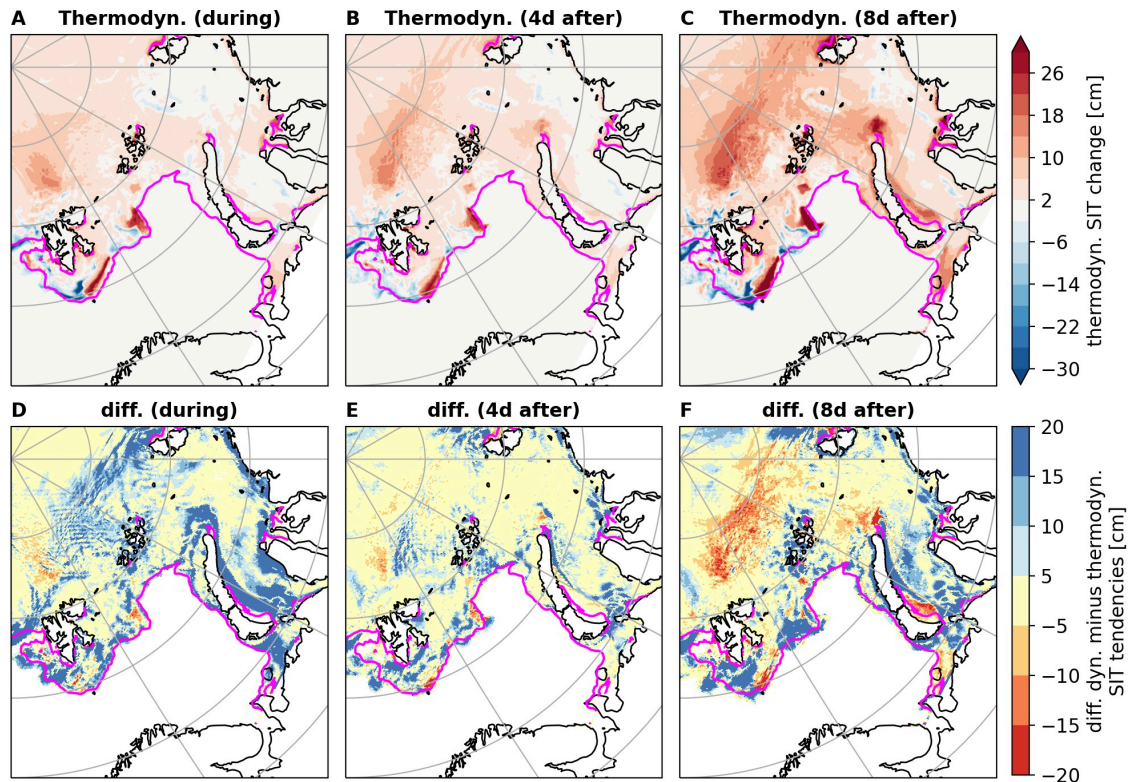
Figure 4.8: Temporally integrated thermodynamic SIT change (A–C) and difference between absolute values of temporally integrated dynamic and thermodynamic SIT change (D–F) during (20.2. – 24.2.2020), shortly after (24.2.20 – 28.2.2020) and for a longer period after (24.2. – 3.3.2020) cyclone 3 based on the HIRHAM–NAOSIM simulation. Pink lines indicate the position of the ice edge (15 % SIC) at the start of the cyclone passage.

4.4.5 Context to other cyclone cases during the MOSAiC winter

To generalize the results from this case study and move towards more solid conclusions on dynamic and thermodynamic contributions to cyclone-driven sea-ice changes, we extend our analysis period to the whole winter of our selected year, specifically to January-March 2020. The time series of the daily SLP averaged over the BKS region (Figure 4.9, domain shown in Figure 4.4) is an indicator for cyclone activity in the BKS. The figure highlights the main cyclone cases during the period and their tracks are shown in the Supplementary Figure S4.9. The cyclone at the beginning of February affected the western BKS around Svalbard for several days starting at February 2, before moving southeastward through the Barents Sea while decaying. The mid-February case of three successive cyclones was discussed in detail in the previous sections. The two March events affected the BKS for several days each, with one cyclone taking a similar path as the mid-February cases (through the southern Barents Sea to the Kara Sea into the central Arctic) and the other cyclone entering
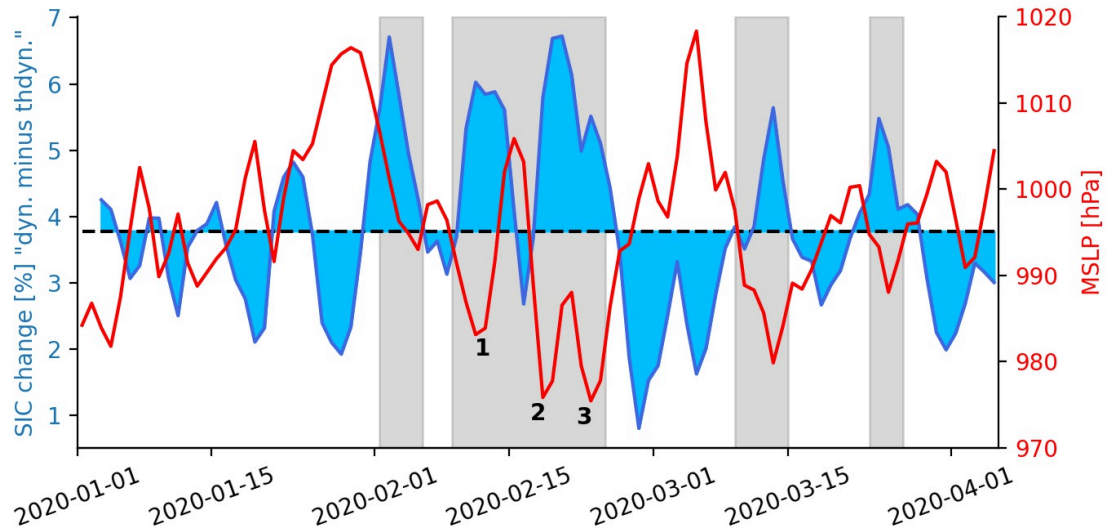
Figure 4.9: Difference of "absolute value of dynamic SIC change" minus "absolute value of thermodynamic SIC change" (blue line), both integrated over 5 days and averaged over the BKS (domain shown in Figure 4.4). Blue filled areas indicate the anomaly compared to the Jan. to March 2020 mean (black dotted line). Red line indicates SLP averaged over the BKS (domain shown in Figure 4.4). Grey areas highlight the main cyclone cases in Jan. to March 2020, numbers indicate the three cyclones analyzed in previous sections.

the BKS on a more northerly track close to Svalbard. They occurred one after the other at intervals of approximately one week.

To discuss the importance of dynamics and thermodynamics for the related SIC changes, we follow the approach of the previous sections and show in Figure 4.9 the time series of the difference between the absolute value of the temporally integrated dynamic SIC change and its thermodynamic counterpart, integrated over 5 days and averaged over the BKS region. Based on our previous analysis, 5 days are an appropriate time period to capture the SIC impacts of individual cyclones (see e.g. Figure 4.5).

First of all, the SIC difference is positive throughout the three months with a mean value of approximately 4 % (indicated by the black dashed line in Figure 4.9). This indicates that for the complete January-March 2020, dynamic SIC changes dominate the overall SIC changes in the BKS region. This is in accordance with our previous analysis (Figure 4.4). Importantly, there is a significant temporal variability in the SIC difference, and thus in the relative importance of dynamics and thermodynamics, often associated with changes in SLP as indicated by the red line in Figure 4.9.

In agreement with our previous analysis of three consecutive cyclones in mid-February (Figures 4.4 and 4.6), the SIC difference is shifted towards more positive values (compared

to the mean value) during these cyclone passages. This indicates a dominance of dynamic over thermodynamic contributions for up to two weeks. After the last of the three cyclones however, a shift towards smaller values indicates an increasing relative importance of thermodynamic processes for SIC changes, which lasts for about 2 weeks with comparatively high air pressure. A similar phase of higher relative importance of thermodynamic SIC changes under high air pressure conditions can be found end of January.

The process of enhanced dynamic SIC changes during and enhanced thermodynamic SIC changes after a cyclone passage is also found for the two cyclone cases that affected the BKS in March 2020 (Figure 4.9). After both of these cyclones, it took approximately one week before the next cyclone arrived in the BKS. Consequently, there was time for thermodynamic SIC changes to take the lead. This supports the hypothesis raised in previous sections that enhanced thermodynamic SIC changes can take place after cyclone passages if not another cyclone follows in quick succession. In accordance with this, Figure 4.9 does not show a period of enhanced thermodynamic SIC changes after the passage of the early February cyclone case. This can be related to the fact the series of the mid-February cyclones started shortly afterwards.

4.5   Discussion and conclusions

The main objective of our study is to quantify cyclone-related dynamic and thermodynamic impacts on the sea-ice cover in order to clarify which of these mechanisms is more important in Arctic winter. It turns out that for the presented sequence of three intense cyclones in February 2020 dynamic contributions are the dominating mechanism for changes in SIC and SIT. Especially cyclone-related decreases in SIC and SIT are almost exclusively driven by dynamic processes. The role of thermodynamics is limited to drive increases in SIC and SIT due to refreezing of leads after the cyclone passages, and to enhance ice growth under cold and dry conditions on the cyclones' western flank. However, after the passing of the cyclones the increased thermodynamic ice growth of the now thinner ice continues, while the dynamic changes only have an immediate effect during the cyclones passing.

For SIT, our results are in accordance with findings by Clancy et al. (2022), who emphasized that dynamic processes are dominant for this quantity in Arctic winter. Apart from that, our findings are partly in contradiction to recent studies by Cai et al. (2020) and Schreiber and Serreze (2020), who found evidence that thermodynamics are the more important factor of the cyclones' impact on sea ice in the cold season. On the one hand, this could be related to the fact that the presented work is a case study of three particular cyclones. Obviously, there can be differences in cyclone impacts on sea ice for different

cases. However, since the tracks of the chosen cyclone cases closely resemble the main cyclone track in the Atlantic sector of the Arctic Ocean in winter, we argue that the sequence of storms presented here is representative. On the other hand, our findings reveal that the considered time scale has a strong impact on the ratio of dynamic and thermodynamic sea-ice changes. This can explain differences between studies. A detailed analysis of the last of the three presented cyclones emphasizes that thermodynamic sea-ice changes become more important on a longer time scale (weekly) following the cyclone passage. This agrees with results by Park et al. (2015) for sea-ice changes related to moisture intrusion events. For the here presented mid-February case, thermodynamics locally outweigh the importance of dynamics on timescales of about one week following the cyclone passage, mostly in the consolidated ice pack and less frequently in the MIZ close to the ice edge, where dynamic sea-ice changes are most pronounced.

A comparison of the mid-February case with other cyclone cases from January to March 2020 suggests that an initial dominance of dynamically caused SIC changes, followed by enhanced thermodynamic impacts, is typical of cyclone passages in the BKS in winter. Further analysis covering more cases from different years is necessary to confirm this hypothesis. Recent statistical studies have reported on cyclone-related increases in SIC in the Arctic winter (Schreiber and Serreze, 2020; Aue et al., 2022), mostly taking place a couple of days after the cyclone passage. If our findings are representative for winter cyclones, this would suggest that the reported SIC increases are likely driven by thermodynamics. In that case, dynamical mechanisms could reasonably explain the strong SIC changes initially taking place during most cyclones by redistributing the sea ice, while enhanced ice growth in leads in the more consolidated ice pack offers an explanation for the positive ice mass balance impact after the cyclone passage.

It should be noted that this mechanism only works in regions with cold surface waters. For instance, if sea ice is advected over warmer Atlantic water south of the polar front in the Barents Sea or over the Yermack Plateau north of Svalbard, the ice will be subject to basal melt. If cyclones mix up warmer sub-surface waters, this can further change the regions with stronger oceanic heat flux impact (Duarte et al., 2020). Another factor that seems to restrict the thermodynamic increase in SIC after the cyclones is the time available until the following cyclone passage. Decomposing the sea-ice changes for the whole sequence of cyclone events reveals that dynamics can be the dominating mechanism for changes in SIC and SIT on time scales of more than two weeks if cyclone passages occur in quick succession.

Apart from the importance of the timing of cyclone passages, our findings further indicate that comparatively minor differences in the location of a cyclone track can result in strong differences in the cyclone impact on the sea-ice cover, particularly in the MIZ. Recently,

Lukovich et al. (2021) came to similar conclusions regarding the importance of the exact position (and timing) of cyclones when analyzing the impacts of extreme summer cyclones on Arctic sea ice. In addition to a cyclone's timing and track, further factors, such as its intensity or the source region of its air masses, presumably contribute to the variability of the impacts of individual cyclones on sea ice. Furthermore, a high spatiotemporal resolution is crucial for capturing cyclone intensification rates and maximum intensity (e.g. Parker et al., 2022). Accordingly, a relatively coarse atmosphere resolution (¼ degree in our model as well as in ERA5) has its limitation in this regard. In conclusion, identifying the key parameters that determine the impact of a specific cyclone on sea ice is not only a complex but also an important research task, particularly in order to make reliable predictions on future cyclone impacts on sea ice in a warming Arctic.

4.6   Supplementary material

1. Figure S4.1: Air temperature and integr. water vapour during cyclone 2.

2. Figure S4.2: Comparison between HIRHAM-NAOSIM and MOSAiC.

3. Figure S4.3: SIC change during sequence of cyclones based on ERA5.

4. Figure S4.4: SIT from HIRHAM-NAOSIM and remote sensing data.

5. Figure S4.5: Meteorological quantities during cyclone 1.

6. Figure S4.6: Meteorological quantities during cyclone 3.

7. Figure S4.7: Vertical heat flux at ocean-ice boundary.

8. Figure S4.8: overall and dynamic SIC change for cyclone 3.

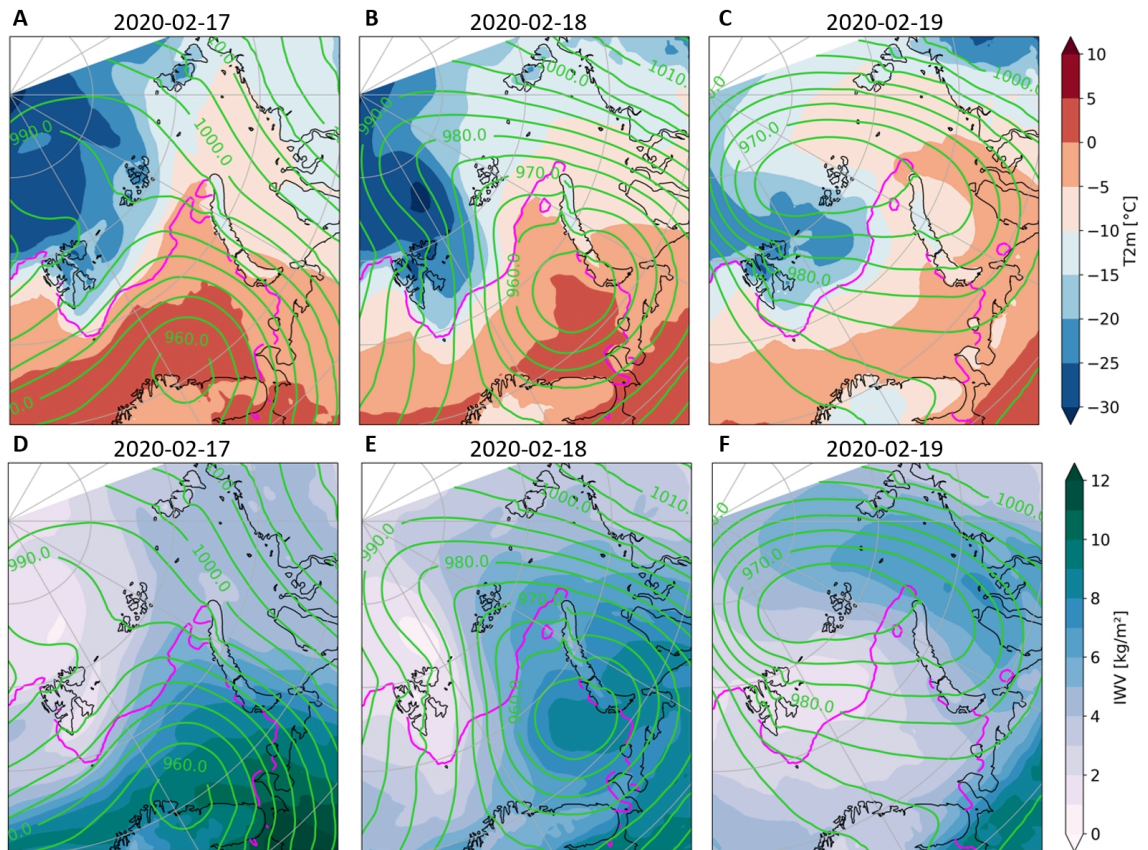9. Figure S4.9: Tracks of further cyclone cases.

Figure S4.1: Daily means of 2-m air temperature (A–C) and integrated water vapour (IWV) (D–F) during cyclone 2 (17.2.–19.2.2020) based on ERA5. Green contour lines represent daily mean sea level pressure (in steps of 5 hPa); pink lines indicate the position of the ice edge (15 % SIC).
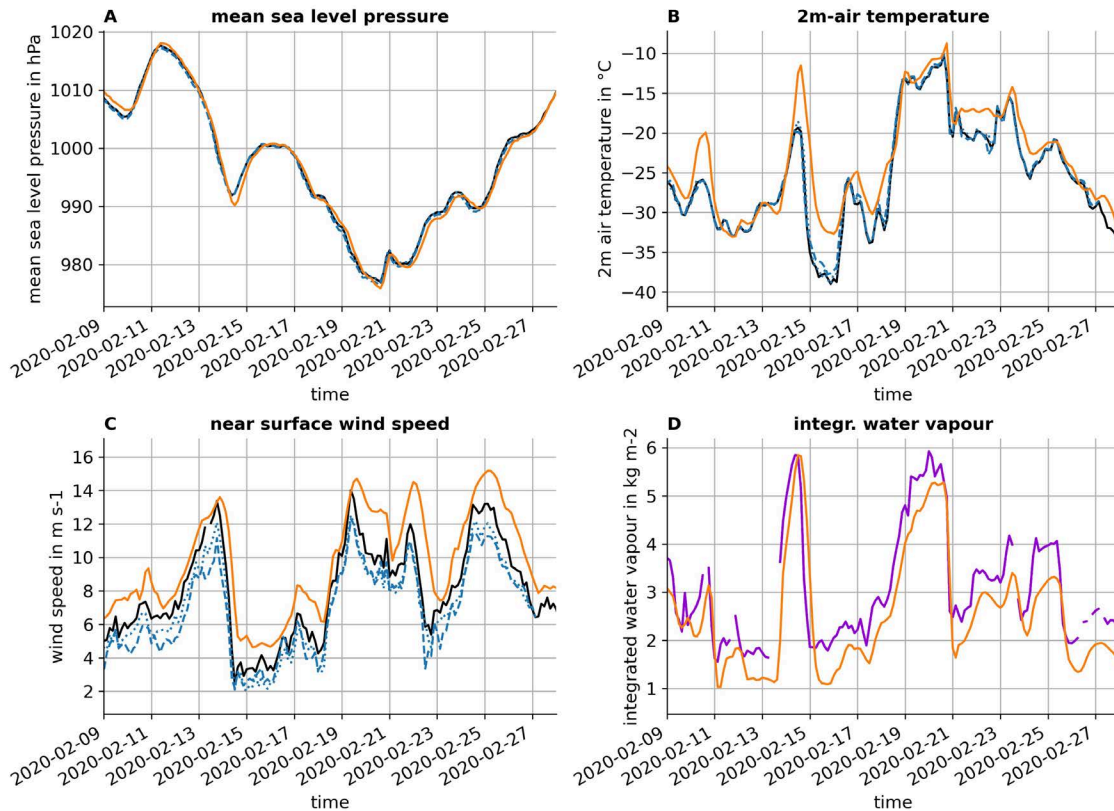
Figure S4.2: Time series of mean sea level pressure (A), 2-m air temperature (B), near surface wind speed (C) and integrated water vapour (IWV) (D) based on HIRHAM-NAOSIM's closest grid cell to the Polarstern position (orange) as well as based on various measurements obtained during MOSAiC: Measurements at Met City (solid black line), at three autonomous Atmospheric Surface Flux Stations (blue lines of different line styles), and HATPRO IWV measurements (violet line).
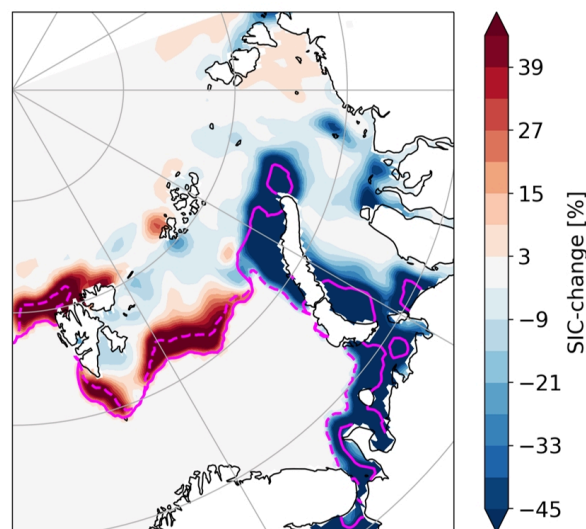
Figure S4.3: SIC change during the whole sequence of cyclones (25.2.2020 minus 9.2.2020) based on ERA5. Solid (dashed) pink lines indicate the position of the ice edge on 9.2.2020 (25.2.2020).
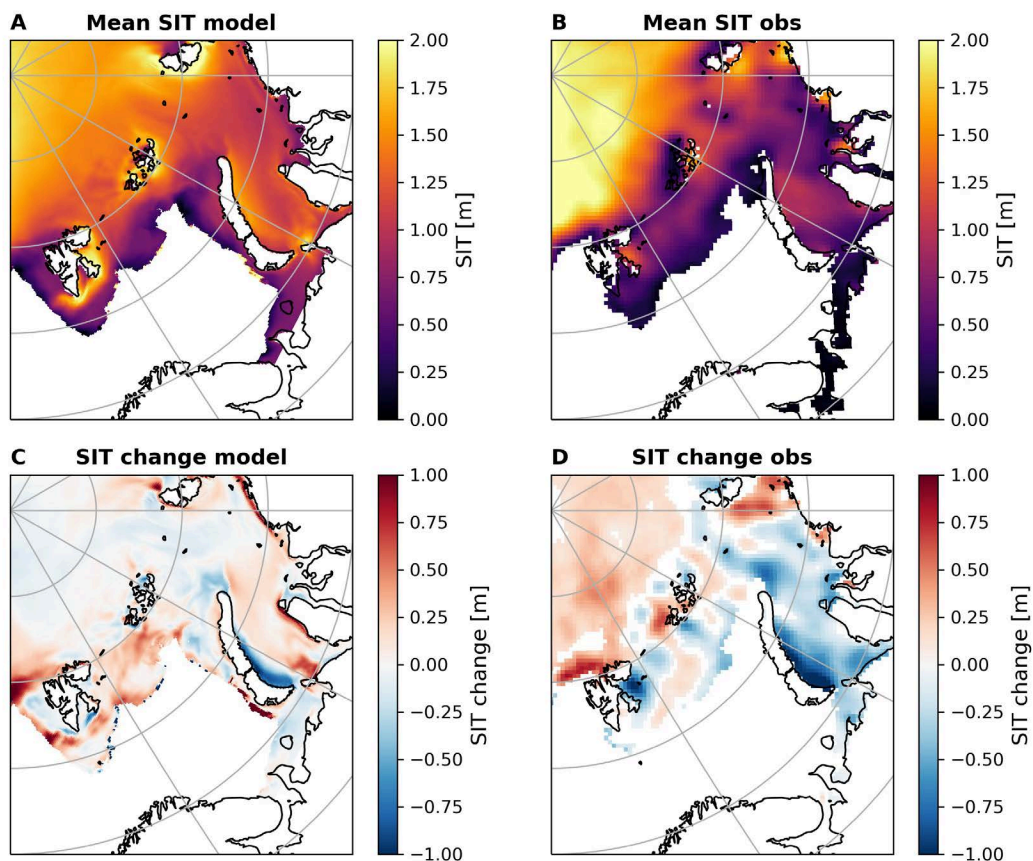
Figure S4.4: Mean SIT from 9.2.2020 to 22.2.2020 (A–B) as well as SIT change (C–D) from 9.–15.2.2020 (weekly mean) to 19.–25.2.2020 (weekly mean) based on HIRHAM-NAOSIM simulation and merged CryoSat-2 and SMOS satellite data.
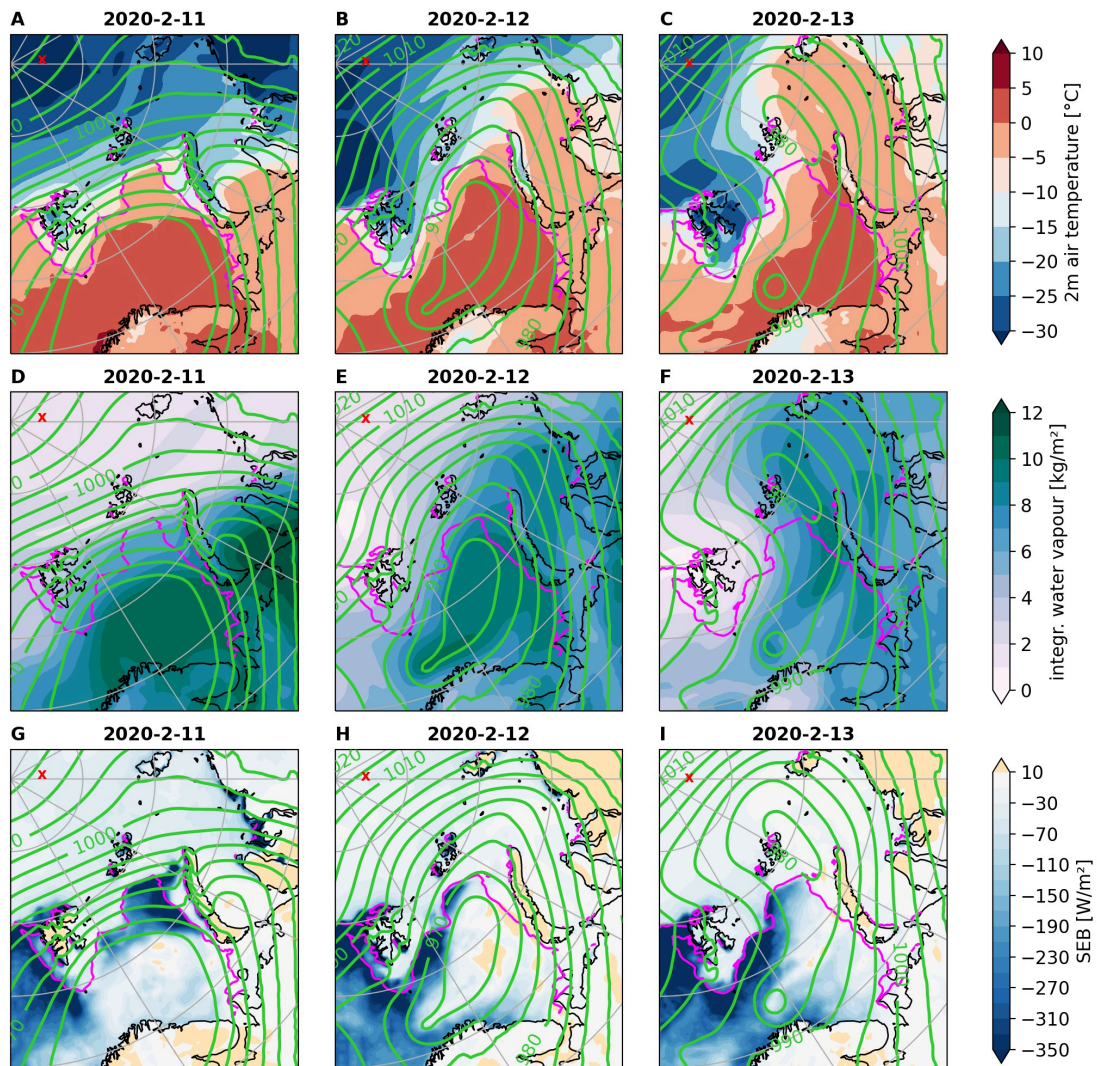
Figure S4.5: Daily means of 2-m air temperature (A–C), integrated water vapour (IWV) (D–F) and surface energy budget (SEB) (G–I) during cyclone 1 (11.2.–13.2.2020) based on the HIRHAM–NAOSIM simulation. Green contour lines represent daily mean sea level pressure (in steps of 5 hPa); pink lines indicate the position of the ice edge (15% SIC). The position of RV Polarstern at the corresponding days of the MOSAiC expedition is marked as red cross.
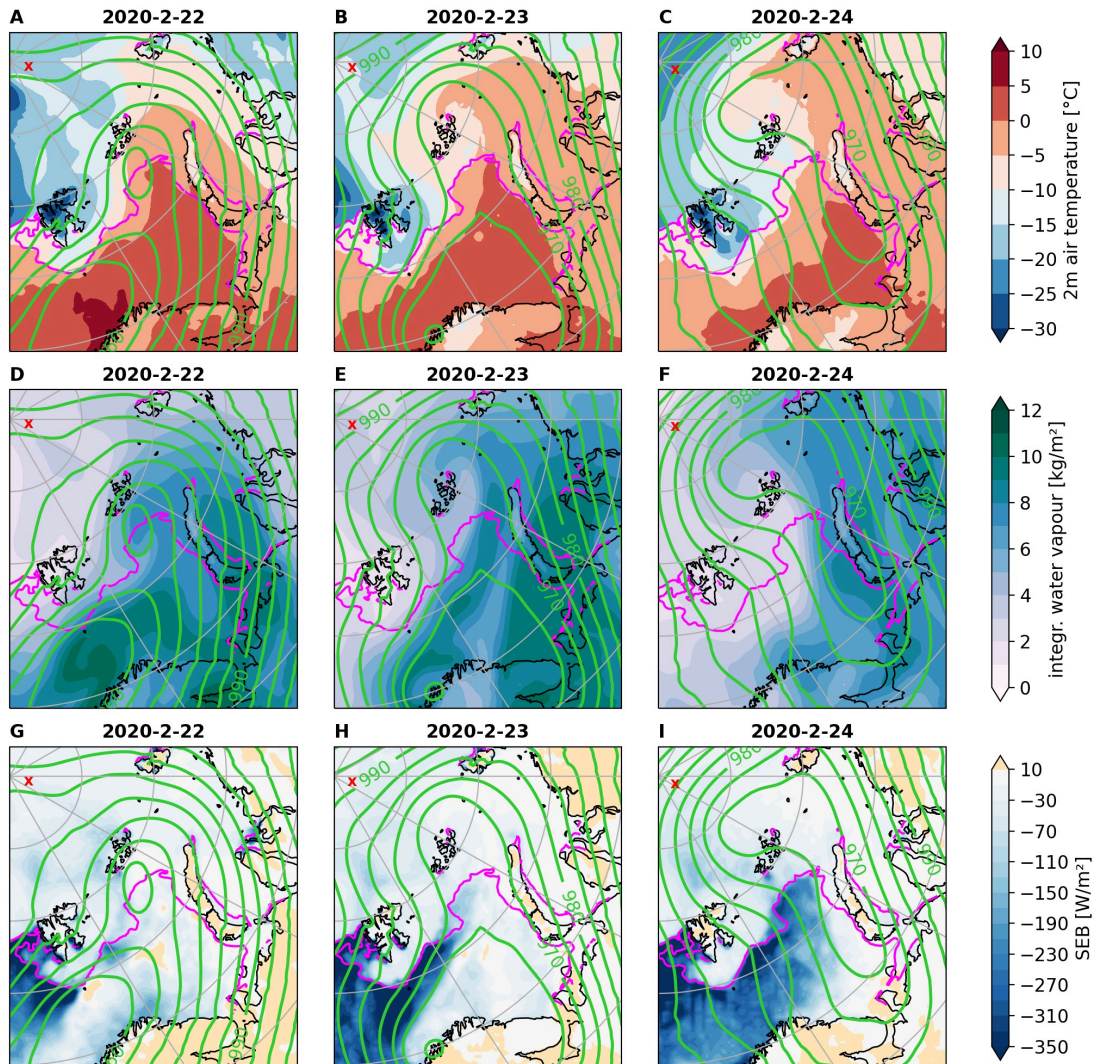
Figure S4.6: Daily means of 2-m air temperature (A–C), integrated water vapour (IWV) (D–F) and SEB (G–I) during cyclone 3 (22.2.–24.2.2020) based on the HIRHAM–NAOSIM simulation. Green contour lines represent daily mean sea level pressure (in steps of 5 hPa), pink lines indicate the position of the ice edge (15 % SIC). The position of RV Polarstern at the corresponding days of the MOSAiC expedition is marked as red cross.
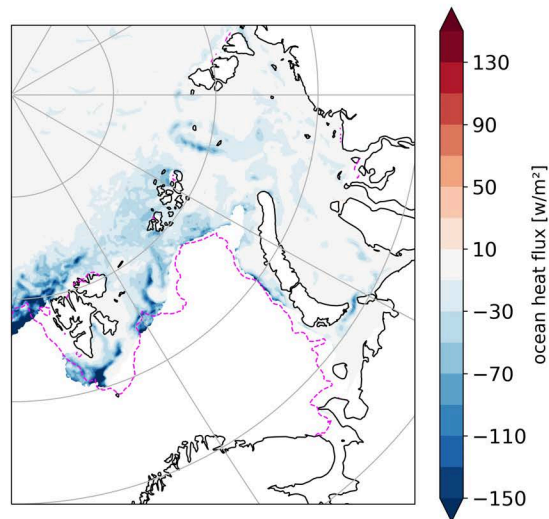
Figure S4.7: Mean vertical oceanic heat flux at the ice/atmosphere surface during the sequence of cyclones (9.2.–25.2.2020), limited to time steps and grid cells with at least 80 % SIC, based on HIRHAM–NAOSIM. Negative (positive) values correspond to upward (downward) fluxes; pink lines indicate the position of the ice edge (15 % SIC) on 9.2.2020.
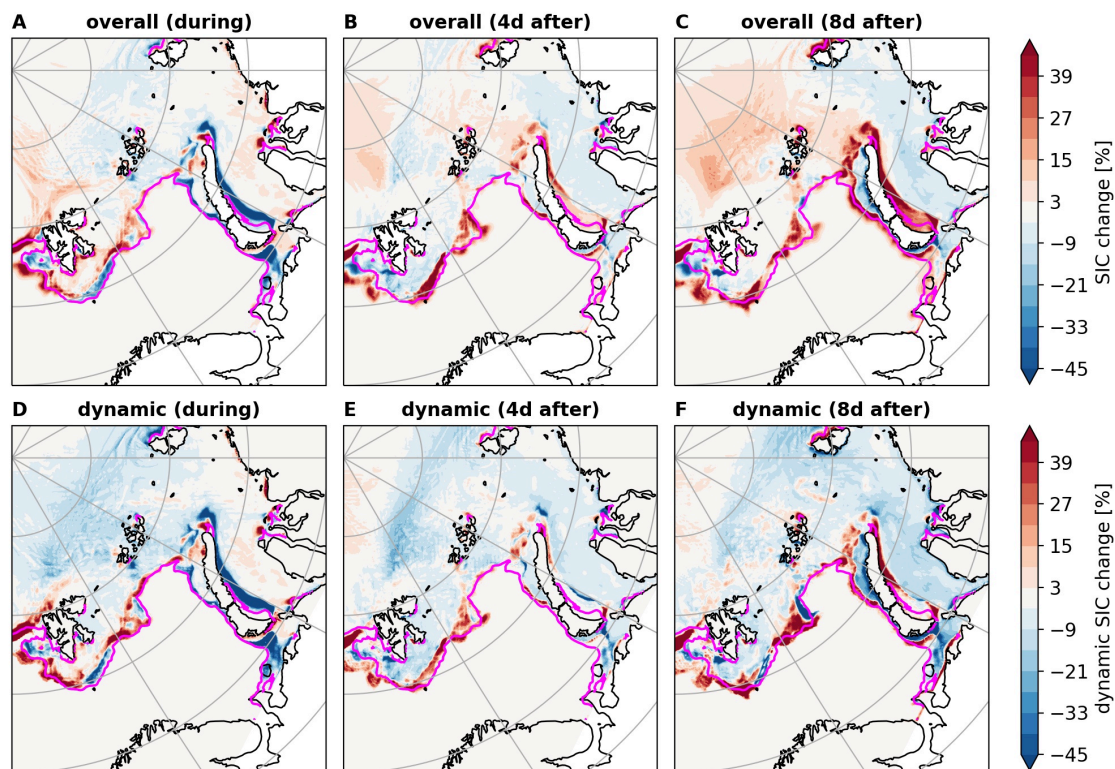

Figure S4.8: Overall SIC change (A–C) and temporally integrated dynamic SIC change (D–F) during (20.2.–24.2.2020), shortly after (24.2.–28.2.2020) and for a longer period after (24.2.–3.3.2020) cyclone 3 based on the HIRHAM–NAOSIM simulation. Pink lines indicate the position of the ice edge (15 % SIC) at the start of the cyclone passage.
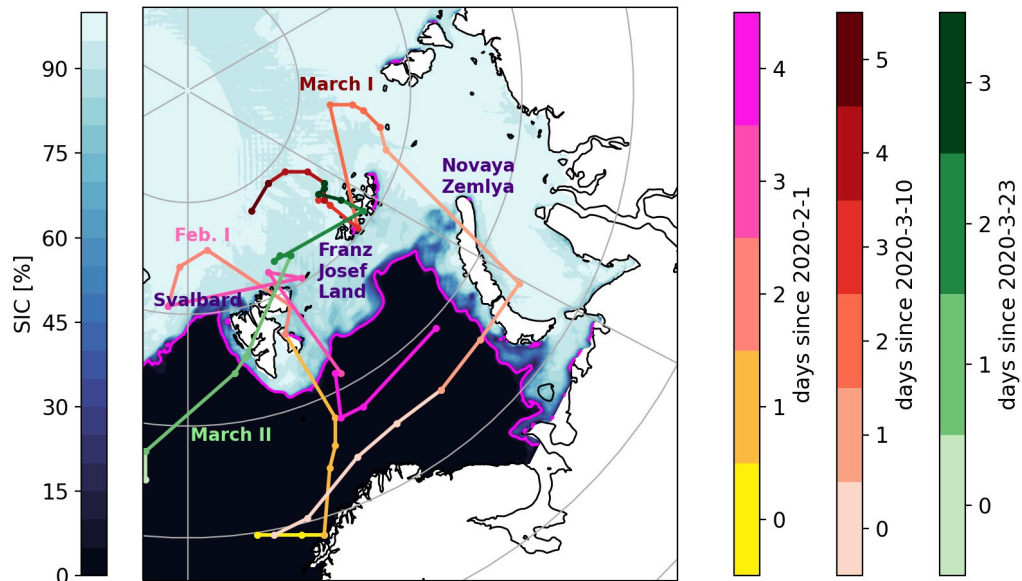
Figure S4.9: Track of cyclone cases from beginning of Febr. 2020 ('Feb. I', yellow-pink line) as well as from mid March ('March I', orange line) and end of March ('March II', green line) 2020 based on 6-hourly SLP minima in the study domain. Daily mean SIC and the 15 % SIC contour (pink line) are shown for the first day within the February cyclone passage (February 1, 2020). SIC and cyclone tracks are based on the HIRHAM–NAOSIM simulation.

Supplementary model description

Compared to the base version 2.0 of HIRHAM–NAOSIM, described in detail by Dorn et al. (2019), the new version 2.2 includes modified parameterizations with respect to (a) the sea-ice albedo and (b) the transfer coefficients for momentum and heat over polar sea ice, reformulations with respect to (c) the ice–water stress, (d) the ice strength, and (e) the ocean–ice heat flux, and an adjustment of (f) the mixing ratios of greenhouse gases. In addition, version 2.2 uses a constant reference thickness for lateral freezing $h_0 = 0.65\,\mathrm{m}$ instead of minimum/maximum values $h_{0\mathrm{min}} = 0.3\,\mathrm{m}$ and $h_{0\mathrm{max}} = 0.8\,\mathrm{m}$ in version 2.0 (see Dorn et al., 2009, Equation (14)).

(a) Sea-ice albedo Concerning snow on sea ice, version 2.2 uses the revised snow albedo parameterization by Jäkel et al. (2019), which includes an observational-based cloud-cover dependency of the snow albedo as innovation. The albedos of bare ice and melt ponds have not been changed. However, the linear transition towards the water albedo for thin ice (Dorn et al., 2009, Equation (33)) and of the restriction of the melt pond fraction to the fraction of the sea-ice surface not covered with snow (Dorn et al., 2009, Equation (37)), which were switched off in version 2.0, have been reactivated in version 2.2.

(b) Transfer coefficients   Version 2.2 includes two new options of improved stability-dependent parameterization of the transfer coefficients for momentum and heat over polar sea ice. The first option is the parameterization by Lüpkes and Gryanik (2015), which especially includes form drag caused by the edges of ice floes and melt ponds. The effects of this parameterization in HIRHAM–NAOSIM were analyzed by Yu et al. (2020), who showed that the agreement of sea-ice drift speed and wind speed ratio between model and observations does not improve. They argue that the additional inclusion of a countering form drag at the ice–ocean interface might improve the agreement. This option has not been activated in version 2.2. The second option is the parameterization by Gryanik and Lüpkes (2018), which includes adapted roughness lengths and a new formulation of the stability functions for stable atmospheric conditions over polar sea ice. The effects of this parameterization were demonstrated in a set of uncoupled HIRHAM experiments by Schneider et al. (2022). This option has been activated in version 2.2 and corresponds to parameterization P1 in the paper of Schneider et al. (2022).

(c) Ice–water stress   In version 2.0, the total ocean surface stress was simply determined as residual of total atmospheric wind stress minus internal ice stress. This approach satisfies the law of conservation of momentum, but does not distinguish different contributions of atmospheric wind stress over open water and over sea ice in solving the ice momentum equation. Since HIRHAM provides atmospheric wind stress over open water and over sea ice separately, an analogous distinction was made in version 2.2 with respect to the ocean surface stress following equations (1) and (2) by Martin et al. (2016). For the solution of the ice momentum equation, only stress terms for the ice-covered part of the grid cell are used now. In addition, a couple of minor adaptations were made for reasons of consistency, but also in order to increase finding an iterative solution of the ice momentum equation. These adaptations include:

1. Use of the uppermost ocean velocities for the calculation of the ice–water stress with drag coefficient $C_{\mathrm{dw}} = 0.0125$ and turning angle $\theta_{\mathrm{w}} = 0°$, instead of geostrophic ocean velocities with $C_{\mathrm{dw}} = 0.0055$ and $\theta_{\mathrm{w}} = 25°$.

2. Use of instantaneous ocean velocities in the ice model, instead of applying a damping time constant of 4 days to the ocean velocities.

3. Use of a free drift solution as initial approximation to the iterative solution of the ice momentum equation, instead of ice velocities from the previous time step.

4. Weighting of the stress terms in the ice momentum equation with the ice concentration, instead of unweighted stress terms.

(d) Ice strength   In consequence of the reformulated ice–water stress, it was found that the model tends to accumulate thick sea ice at the coasts of narrow straits and bays, in particular in the region of the Canadian Arctic Archipelago, caused by strong deformation in case of onshore ice motion. To reduce the deformation of thick ice, the ice strength was formulated as

$$P = P^* h^2 \exp[-C(1 - A)] \,, \tag{4.8}$$

where h is the mean ice thickness, A is the ice concentration, and $P^* = 25000 \, \mathrm{N \, m^{-2}}$ and $C = 20$ are empirical constants. The difference to the formulation by Hibler (1979) used in version 2.0 is the quadratic dependence of the ice strength on the ice thickness instead of a linear dependence. This reformulation follows the idea by Chikhar et al. (2019), who discussed the weakening of thinner ice and strengthening of thicker ice by means of a higher dependence of the ice strength on the ice thickness.

(e) Ocean–ice heat flux   The oceanic heat flux towards the ice–ocean interface is parameterized in HIRHAM–NAOSIM as

$$Q_{\mathrm{oi}} = \rho_{\mathrm{w}} c_{pw} \gamma_{\mathrm{h}} (T_{\mathrm{o}} - T_{\mathrm{fs}}) \,, \tag{4.9}$$

where ρ_{w} is the density and c_{pw} the specific heat capacity of sea water, T_{o} is the ocean mixed layer temperature, and T_{fs} is the freezing temperature of sea water. The parameter γ_{h} represents a heat transfer rate. In version 2.0, the heat transfer rate was parameterized as

$$\gamma_{\mathrm{h}} = \frac{\Delta z}{\tau_0} \,,$$

where Δz is the ocean mixed layer depth and τ_0 is a damping time constant for a delayed adaptation of the mixed layer temperature, meaning that γ_{h} is a constant in version 2.0. To allow for the effects of strong or weak turbulent mixing in the ocean boundary layer, the heat transfer rate is parameterized in version 2.2 as

$$\gamma_{\mathrm{h}} = C_{\mathrm{h}} \cdot u_* \,, \tag{4.10}$$

where $C_{\mathrm{h}} = 0.006$ is a constant heat transfer coefficient and u_* is the friction velocity at the ice–ocean interface (see, e.g., McPhee, 1992; Omstedt and Wettlaufer, 1992).

(f) Greenhouse gases   In version 2.0, the mixing ratios of greenhouse gases were accidentally preset with pre-industrial values for the year 1860. Version 2.2 uses time-adjusted greenhouse gases according to the RCP4.5 scenario (Thomson et al., 2011). In addition,

the time-interpolated mixing ratio of carbon dioxide from RCP4.5 (r_{RCP}) is superimposed
by a seasonal cycle, leading to the time-adjusted mixing ratio

$$r(t) = r_{\mathrm{RCP}}(t) + 5.921 \cdot 10^{-6} \sin[2\pi\, x(t) + 0.135] \tag{4.11}$$

where t is the time and $x(t)$ is the fractional time of the current year. Amplitude and
phase of the sine function were derived from measurements made in Ny-Ålesund, Svalbard
(Buschmann et al., 2017, 2022).

5 Cyclone impacts on sea ice concentration in the Atlantic Arctic Ocean: Annual cycle and recent changes

Summary of the publication:

Objectives	• Quantify the impacts of cyclones on SIC in the Atlantic Arctic Ocean separately for each month of the year. • Quantify changes in (monthly) cyclone impacts on SIC in the Atlantic Arctic Ocean during the period from 1979 to 2018.
Contributions to RQs	• This study contributes to **RQ1** by providing monthly quantifications of cyclone impacts on SIC and to **RQ3** by quantifying monthly trends in these cyclone impacts over the last four decades.
Key points	• Cyclones can significantly impact the sea ice in the Atlantic Arctic in all months of the year, but with strong spatiotemporal variations. • Impacts are stronger in the cold season than in summer due to variations in cyclone intensity and traversed sea ice conditions. • Significant changes emerged throughout the year, recently strongest in the Barents Sea in autumn due to a reduced mean ice concentration.
Own Share	• I processed the utilized data sets, carried out the scientific analysis and designed all figures contained in the manuscript. • I wrote the first draft of the manuscript and was in charge of leading the manuscript revision and managing the submission and peer-review process.

5.1 Abstract

We quantify sea-ice concentration (SIC) changes related to synoptic cyclones separately for each month of the year in the Greenland, Barents and Kara Seas for 1979-2018. We find that these SIC changes can be statistically significant throughout the year. However, their strength varies from region to region and month to month, and their sign strongly depends on the considered time scale (before/during vs. after cyclone passages). Our results show that the annual cycle of cyclone impacts on SIC is related to varying cyclone intensity and traversed sea-ice conditions. We further show that significant changes in these cyclone impacts have manifested in the last 40 years, with the strongest changes occurring in October and November. For these months, SIC decreases before/during cyclones have more than doubled in magnitude in the Barents and Kara Seas, while SIC increases following cyclones have weakened (intensified) in the Barents Sea (Kara Sea).

5.2 Introduction

Over the last decades, surface temperatures in the Arctic have been rising rapidly, associated with pronounced environmental changes such as a strong sea-ice decline (IPCC, 2021). These changes potentially have implications for various climate interaction processes; one of these is the strong coupling between synoptic scale cyclones and sea ice (Valkonen et al., 2021; Crawford et al., 2022).

It has been shown that synoptic cyclones can exert significant impacts on the Arctic sea ice (recently, Schreiber and Serreze, 2020; Clancy et al., 2022; Aue et al., 2022; Finocchio et al., 2022), including both dynamically caused sea-ice changes via enhanced ice drift and deformation as well as thermodynamic sea-ice changes associated with the advection of warm-moist/cold-dry air (Clancy et al., 2022; Aue et al., 2023). Additionally, there is evidence on enhanced basal melting of sea ice due to up-mixing of relatively warm ocean water following some (extreme) summer cyclones (Zhang et al., 2013; Stern et al., 2020; Tian et al., 2022). It is, however, still an open research question how the interplay of these mechanisms and thus the resulting cyclone impact on SIC might change under the changing conditions in the Arctic.

For example, the Arctic sea ice is getting thinner (Kwok, 2018; Meier and Stroeve, 2022) and more mobile (Spreen et al., 2011). This facilitates e.g. the occurrence of break-up events under strong wind conditions (Rheinlænder et al., 2022) and could lead to a future intensification of cyclone impacts on sea ice. The Arctic sea-ice retreat and related changes

in ocean-atmosphere heat fluxes in winter can potentially also impact the atmosphere by favoring local cyclonic circulation conditions (Heukamp et al., 2023a) and intensified winter storms (Crawford et al., 2022), creating possible feedback loops involving cyclones and sea ice.

A better understanding of how cyclone impacts on sea ice are affected by these "new Arctic" conditions can help to improve short-term sea-ice forecasts during cyclone events. Such forecasts are important for Arctic navigation, particularly during hazardous weather conditions (Inoue, 2021), and will presumably gain further importance in future due to increasing shipping activities in the Arctic (Cao et al., 2022). Additionally, this understanding can feed into an improved representation of cyclone-sea ice interactions in climate models (Valkonen et al., 2023) and potentially contribute to more accurate predictions on the future Arctic sea-ice cover, since cyclones drive a substantial part of regional sea-ice concentration (SIC) variability (e.g., Schreiber and Serreze, 2020).

Recent studies provided first insights into ongoing changes in cyclone impacts on sea ice. Aue et al. (2022) found an intensification of SIC changes during and following cyclone passages in the Barents Sea in winter, while Schreiber and Serreze (2020) found that anomalous SIC increases following cyclones in summer and autumn have generally weakened in the Arctic. Considering a monthly time scale in summer, Finocchio et al. (2022) revealed that cyclone impacts on sea ice are different for June (slow down of seasonal sea-ice loss) and August (acceleration of seasonal sea-ice loss), and that particularly the cyclone-related sea ice decreasing effects in August have intensified recently. Their results highlight the importance to study the cyclone impacts on sea ice on monthly instead of only seasonally averaged time scales. However, no study has investigated this throughout the whole year on a monthly basis yet. Thus, a comprehensive view on the complete annual cycle of cyclone impacts on sea ice combined with an analysis of trends over the last four decades during the ongoing warming of the Arctic is missing.

Given the rapidly changing Arctic environment, addressing this knowledge gap to improve understanding on (changing) cyclone impacts on sea ice is urgent. Thus, we present the first quantification of (i) the impacts of synoptic cyclones on Arctic SIC separately for each month of the year and (ii) their changes during the period from 1979 to 2018. We further relate both the annual cycle and recent changes of cyclone impacts to varying relevant background conditions, namely mean sea-ice thickness (SIT), SIC, air temperature, as well as cyclone intensity. We focus on the Atlantic Arctic ocean (covering the Greenland, Barents and Kara Seas, hereafter GBKS; Figure 5.1), as this is the Arctic hot spot region with largest warming and sea-ice reduction in recent decades (Isaksen et al., 2022; Rieke et al., 2023).

5.3 Data and methods

Following Aue et al. (2022), cyclone impacts on SIC are calculated as follows: i) The Akperov et al. (2020) cyclone tracking algorithm is applied to the ERA5 reanalysis at $0.25°$ horizontal resolution to obtain 6-hourly cyclone positions and characteristics, ii) cyclone and non-cyclone-days are separated at each grid-cell depending on whether it was or was not situated within the outermost closed isobar of a cyclone (for a least one, 6-hourly timestep), iii) at each grid-cell, the SIC change is calculated over a few days associated with each cyclone occurrence (before/during cyclone: day -3 to day 0; following cyclone: day 0 to day 5; overall effect: day -3 to day 5), iv) this result is averaged for all cyclone occurrences and compared to the non-cyclone-days SIC change reference. We utilize daily SIC data from ERA5 (based on HadISST2 and OSI SAF satellite data; Hersbach et al., 2020), which have been shown to be suitable for the purpose of our study (Aue et al., 2022) as the SIC response to cyclones agrees with the one derived from passive microwave data (Schreiber and Serreze, 2020). To assess the background state, we further analyze 2m air temperature (based on ERA5) as well as SIT. The latter is taken from ORAS5 ensemble means (available until 2018; Zuo et al., 2019), which have been shown to be suitable to assess the general background state and long-term changes in the Atlantic Arctic ocean (e.g., Tietsche et al., 2018; Shu et al., 2021) and provide complete coverage both in space and time (in contrast to satellite-derived SIT).

We analyze cyclone impacts on SIC for all individual months for 1979–2018, and quantify their recent changes with two approaches: First, we calculate 11-year running means of domain averaged cyclone impacts on SIC within the analysis period. Statistical significance is reported on 95 % confidence level utilizing the students t-test; 11-year periods with a mean sea-ice extent in the domain below 50 % of its value for 1979–1999 are excluded to ensure a certain consistency of the averaged ice-covered area and an adequate sample size. In addition, trends of these means are assessed based on Theil-Sen's Slope Estimator and a Mann-Kendall test for statistical significance (on 95 % confidence level) utilizing the "pymannkendall" python package (Hussain and Mahmud, 2019). Second, we divide the analysis period into two parts, which are in the following referred to as "old Arctic" (1979–1999) and "new Arctic" (2000–2018), and conduct a composite analysis for both.

5.4 Changes in cyclones and traversed sea ice

Before analyzing cyclone impacts on SIC in the study domain of the GBKS, we provide context on the background conditions that control them. Specifically, we analyze the
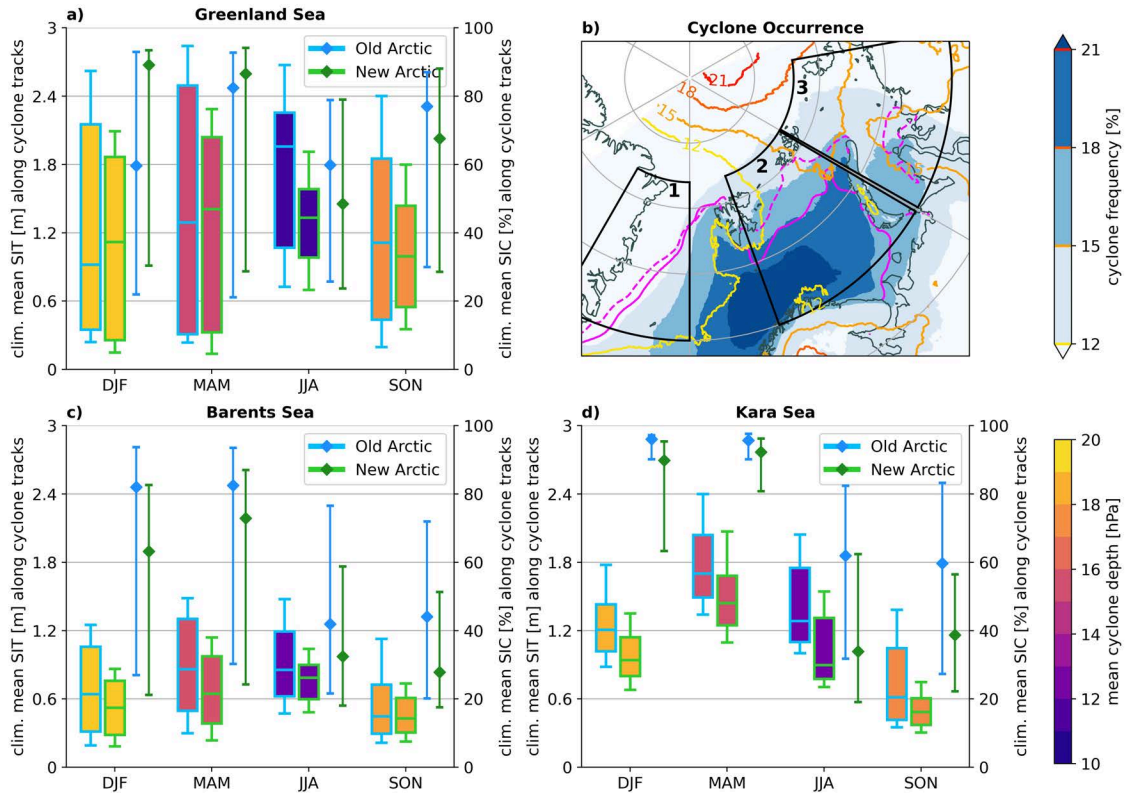
Figure 5.1: Box-Whisker-Plots of mean SIT (with boxes) and SIC (no boxes) along cyclone tracks for the Greenland Sea (a, domain 1), Barents Sea (c, domain 2) and Kara Sea (d, domain 3) for 1979–1999 (blue) and 2000–2018 (green). Extend of boxes (whiskers) indicates 25th/75th (10th/90th) percentile, line/marker indicates median. Color of boxes indicates mean cyclone depth. Subfigure (b) shows the cyclone frequency for winter (DJF, blue colors) and summer (JJA, colored contour lines) and the mean position of the 15 % SIC-contour for winter (summer) as solid (dashed) magenta line, as well as domains for the box-plots.

seasonally averaged cyclone occurrence frequency and cyclone depth as well as the mean SIC and SIT conditions along the cyclone tracks for the old and new Arctic (Figure 5.1).

Generally, maxima in cyclone occurrence frequency (Figure 5.1b) are found in the Norwegian/southern Barents Sea (in the central Arctic) in winter (summer) related to the prevailing North Atlantic storm track (frontal zone), which is a well known feature (pioneered by Serreze, 1995). We further demonstrate that the pronounced annual cycle of mean cyclone depth (i.e. intensity) being twice as high in winter (ca. 20 hPa) as in summer (ca. 10 hPa) is the same in all three regions (Figure 5.1a,c,d). Additionally, the sea-ice conditions over which the cyclones pass show distinct regional and seasonal characteristics.

Cyclones move over the thinnest ice in the Barents Sea, compared to the other two regions (Figure 5.1a,c,d). That makes the Barents Sea potentially more susceptible to the

cyclones' forcing than the other regions. The median SIT along cyclone tracks in the Kara and Greenland Seas is generally higher in all seasons, compared to the Barents Sea. But, in the Greenland Sea, the SIT distribution ranges widely, particularly in winter and spring, which is in accordance with the observed broad (and bimodal) SIT distribution of sea ice that is exported through the Fram Strait (e.g., Sumata et al., 2023). High (low) SIC values underneath cyclones are found in winter-spring (summer-autumn) in the Barents and Kara Seas, while in the Greenland Sea, the seasonal cycles of both SIC and SIT are less pronounced and comparatively low SIC values are mainly found in summer. In the Kara Sea, the 10th percentile of SIC underneath cyclones is approx. 90 % in winter and spring in the old Arctic, indicating a closed ice cover for almost all cyclone passages.

Importantly, our results do not show significant changes in mean cyclone depth (Figure 5.1) between the old and new Arctic neither for any season nor any region. However, we show that the sea-ice conditions along cyclone tracks have changed throughout the year. In the new Arctic, cyclones pass over sea ice of much lower thickness and concentration, compared to the old Arctic (except for the Greenland Sea in winter-spring, see below; Figure 5.1a,c,d). In the Barents Sea, the largest SIC (SIT) reduction along the cyclone tracks occurs in autumn-winter (spring), while in the Kara Sea, this is shifted to summer-autumn (summer), respectively. Our analysis shows evidence that changes in sea-ice conditions (rather than in cyclone characteristics) can be expected to be mostly responsible for a changed cyclone impact - a hypothesis which was raised earlier by Aue et al. (2022) and will be discussed further in the next sections. In the Greenland Sea, a striking result is that both the cyclone track related median SIT and SIC for winter and spring are higher in the new Arctic than in the old Arctic (Figure 5.1a), which is in contrast to all other domains and seasons. For the SIC, also the 10th and 90th percentile are increased, indicating a shift of the whole SIC distribution towards higher SIC, while for SIT, the shift is de facto limited to the median value.

5.5   Cyclone impacts on SIC

Figure 5.2 shows the changes of cyclone impacts on SIC (based on 11-year running means; see Section 5.3) as regional averages for the Greenland, Barents and Kara Seas, separately for each month and for different daily time scales (days before/during and following cyclone passages as well as both time scales combined). Our results are insensitive to the length of the running mean and can also be found for a shorter window length (Supplementary Figure S5.1). Further, our results clearly demonstrate that the separation of
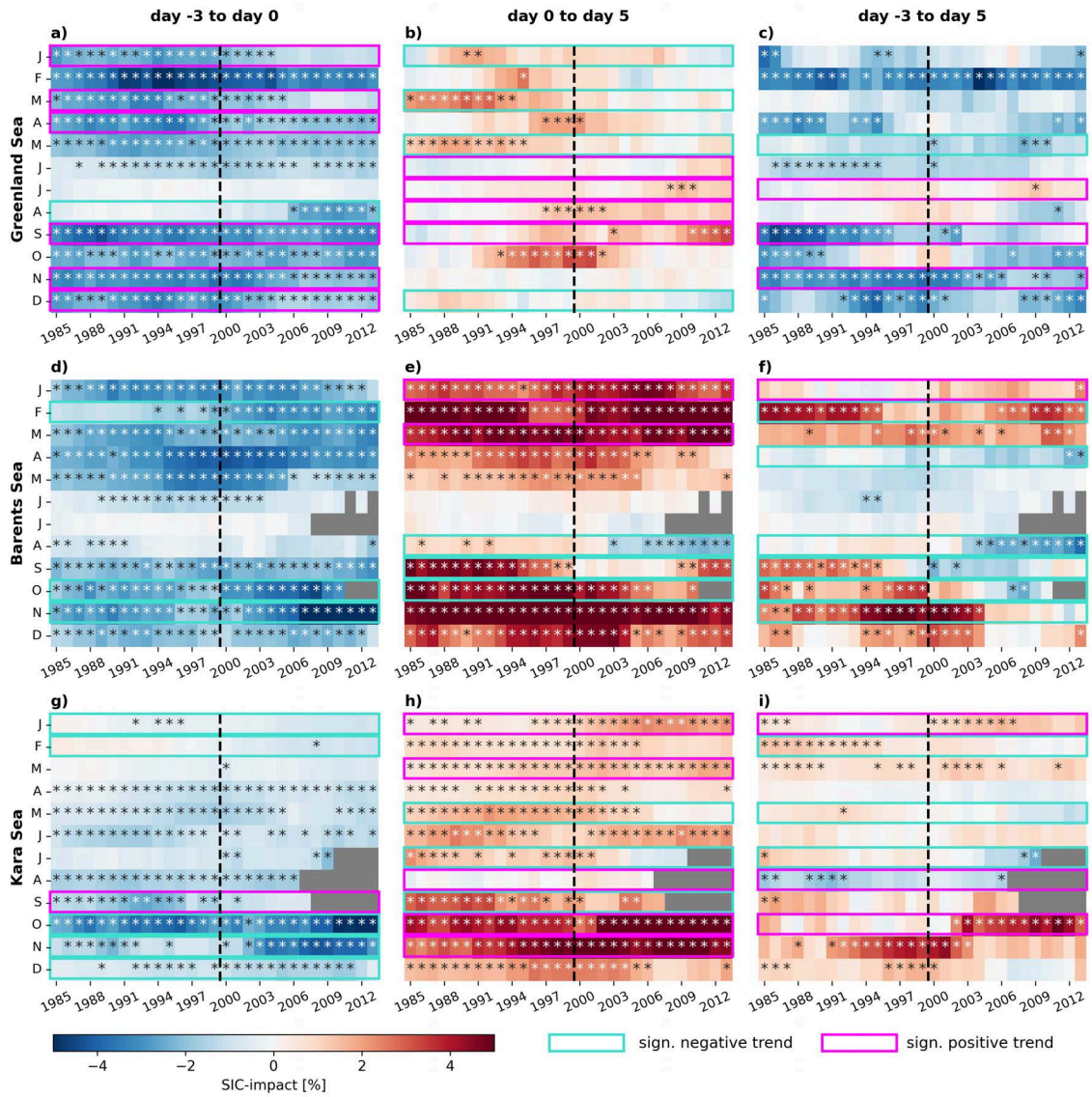
Figure 5.2: 11-year running means of anomalous SIC changes associated with cyclone passages (SIC-impact in %) in the Greenland (a-c), Barents (d-f) and Kara Seas (g-i) for each month. Stars indicate statistical significance, magenta (turquoise) boxes indicate significant positive (negative) trends of these changes. Black dashed line separates old and new Arctic time period. Grey colored time steps are excluded due to a too low sea-ice extent in the region. All statistical significance is at the 95 % level.

cyclone-related SIC decreases and increases by the time scale, i.e. the time considering before/during and after cyclone passages (Aue et al., 2022), is valid throughout the complete annual cycle (Figure 5.2). In the following Section 5.5.1 we assess the annual cycle of cyclone impacts under old Arctic conditions, while recent changes towards the new Arctic are discussed afterwards in Section 5.5.2.

5.5.1 Annual cycle in the old Arctic

At the beginning of the year (January to May), a significant decrease in SIC of up to 4 % is found before/during cyclones in the Greenland and Barents Seas (Figure 5.2a,d). The magnitude of this SIC decrease before/during cyclones is decreasing towards summer, and in July-August, no significant impact is found anymore. This demonstrates that cyclone-related summer SIC changes are much less relevant in the GBKS than in the Laptev and East Siberian Seas and in the Amerasian Arctic Ocean (Schreiber and Serreze, 2020; Finocchio et al., 2022). These findings are consistent with the generally decreased cyclone depth in summer compared to winter and the higher median SIT underneath cyclones in the Greenland Sea in summer (Figure 5.1; see Section 5.4), which can hamper the cyclones' ability to impact the ice. The SIC impacts following cyclones show a similar seasonal behavior as those during cyclones with insignificant impacts in summer (Figure 5.2b,e). The SIC increase following cyclones in winter-spring is regionally different, strong in the Barents Sea, but absent or weak in the Greenland Sea (significantly only in March, May, and occasionally in January).

The annual cycle of cyclone impacts on SIC in the Kara Sea exhibits some differences to the other two regions (Figure 5.2g-i). In winter and spring, SIC decreases before/during cyclones are much weaker and are only significant in April-May. This is in accordance with the extraordinarily high SIC in the Kara Sea in winter-spring and the high SIT in spring (Figure 5.1). Significant SIC increases following cyclones are found for all months (except August), but are not as strong as in the Barents Sea (Figure 5.2e vs. 5.2h).

Cyclone impacts on SIC are generally more intense in autumn than in the preceding summer months in all three regions. In the Barents Sea, cyclone impacts both before/during and following cyclones are strong throughout September-November (Figure 5.2d,e), while in the Kara Sea, particularly the October stands out (Figure 5.2g,h). These findings are consistent with results from Section 5.4, SIC and particularly SIT along cyclone tracks are lowest in autumn (Figure 5.1), so that cyclones can act effectively on the ice cover. At the same time, the mean cyclone depth returns to higher intensity in this season.

5.5.2 Changes in the new Arctic

Figure 5.2 further highlights that cyclone impacts on SIC have been subject to significant changes over the past 40 years (slope of linear trends can be found in Supplementary Figure S5.2). Those are regionally different, depend on the considered time scale (before/during and after the cyclone passage), and show intra-seasonal (month to month) differences.

Between January and April, cyclone impacts on SIC exhibit opposing trends in the Greenland Sea and the Barents-Kara Seas. In the Greenland Sea, decreases in SIC before/during cyclones have weakened (significantly in January, March, April; Figure 5.2a), while they have intensified in the Barents and Kara Seas (significantly in January, February; Figure 5.2d,g). Similarly, also the SIC increasing effects following cyclones have intensified in the Barents and Kara Seas (significantly in January, March; Figure 5.2e,h), while they have weakened (for the same months) in the Greenland Sea (Figure 5.2b). These findings agree with results from Section 5.4: In the Greenland Sea, the traversed mean SIT and particularly SIC have increased in the new Arctic in winter and spring, presumably making the ice cover more resistant against the cyclones' forcing. In contrast, SIC and SIT have decreased in the Barents and Kara Seas in the new Arctic, thus favoring the sea-ice impact of cyclones.

In summer, the changes in August point to interesting regional differences. In the Barents Sea, SIC changes following cyclones shift from slightly positive (SIC increase after cyclone passage) to significantly negative (SIC decrease) (Figure 5.2e). This results in significant negative cyclone impacts on SIC on the overall time scale starting around the year 2000. Differently, the Greenland Sea experiences a positive trend in SIC increase following cyclones, which offsets a strengthening of the decrease in SIC before/during cyclones (emerges around 2005). Accordingly, no significant trend is found in the overall cyclone impact on SIC (Figure 5.2c).

In autumn, strong changes in the cyclone impacts on SIC occur in the whole study domain of the GBKS, but they differ among the regions and months. In the Greenland Sea, the SIC decrease before/during cyclones is consistently weakened (significantly in September, November; Figure 5.2a), which determines the overall weakened cyclone-related SIC decrease (Figure 5.2c). In contrast, the Barents Sea experiences an intensification of the SIC decreasing effects before/during cyclones (significantly in October, November), but the SIC increase following cyclones is weakened (significantly in September, October) (Figure 5.2d,e). Consequently, the overall cyclone impact on SIC shifts from increasing SIC in the old Arctic to neutral/slightly decreasing SIC in the new Arctic (significantly between September and November; Figure 5.2f). In the Kara Sea, the trends in the cyclone impact on SIC are not uniform among the autumn months. While in September both the SIC decrease before/during and the SIC increase following cyclones have weakened, they have both intensified in October and November (Figure 5.2g,h). Still, the overall change in the impact of cyclones is different for October and November (Figure 5.2i). In October, the intensified SIC increase following cyclones outweighs the intensified SIC decreases before/during cyclones, resulting in a significant overall cyclone-related SIC increase. Again, a step change

appears around the year 2000. In November, both effects are of similar strength (Supplementary Figure S5.2), but the intensification of the SIC increase after cyclones emerges earlier in time than the occurrence of the significant SIC decrease before/during cyclones. Thus, a significant overall increase in SIC due to cyclones started to appear around the year 1990, but then disappeared around the year 2000 due to the cancellation of both intensification effects.

As indicated above, autumn is a season of interesting contrasting regional differences in the recent changes of cyclone impacts on SIC. Therefore, we have selected the two months of October and November for a composite analysis to elucidate in the following Section 5.5.3 the regional changes between the old and new Arctic in more detail. Reasons for the month selection include the following features: The strongest trend (ca. -1 % per decade) before/during cyclone passages is found in November in the Barents and Kara Seas. For the days following cyclones, the strongest trend (+1.83 % per decade) occurs in October in the Kara Sea. The overall cyclone impact shows in October a regional difference between the Barents and Kara Seas (negative trend in the Barents Sea vs. positive trend in the Kara Sea).

5.5.3   Regional changes in autumn

Cyclone impacts on SIC in October and November consist of a decrease (increase) in SIC before/during (after) the cyclone passage in the entire GBKS (Figure 5.3a-b), which is consistent with our previous region-averaged analysis (Figure 5.2). Considering the overall impact from day -3 to day 5 (Figure 5.3c), a significant decrease in SIC is found along the Greenland Sea ice edge and around Svalbard, while a significant increase is found at the ice edge in the central Barents and southern Kara Seas as well as in the northern Kara Sea.

Strong changes between the old and new Arctic in October (Figure 5.3d-f) are found for the five days following cyclone passages (Figure 5.3e), which is consistent with the strong trends on this time scale (Supplementary Figure S5.2). Here, SIC increasing impacts of cyclones have weakened in a broad region extending from Svalbard into the Kara Sea north and east of Novaya Zemlya, but newly emerge in the northern Kara Sea, west of Severnaya Zemlya, where cyclones previously did not have an impact on SIC. These differences determine the overall impact of cyclones on sea ice (Figure 5.3f). Contrary, the changes in overall cyclone impacts in November (Figure 5.3i) are dominated by a strong intensification of SIC decreases before/during cyclones (Figure 5.3g), which extend across almost the complete ice-covered parts of the Barents and Kara Seas. After cyclone passages, SIC increases become more intense in the northeastern Kara Sea and west of Franz-Josef-Land and less intense close to the ice edge (Figure 5.3h).
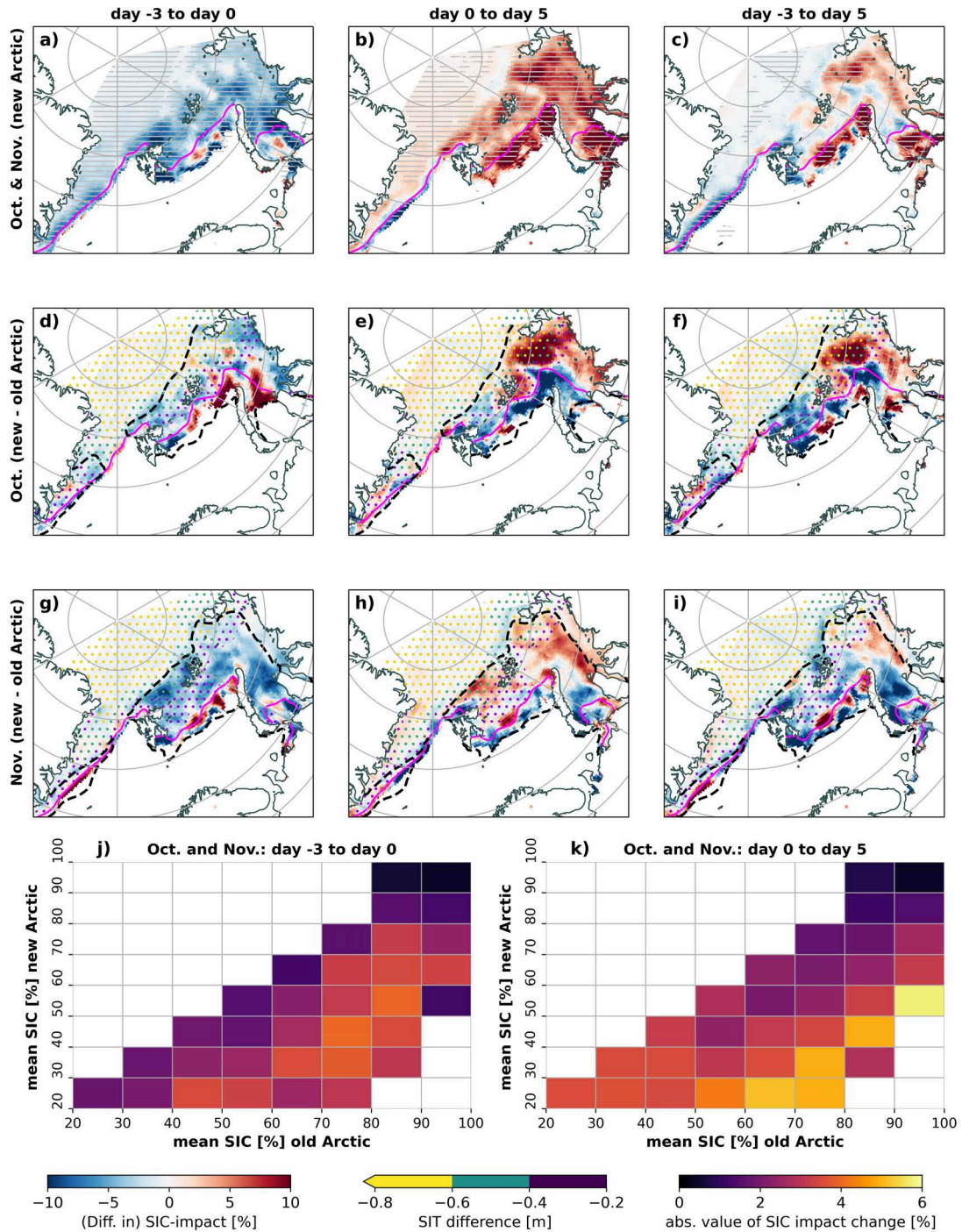
Figure 5.3: Subplots (a-c) show cyclone impacts on SIC for different daily time scales averaged for October and November 2000–2018. Hatches indicate statistical significance on 95 %-level. Subplots (d-i) show difference (2000–2018 minus 1979–1999) in cyclone impacts on SIC (blue-red colors) and SIT (colored dots) for October (d-f) and November (g-i). Black dashed line indicates grid-cells with at least 10 % SIC decline. Solid magenta line in (a-i) shows 15 % SIC contour for 2000–2018. Subplots (j-k) show absolute values of changes in cyclone impacts on SIC (2000–2018 minus 1979–1999) for different SIC bins.

The vast majority of these changed cyclone impacts between the new and old Arctic occurs in regions with a decline in mean SIC between both time periods (Figure 5.3d-i). In contrast, regions with simultaneous intensified cyclone impacts and comparatively strong SIT decline, as e.g. found in October and west of Severnaya Zemlya, are more limited. To follow-up on this, we group changes in cyclone impacts between the old and new Arctic across all grid-cells in the study domain (and for October and November combined) by the respective mean SIC and SIT in both periods (Figure 5.3j,k, Supplementary Figure S5.3).

Our results clearly demonstrate that the absolute values of changes in the SIC decreases before/during cyclones (Figure 5.3j) are higher, wherever SIC is declined in the new Arctic. This relationship is not equally clear for SIT (Supplementary Figure S5.3), confirming that particularly the decline in mean SIC (which results in a more mobile ice cover; e.g., Spreen et al., 2011) is the primary driver of amplified destructive cyclone impacts on SIC. This finding is in accordance with the linear (exponential) relation between ice strength and SIT (SIC) (ice strength parameterization of Hibler, 1979).

For the days following cyclones, the relation between decreased mean SIC and intensified SIC changes is even stronger than before/during cyclones, but only for grid-cells with medium-high SIC (above 50 %) in the old Arctic (Figure 5.3k). Presumably, the decline in mean SIC enhances the potential for sea-ice growth, when the ocean is exposed to cold air temperatures after the cyclone passage (e.g., Aue et al., 2023). However, for grid-cells that already had a rather low SIC (below 50 %) in the old Arctic, the change of cyclone impacts does not really depend on mean SIC changes anymore. This indicates that the weakening of previously existing SIC increases following cyclones in the old Arctic, which occurs at grid-cells close to the ice edge (see e.g. blue colors in Figure 5.3e), seems to be driven differently, namely by thermodynamic processes.

To substantiate this, we compare the mean 2m air temperature between old and new Arctic for October and November (Supplementary Figure S5.4). This reveals that the mean position of the $-1.8°C$ isotherm (freezing point of sea water) is significantly displaced northwards in the new Arctic in the Barents (and southern Kara) Sea, particularly in October. This suggests that, close to the ice edge, a rise in mean air temperature hampers a thermodynamic recovery of the ice cover after it has been damaged by strong winds during a cyclone passage. This mechanism could thus explain the weakened SIC increase following cyclones and the less pronounced relation between SIC changes (following cyclones) and the mean SIC in grid-cells close to the ice edge.

5.6   Conclusions

Our analysis of cyclone impacts on SIC in the Greenland, Barents and Kara Seas revealed statistically significant impacts for all months of the year. Those i) are subject to strong variability in space (region to region) and time (before/during vs. after cyclone passages, month to month), and ii) exhibit a distinct seasonal cycle (stronger impacts in the cold season, but weaker in summer) associated with variations in cyclone intensity and sea-ice conditions (SIC and SIT) underneath the cyclone tracks. We further reveal year-round, statistically significant changes in cyclone impacts on SIC during the last four decades, which are magnitude-wise strongest in autumn. The pronounced spatiotemporal variability is striking and should be considered in future research on trends in cyclone impacts on sea ice, e.g. focusing on different regions or exploiting model projections. For the Barents and Kara Seas in October and November, we relate an intensification of SIC decreases during cyclone passages to a preceding decrease in mean SIC. Notably, however, the thermodynamic SIC increasing effects following cyclones intensify only in sufficiently cold regions, resulting in opposing trends of overall cyclone impacts on SIC in the Barents Sea (negative trend) and the Kara Sea (positive trend) in October.

Our finding that changes in ice conditions (rather than cyclone intensity changes) are responsible for intensified cyclone impacts is consistent with studies, which attribute an observed acceleration of ice drift speed mainly to ice thinning (rather than to wind speed increase) (Spreen et al., 2011; Zhang et al., 2022). An ongoing shift in cyclone impacts on SIC in the Barents Sea from overall SIC-increasing towards overall SIC-decreasing in summer/autumn emphasizes that cyclone-sea ice feedbacks are important for future changes of the Arctic sea ice and that it is crucial to capture them correctly in model simulations. To assess cyclone impacts on smaller scale sea-ice deformation characteristics such as leads, which cannot be covered by ERA5, future research exploiting sea ice data at high horizontal resolution would be beneficial.

5.7   Supplementary material

1. Figure S5.1: 7-year running means of Cyclone impacts on SIC.

2. Figure S5.2: Trends in cyclone impacts on SIC.

3. Figure S5.3: Changes in cyclone impacts between the old and new Arctic in October and November depending on mean sea-ice thickness.

4. Figure S5.4: Recent changes in 2m air temperature in October and November.
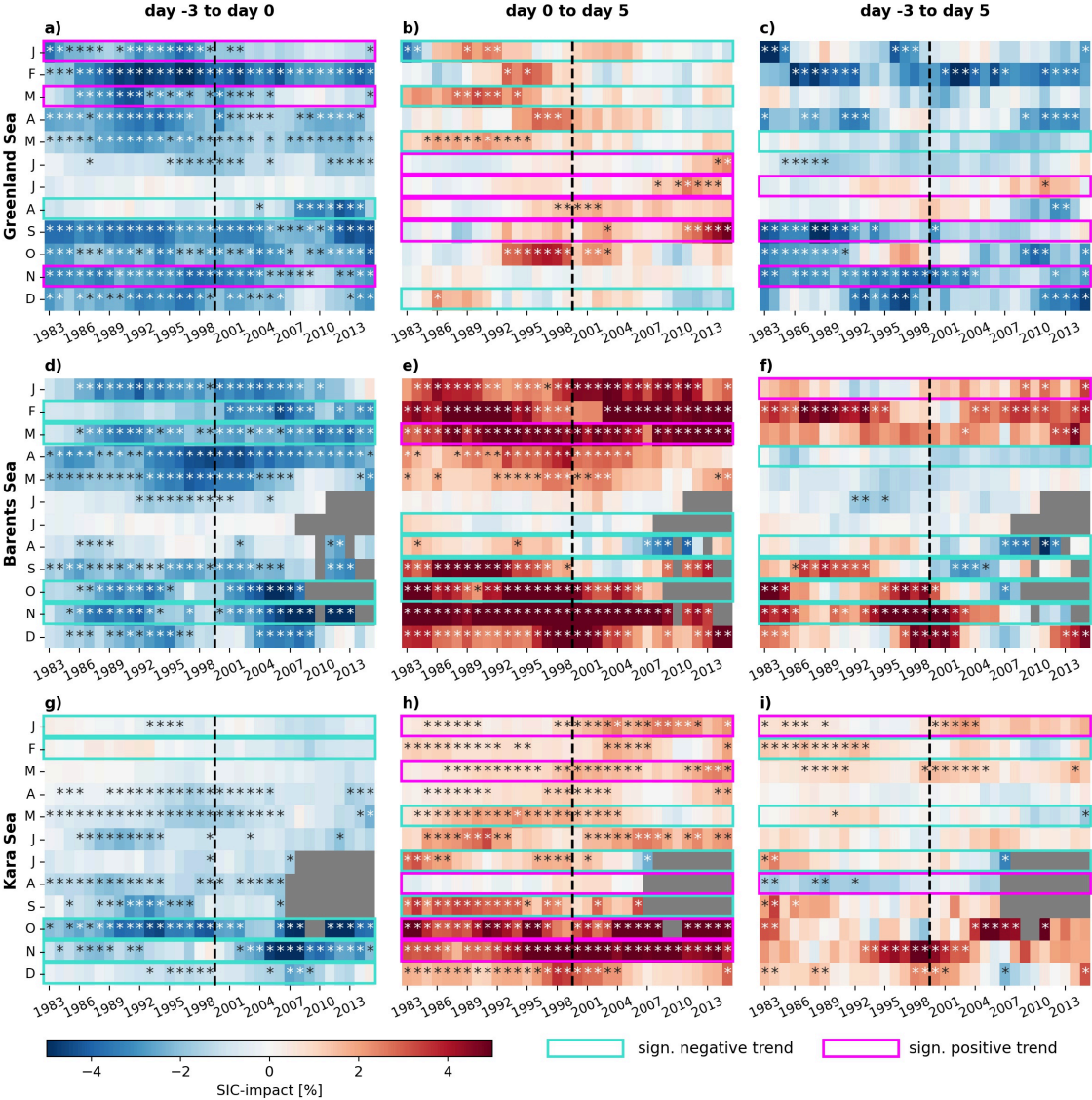
Figure S5.1: 7-year running means of anomalous SIC changes associated with cyclone passages (SIC-impact in %) in the Greenland (a-c), Barents (d-f) and Kara Seas (g-i) for each month. Stars indicate statistical significance, magenta (turquoise) boxes indicate significant positive (negative) trends of these changes. Black dashed line separates old and new Arctic time period. Grey colored time steps are excluded due to a too low sea-ice extent in the region. All statistical significance is at the 95 % level.

	day -3 to day 0				day 0 to day 5				day -3 to day 5		
	Greenland Sea	Barents Sea	Kara Sea		Greenland Sea	Barents Sea	Kara Sea		Greenland Sea	Barents Sea	Kara Sea
Jan	**0.64**	0.12	**-0.36**	Jan	**-0.46**	**0.4**	**0.8**	Jan	0.2	**0.54**	**0.43**
Feb	0.41	**-0.88**	**-0.58**	Feb	-0.27	0.25	0.02	Feb	-0.09	**-0.56**	**-0.54**
Mar	**0.86**	-0.22	-0.25	Mar	**-1.07**	**0.35**	**0.4**	Mar	-0.23	0.11	0.14
Apr	**0.44**	-0.26	-0.26	Apr	0.03	-0.44	0.06	Apr	0.35	**-0.62**	-0.27
May	0.22	0.23	-0.13	May	**-0.62**	0.04	**-0.62**	May	**-0.44**	0.26	**-0.7**
June	-0.24	0.12	0.09	June	**0.56**	0.05	0.08	June	0.21	0.19	0.11
July	-0.04	0.02	-0.3	July	**0.46**	-0.32	**-0.94**	July	**0.46**	-0.23	**-1.16**
Aug	**-0.84**	-0.07	-0.0	Aug	**0.6**	**-1.31**	0.34	Aug	-0.26	**-1.26**	**0.36**
Sep	**0.35**	-0.17	**0.49**	Sep	**1.16**	**-1.67**	**-0.81**	Sep	**1.39**	**-1.56**	-0.48
Oct	-0.11	**-0.7**	**-0.55**	Oct	0.08	**-0.96**	**1.82**	Oct	-0.07	**-1.47**	**1.63**
Nov	**0.41**	**-1.04**	**-1.1**	Nov	0.06	-0.16	**0.99**	Nov	**0.5**	**-1.08**	-0.05
Dec	**0.47**	-0.06	**-0.41**	Dec	**-0.6**	0.02	-0.07	Dec	-0.09	0.01	-0.44

Figure S5.2: Trend in 11-year running means of cyclone impacts on SIC between 1979 and 2018 in % per decade. Statistically significant trends are printed bold. Trends above (below) 1 (-1) % per decade are printed in red (blue) to highlight the strongest trends.
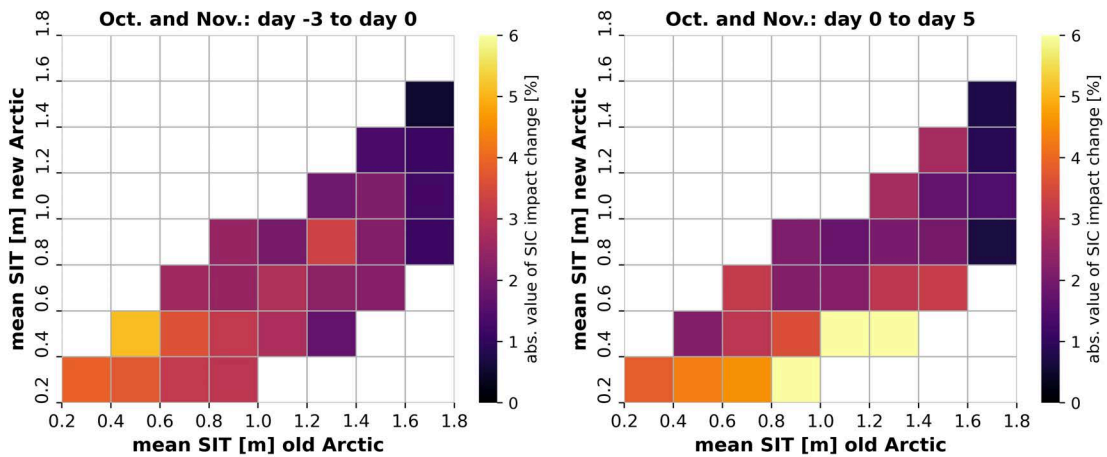
Figure S5.3: Absolute values of changes in cyclone impacts on SIC between 2000-2018 and 1979-1999 (new minus old Arctic) for different SIT bins for October-November.
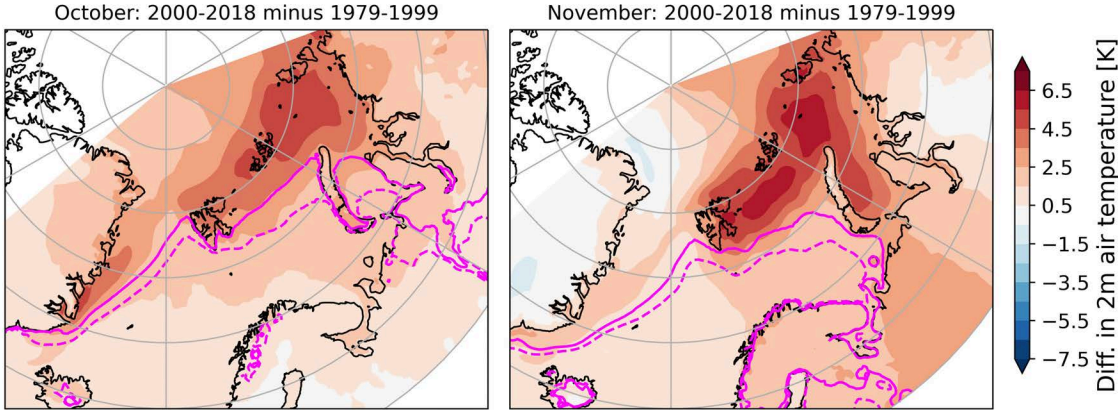
Figure S5.4: Difference in mean 2m air temperature for October (left) and November (right) between 2000-2018 and 1979-1999 (new minus old Arctic). Solid (dashed) magenta line indicates $-1.8°$ isotherm for 2000-2018 (1979-1999). The difference is statistically significant in the whole study domain at the 95 % level.

6 Conclusions and Outlook

The topic of this thesis is the impact of cyclones on the sea-ice cover in the Atlantic Arctic Ocean. Findings that emerged from the three presented publications (chapters 3–5) have substantially expanded the state of knowledge within this field. In the following, final chapter of this thesis, these findings are synthesized in the context of the three initially raised research questions (RQs). Finally, this thesis is concluded by an outlook on promising paths for future research regarding cyclone impacts on sea ice.

6.1 What is the statistical impact of cyclone passages on sea-ice concentration (SIC) in the Atlantic Arctic Ocean?

In order to address RQ1, the impact of cyclone passages on SIC in the Atlantic Arctic Ocean has been statistically quantified. Hereby, the following new aspects have been considered: The dependency of cyclone impacts on the considered time scale, detailed regional differences between the Greenland, Barents and Kara Seas, the dependency on cyclone depth, the state of ice cover, and the time of year. Considering these new aspects, cyclone impacts on SIC in the Atlantic Arctic Ocean can be summarized as follows:

Conclusion 1: Cyclones significantly impact SIC in the Atlantic Arctic Ocean from autumn to spring:

Results from chapter 5 of this thesis provided the first quantification of monthly cyclone impacts on SIC covering the whole year. This analysis revealed that cyclones are a significant driver of SIC variability in the Greenland and Barents Seas from autumn to spring (chapter 5, Figure 5.2). In contrast, cyclone-related SIC changes are pronounced weakly or are completely absent in the summer months in these regions. The weakened cyclone impacts in summer compared to the remaining seasons are related to an on average lower intensity of cyclones in this season (chapter 5, Figure 5.1). In the Kara Sea, cyclone impacts on SIC are strongest in autumn and comparatively weak throughout the rest of the year. This different annual cycle compared to the Greenland and Barents Sea was shown to be related to a higher mean SIC and SIT in the Kara Sea in winter and spring. In conclusion, findings from this thesis demonstrate that variations in I) cyclone intensity and II) local sea-ice conditions (mean SIC, SIT) generally affect cyclone impacts on SIC and

result in a pronounced annual cycle of these impacts. For winter (December to February), the effects of varying cyclone intensity were specifically quantified: SIC changes during intense winter cyclones (maximum depth above 20 hPa) in the Greenland and Barents Seas were shown to be roughly twice as high as during non intense winter cyclones, when both are situated over low to medium SIC (chapter 3, Figure 3.1).

Conclusion 2: Cyclone impacts on SIC can be separated in an initial SIC-decreasing phase followed by a SIC-increasing phase:

Within this thesis, the temporal variability of cyclone impacts on SIC on time scales of up to a week before/after each cyclone occurrence has been analyzed. This analysis revealed that throughout the year, cyclone impacts on SIC can be separated into two phases:

The first phase consists of a decrease in SIC starting up to three days before the cyclone passage. This initial decrease in SIC can be found in all regions of the study domain, namely in the Greenland, Barents and Kara Seas, and for most parts of the year (see conclusion 1). The second phase consists of a SIC increase starting directly after the cyclone arrival and lasting for up to a week. This SIC-increasing phase of cyclone impacts is mostly limited to the Barents and Kara Seas and can only be found occasionally in the Greenland Sea. Quantitative values of both the initial cyclone-related SIC decrease and the following cyclone-related SIC increase range from -5 % to +5 % on regional average (chapter 5, Figure 5.2), but are higher for individual grid-cells (chapter 3, Figure 3.1).

The determined SIC increase following cyclones agrees with results from a recent study by Schreiber and Serreze (2020), who focused on day 0 to day 4 relative to the cyclone passage in their analysis. Findings from this thesis suggest, however, that overall impacts of cyclones on SIC are captured more accurately considering a larger time window including the initial, cyclone-related SIC decrease, such as day -3 to day 5 relative to each cyclone. Results from this thesis further demonstrate that the SIC increase following cyclones acts over a longer time (up to a week) than the initial SIC decrease before/during cyclones (up to 3 days). This indicates that both phases of cyclone impacts are related to different, physical mechanisms (see following section 6.2).

Conclusion 3: Cyclone impacts on SIC exhibit a pronounced regional difference between the Greenland Sea and the Barents and Kara Seas:

Throughout autumn to spring, regionally different SIC changes following cyclone passages are found in the Greenland Sea compared to the Barents and Kara Seas. Following cyclones, significant increases in SIC occur regularly in the Barents and Kara Seas, while no significant changes in SIC are found in the Greenland Sea for most parts of the year and

most time periods within 1979–2018 (chapter 5, Figure 5.2). Occasionally, comparatively weak but significant increases in SIC following cyclones occur also in the Greenland Sea, e.g. for March and May 1979–1995. The most likely explanation for these temporary deviations from the regular pattern is natural variability of the climate system, causing e.g. variations in the tracks and properties of cyclones or in the state of the sea-ice cover.

The regionally different response of the sea ice following a cyclone passage results in contrasting overall SIC impacts of cyclones (day -3 to day 5). This contrast between *overall SIC-decreasing* cyclone impacts in the Greenland Sea and *overall SIC-increasing* cyclone impacts in the Barents Sea (and to a smaller degree in the Kara Sea) is strongly pronounced on winter average (December to February). For winter 2000–2020, regionally averaged overall SIC decreases of up to -7 % in the Greenland Sea are contrasted by overall SIC increases of up to +4 % in the Barents Sea (Chapter 3, Figure 3.1). A qualitative summary on seasonally and regionally different cyclone impacts on SIC based on the findings of this thesis is provided in Figure 6.1.

Open scientific questions related to RQ1

First, the study domain of the here presented work is limited to the Atlantic Arctic Ocean consisting of the Greenland, Barents and Kara Seas. Thus, further analysis covering the central Arctic Ocean and the Pacific Arctic marginal seas would be beneficial. Results from other studies already indicate, that these regions might be particularly interesting for cyclone impacts on SIC in summer (e.g., Finocchio and Doyle, 2021), a season which did reveal only comparatively few statistically significant results for the Atlantic Arctic Ocean.

Second, the focus of the here presented work is on cyclone-related SIC changes over a few days or at most a few weeks. On this particular time scales, statistically significant cyclone impacts on SIC have been revealed. A remaining question is, however, if the sum of these short-term cyclone impacts is also relevant for sea-ice variability on longer time scales. For example, does the number of cyclone passages in a region significantly impact seasonally averaged anomalies of the sea-ice area? Do winters with comparatively high cyclone activity in the Barents Sea result in positive, regional SIC anomalies, as could be assumed based on the cyclones' overall SIC-increasing effect on daily time scales? Results from this thesis emphasize that the answer to these questions presumably depends on several factors including the mean intensity of cyclones and the local SIC conditions. Another related question is whether the Arctic sea-ice cover has a memory on cyclone passages over longer time scales, e.g. from the preceding month/season to the following one. For example, results from Valkonen et al. (2021) indicate a significant correlation between cyclone counts in the cold season and SIC anomalies in the following warm season.

Cyclone impacts on SIC	Spring 🌱		Summer ☀️		Autumn 🍃		Winter ❄️	
	during	after	during	after	during	after	during	after
Greenland Sea	↘ +	➡ –	↙ –	➡ +	⬇ +	➡ +	↙ +	➡ –
Barents Sea	⬇	↗ +	➡	↘ –	⬇ –	↗ –	⬇ –	⬆ +
Kara Sea	↘	↗ +/–	↘	↗ +/–	↘ +/–	↗ +/–	↘ –	↗ +

Figure 6.1: Red/blue arrows pointing upwards/downwards (obliquely upwards/downwards) indicate significant SIC increasing/decreasing cyclone impacts in all months (at least one month) of a season for 2000–2018. "+"/"-" symbols indicate significant positive/negative trends in at least one month of a season for 1979–2018. For disagreeing monthly trends, two symbols are depicted. Red (blue) "+" ("-") symbols indicate strong trends above (below) +1 % (-1 %) per decade.

6.2 What are the individual contributions of dynamic and thermodynamic processes to sea-ice changes related to cyclones?

Dynamic and thermodynamic sea-ice changes have rarely been quantified separately during cyclone events, mostly due to a lack of suitable data. In this thesis, a simulation of the coupled atmosphere-ocean-sea ice model HIRHAM-NAOSIM 2.2 has been utilized to reveal new insights into this topic based on a case study (chapter 4). The simulation was nudged to the ERA5 reanalysis and the analysis was accompanied by field observations from the MOSAiC expedition as well as remote sensing sea-ice data. Results from this case study are complemented by a composite analysis of SEB and wind speed and direction for cyclone conditions based on ERA5 data (chapter 3). Based on this set-up, the following main conclusions can be drawn:

Conclusion 1: Sea-ice changes during three intense cyclones in February 2020 are dominated by dynamic mechanisms:

An analysis of three specific cyclone events in February 2020 based on a coupled model simulation revealed a dominance of dynamic mechanisms (such as ice drift and deformation) for the caused overall sea-ice changes. This was found for changes in both SIC (chapter 4, Figure 4.4) and SIT (chapter 4, Figure 4.7). The dominance of dynamic sea-ice changes lasted not only for the comparatively short time scales of individual cyclones (up to 5 days), but also for more than two weeks covering all three consecutive cyclone events.

Analyzing the last of the three consecutive cyclones, however, revealed a dependence of the
relative importance of dynamic and thermodynamic SIC changes on the time scale (chap-
ter 4, Figure4.6). Specifically, the dominance of dynamic sea-ice changes was particularly
pronounced in the early stage of the cyclone passage, whereas following the cyclone event,
thermodynamic sea-ice changes locally took the lead.

The southerly winds during the initial phase of a cyclone passage are often related to warm
air intrusions and/or atmospheric rivers (Guo et al., 2020). The thermodynamic impact of
such events on the surface energy budget and the sea-ice cover is a very recent research topic
(e.g., Zhang et al., 2023). In this regard, findings from chapter 4 of this thesis emphasize
the possibility that a thermodynamic stalling of ice growth in winter during such events
promoting a thinner ice cover can potentially be out weighted by a dynamic thickening of
the ice under convergent ice drift due to the associated southerly winds. This highlights the
complexity of the interplay of dynamic and thermodynamic sea-ice changes in the context
of cyclone events (and related warm air intrusions and atmospheric rivers) and emphasizes
the need for further dedicated research on this topic.

**Conclusion 2: Winter cyclones (in the Barents Sea) typically cause strong dynamic
redistribution of sea ice followed by enhanced thermodynamic ice growth:**

From a broader perspective, statistical results from chapter 3 of this thesis revealed positive
SEB anomalies (more energy gain/less energy loss of the surface) and enhanced on-ice
wind speed prior to and during cyclone passages in the Barents Sea in winter based on
ERA5 data. Such conditions principally favor both dynamically and thermodynamically
driven SIC decreases. For the days following cyclones, anomalies in SEB and wind speed
are of opposite sign, thus favoring dynamic and thermodynamic SIC increases.

To separate both mechanisms, further data e.g. from a coupled model simulation (chapter
4) is needed. Hereby, results from a case study of three intense cyclones from February
2020 (see conclusion 1) revealed an initial dominance of dynamic sea-ice changes followed
by enhanced thermodynamic sea-ice changes for the last of the three cyclones. Extending
the analysis of the model simulation to all MOSAiC winter (January–March 2020) cyclones
suggests that this pattern is typical of winter cyclones (chapter 4, Figure 4.9). Results from
this thesis thus provide quantitative evidence for the hypothesis raised earlier by Schreiber
and Serreze (2020), whereas anomalous SIC changes following cyclones are dominated by
thermodynamic mechanisms.

Importantly, the findings of this thesis further indicate that the enhanced thermodynamic
ice growth following a cyclone is only possible, if not another cyclone follows in quick
succession (chapter 4, Figure 4.9). Thus, particularly cyclone clusters (a group of cyclones

traversing the sea ice within short time) can have strong destructive impacts on the Arctic sea ice. Results from this thesis thus emphasize that the strongest cyclone-related SIC decreases might not necessarily occur during the most intense cyclones, but rather during a group of several, consecutive events, which should be considered in future research.

Conclusion 3: The overall SIC-increasing effect of winter cyclones is presumably related to divergence-induced new ice formation:

In chapters 3 and 5, statistically significant overall (day -3 to day 5) SIC-increasing effects of cyclones were found in the Barents Sea and (to a smaller degree) in the Kara Sea in the cold season. These overall SIC increases are determined by comparatively long lasting SIC increases following the cyclone passage, which were shown to be primarily related to thermodynamic processes (see previous conclusion 2).

More specifically, the overall SIC increases due to cyclones in the cold seasons are presumably related to divergence-induced new ice formation. Hereby, the formation of open water areas (such as leads) in the ice cover due to divergent ice drift provides room for the growth of new ice, thus potentially increasing the regional sea-ice area. It was recently shown that in divergent ice drift regimes in the Arctic, new ice formation in leads contributes up to 30 % to the sea-ice mass balance (von Albedyll et al., 2022). Winter cyclones in the Barents (and Kara) Seas seemingly contribute to this process by opening up the sea-ice cover and transporting cold-dry air masses over these openings along with the northerly winds on their western flank. It should be noted that a requirement for such enhanced ice growth under cold atmospheric conditions is the presence of sufficiently cold surface waters.

Based on the combined findings of chapters 3–5, the physical mechanisms of cyclone impacts on SIC in the Atlantic Arctic Ocean in winter can be summarized as follows (schematic overview in Figure 6.2): A first phase of SIC decreases is driven by dynamic SIC changes, specifically a shift of the ice edge due to winds directed from the open ocean towards the ice cover. In the following, second phase, winds directed from the ice cover towards the ocean again result in shift of the ice edge and additionally cause lead formation under divergent ice drift. These dynamic SIC changes are accompanied by enhanced ice growth in the newly formed open water areas, eventually resulting in a net gain in sea-ice area. In contrast to the Barents and Kara Seas, this second phase is not found in the Greenland Sea, resulting in regionally different overall cyclone impacts on sea ice.

Open scientific questions related to RQ2

The model-based quantification of dynamic and thermodynamic sea-ice impacts of cyclones within this thesis was limited to a case study covering MOSAiC winter cyclones.
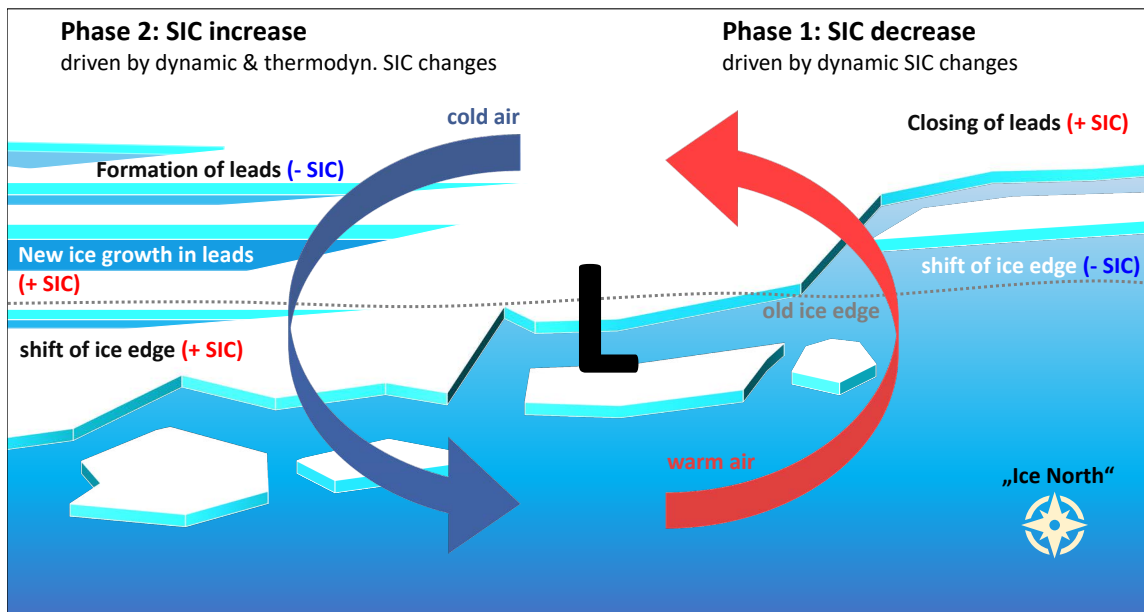
Figure 6.2: Schematic overview on processes contributing to SIC changes related to the passages of winter cyclones in the Atlantic Arctic Ocean. Processes are grouped into two phases: The initial, cyclone-related SIC decrease (phase 1) and the SIC increase following the cyclone passage (phase 2).

In principal, the processes underlying cyclone-related sea-ice changes in winter should be valid in general and not vary from event to event; Nonetheless, in order to gain further confidence in the general validity of the presented results, a statistical analysis covering cyclones from several years would be beneficial. Ideally, such an extended analysis of dynamic and thermodynamic cyclone impacts would not be solely model based but accompanied by e.g. remote sensing based approaches.

As indicated before, results from chapter 4 emphasize that particularly the occurrence of cyclone clusters results in strong SIC decreases, because a thermodynamic recovery of the sea-ice cover is prevented by the continuous cyclonic wind forcing. Future research should aim to quantitatively assess this effect by comparing the sea-ice impacts of cyclone clusters and individual cyclone events. Additionally, the atmospheric conditions that result in the occurrence of cyclone clusters in the Atlantic Arctic Ocean should be analyzed.

Another possible topic for follow-up research consists of a comparison of the relative importance of cyclone-related dynamic and thermodynamic sea-ice changes between winter and summer. In Arctic summer, the incoming shortwave radiation forms an additional factor determining thermodynamic sea-ice changes. Apart from that, a thinner and less concentrated ice cover compared to winter can facilitate dynamic sea-ice changes during cyclones. Thus, there is reason to assume that the interplay of dynamics and thermodynamics related to cyclone passages is different in summer than in winter.

6.3 Do the SIC impacts of cyclones change in a warming Arctic and what are the related mechanisms?

This thesis provides the first assessment of recent trends in cyclone impacts on SIC on a monthly basis for the whole year (chapter 5). The analysis period covers the years between 1979 and 2018 and the following main conclusions can be drawn:

Conclusion 1: Significant trends in cyclone impacts on SIC exist throughout the year:

Results from chapter 5 have demonstrated that statistically significant changes in cyclone impacts on SIC between 1979 and 2018 are found throughout the year. However, these recent changes strongly I) vary between the Greenland, Barents and Kara Seas, and II) depend on the considered time scale (i.e. the days before/during and the days following a cyclone passage). Importantly, trends in cyclone impacts on SIC also vary from month to month (chapter 5, Figure 5.2). Statistically significant trends in cyclone impacts on SIC are visualized in the qualitative summary of seasonal cyclone impacts in Figure 6.1.

In general, the strongest trends in cyclone impacts on SIC are found for autumn (October and November) in the Barents and Kara Seas. In November, the SIC decreases before/during cyclone passages exhibit a negative trend of about -1 % per decade in the Barents and Kara Seas. This corresponds roughly to a doubling of the magnitude of these destructive cyclone impacts on SIC between 1979 and 2018. With respect to the SIC increases following cyclones, a weakening associated with a negative trend of -1.6 % per decade (-1 % per decade) was found in September (October) in the Barents Sea. In the Kara Sea, however, an intensification associated with a positive trend of +1.8 % per decade (+1 % per decade) was found in October (November).

Conclusion 2: Changes in the state of the ice cover rather than changes in cyclone properties drive trends in cyclone impacts on SIC:

The analysis of trends in cyclone impacts on SIC in this thesis was accompanied by an analysis of changes in relevant background conditions, namely in mean SIC, mean SIT and in cyclone intensity. This revealed that changes in the state of the ice cover rather than changes in cyclone properties drive recent changes in cyclone impacts (chapter 5, Figure 5.1, Figure 5.3). This finding agrees well with studies who attribute an observed acceleration of sea-ice drift speed to changes in sea-ice conditions rather than to changes in atmospheric wind forcing (Spreen et al., 2011; Zhang et al., 2022).

Specifically for October and November, an intensification of destructive cyclone impacts on SIC in the Barents and Kara Seas was related to a preceding decrease in mean SIC (chapter 5, Figure 5.3). As was introduced in section 2.3 in equation 2.13, a decrease in mean SIC hampers the ability of the sea ice to resist atmospheric forcing, because it weakens the internal ice strength (which is assumed to depend exponentially on the ice concentration).

Conclusion 3: Previously observed overall-SIC increasing effects of cyclones in the Barents Sea in autumn are disappearing recently:

Assessing recent changes in the overall impact of cyclones on SIC (from day -3 to day 5 relative to the cyclone passage) revealed significant negative trends between -1.1 % per decade and -1.6 % per decade in the Barents Sea in autumn. Particularly for October, a northward displacement of the -1.8 °C isotherm (freezing point of sea water) in the Barents Sea related to a recent increase in the two meter air temperature was found. This suggests that the negative trends in overall cyclone impacts on SIC are (at least partly) related to too high air temperatures, which hamper new ice formation in open water areas such as leads. Recent studies have reported on a shift in the peak of the ice growing season in the Barents and Kara Seas from October/November towards later times of the year (Cornish et al., 2022). This agrees well with the weakening of overall SIC-increasing cyclone impacts in October/November in the Barents Sea as found in this thesis.

Noteworthy, results from chapter 5 provide evidence on an ongoing regime shift in cyclone impacts in the Barents Sea in autumn from *overall SIC increasing* to *overall SIC decreasing*. New, statistically significant overall SIC decreases already emerged in August recently (chapter 5, Figure 5.2), while for September–November, this can be expected to happen in the near future if the current trends continue. In that case, cyclone impacts on SIC in the Barents Sea (between August and November) will become more and more similar to those in the Greenland Sea, and the pronounced regional difference between both marginal seas will disappear.

Open scientific questions related to RQ3

In accordance with the previous conclusion in section 6.1, the analysis of trends in cyclone impacts on SIC could benefit from an extension of the study domain to the Pacific part of the Arctic Ocean. For this region, a significant intensification of cyclone related sea-ice losses in August has been revealed in a recent study (Finocchio et al., 2022), but so far, no quantification of monthly cyclone impact trends throughout the whole year was conducted.

The overarching motivation behind the analysis of trends in cyclone impacts on SIC is to arrive at more reliable predictions on future cyclone impacts in a warming Arctic. Thus,

directly analyzing these future sea-ice impacts based on model projections would be the logical next step. A possible starting point would be to compare I) the absolute values and II) the recent trends of cyclone impacts on SIC between observations/reanalysis data and model simulations for a historic overlap period. That way it could be assessed whether current climate models are able to realistically capture cyclone impacts on SIC and the related trends. Afterwards, model projections could be analyzed.

One of the findings of this thesis regarding RQ3 is that cyclone intensity has not changed significantly over the last four decades. Thus, changes in sea-ice conditions are most likely responsible for trends in cyclone impacts. However, there is scientific evidence that relevant cyclone intensity changes can be expected in a future climate characterized by a further sea-ice retreat (Parker et al., 2022). Consequently, changes in cyclone properties could form another important factor (in addition to sea-ice changes) for cyclone impacts on SIC in a future Arctic.

6.4 Ways forward

Findings of this thesis highlight the importance of cyclone passages for the sea-ice cover in the Atlantic Arctic Ocean and provide a quantitative assessment of cyclone impacts on SIC including several novel aspects. Still, further open questions remain with respect to the coupling between cyclones and Arctic sea ice. Since the Atlantic Arctic Ocean is a key region for the whole Arctic climate system (e.g., Smedsrud et al., 2013), addressing these knowledge gaps is particularly urgent for this region. Hereby, promising opportunities for follow-up research consist of I) processes and feedbacks which are not yet fully understood based on current studies and II) possible future changes of cyclone impacts on sea ice. Concerning I), a potential topic is the impact of cyclone passages on small-scale sea-ice deformation characteristics, such as leads.

Leads in the sea-ice cover are of high importance for the Arctic climate, because they enable fluxes of heat and moisture between the atmosphere and the Arctic ocean. That way, leads in the sea ice can substantially impact the atmospheric boundary layer (Lüpkes et al., 2008). The formation of leads in the Arctic sea ice is related to both oceanic and atmospheric forcing (Willmes et al., 2023). Based on the high wind speeds and abrupt changes in wind direction often associated with cyclone passages, it is a reasonable assumption that cyclones play an important role for lead formation in the Arctic. However, this has not yet been analyzed on a statistical basis. Since horizontally high-resolved sea-ice lead data sets have recently become available, e.g. from MODIS satellite data (Reiser et al., 2020) for approximately the last two decades, such an analysis is in principal achievable.

As mentioned before, the main motivation behind the presented analysis of recent changes in cyclone impacts on sea ice is to predict **future developments of cyclone impacts** in a warming Arctic. For example, findings from this thesis suggest that SIC-increasing effects of cyclones might be hampered in the future by too warm air temperatures. At the same time, a thinner and more mobile ice cover can potentially enhance dynamic sea-ice changes related to cyclones. It will be particularly interesting to see, whether feedback loops including cyclones and sea ice exist. Recent studies suggest that the retreat of the Arctic sea ice already resulted in an intensification of winter cyclones (Crawford et al., 2022) or at least will result in intensified cyclones in the future (Parker et al., 2022). Results from this thesis have demonstrated that more intense cyclones are related to a stronger, initial loss of SIC. This suggests that a positive feedback loop including ice retreat and cyclone intensity is within the realm of possibility.

In addition, a possible **importance of the ocean for cyclone-sea ice feedbacks** should be analyzed in more detail in future research. A recent study by Heukamp et al. (2023b) (see Appendix) relates variations in the transport of warm (cold) water masses into (out of) the Barents Sea to variations in regional cyclone activity. This emphasizes amongst others the possible existence of an additional pathway of cyclone impacts on sea ice including ocean dynamics, specifically the transport of warm water across the Barents Sea Opening. In principal, such an oceanic pathway of cyclone impacts on sea ice could be part of a positive feedback loop (Kovács et al., 2020; Akperov et al., 2020), where the enhanced inflow of warm water due to cyclones results in enhanced local sea-ice retreat and a related intensification of cyclones. In a recent study, however, no evidence for the existence of such a feedback loop was found (Heukamp et al., 2023a). It was shown in another recent study, though, that changes in the upper Arctic Ocean stratification in late summer can potentially enhance SIC-decreasing effects of cyclones, because they facilitate the up-mixing of warm water masses under high wind speed conditions (Finocchio et al., 2022). This mechanisms is a possible source of oceanic-driven changes in future cyclone impacts on sea ice and thus provides another noteworthy opportunity for further research.

Appendix: Cyclones Modulate the Control of the North Atlantic Oscillation on Transports into the Barents Sea

This appendix contains a study which I co-authored during my doctorate and which has not been presented before in this thesis. This study links atmospheric variability including cyclone activity in the Arctic to ocean dynamics.

Summary of the publication:

Abstract	The warm Atlantic Water transported into the Barents Sea plays a crucial role in winter sea ice extent, marine ecosystems, and mid-latitude weather. The North Atlantic Oscillation is known to be an important driver for the Atlantic Water transport variability in the Barents Sea Opening. Here, we find that the dependence of the Barents Sea Opening ocean volume transport variability on the North Atlantic Oscillation is non-stationary. Our results indicate that for the period 1995 to 2005, the link between the North Atlantic Oscillation and the transport variability in the Barents Sea Opening temporarily weakened before an eventual recovery. During this period, synoptic cyclones with unusual trajectories as a consequence of pronounced atmospheric blocking in the North Atlantic sector altered the large-scale and local wind patterns. This temporarily caused a state that the Barents Sea Opening transport variability is largely locally driven instead of being driven by the North Atlantic Oscillation. Our study suggests that an adequate representation of both the North Atlantic Oscillation and cyclone activity is necessary for climate models to better predict future changes in poleward ocean heat transport and Arctic climate.

Own Share	• I processed the cyclone occurrence data utilized in one chapter of the publication and contributed to the conception of this chapter. I further contributed to the design and interpretation of the related figures. • Along with the other co-authors, I contributed to the revision of the whole manuscript.

ARTICLE

Check for updates

Cyclones modulate the control of the North Atlantic Oscillation on transports into the Barents Sea

Finn Ole Heukamp [1✉], Lars Aue [2], Qiang Wang [1], Monica Ionita [1,3], Torsten Kanzow[1,4], Claudia Wekerle [1] & Annette Rinke [2]

The warm Atlantic Water transported into the Barents Sea plays a crucial role in winter sea ice extent, marine ecosystems, and mid-latitude weather. The North Atlantic Oscillation is known to be an important driver for the Atlantic Water transport variability in the Barents Sea Opening. Here, we find that the dependence of the Barents Sea Opening ocean volume transport variability on the North Atlantic Oscillation is non-stationary. Our results indicate that for the period 1995 to 2005, the link between the North Atlantic Oscillation and the transport variability in the Barents Sea Opening temporarily weakened before an eventual recovery. During this period, synoptic cyclones with unusual trajectories as a consequence of pronounced atmospheric blocking in the North Atlantic sector altered the large-scale and local wind patterns. This temporarily caused a state that the Barents Sea Opening transport variability is largely locally driven instead of being driven by the North Atlantic Oscillation. Our study suggests that an adequate representation of both the North Atlantic Oscillation and cyclone activity is necessary for climate models to better predict future changes in poleward ocean heat transport and Arctic climate.

[1] Alfred-Wegener-Institute, Helmholtz Center for Polar and Marine Research, Bremerhaven, Germany. [2] Alfred-Wegener-Institute, Helmholtz Center for Polar and Marine Research, Potsdam, Germany. [3] Faculty of Forestry, Stefan cel Mare University of Suceava, Suceava, Romania. [4] Faculty of Physics/Electrical Engineering, University of Bremen, Bremen, Germany. ✉email: finn.heukamp@awi.de

T he Barents Sea (BS) is one of the two major oceanic gateways for warm and saline Atlantic Water (AW) to enter the Arctic Ocean. The temperature and volume, thus oceanic heat, of the AW entering the BS fundamentally shape winter sea ice conditions and air–sea fluxes in the BS[1,2]. The extent of the sea ice and the strength of air–sea heat exchange are crucial for marine ecosystems and local fishery[3,4], European winter weather[5,6] and terrestrial climate[7], as well as shipping routes[8].

The warm AW originates from the tropical Atlantic Ocean. As part of the Atlantic Meridional Overturning Circulation, it is transported north by the Gulf Stream and the North Atlantic Current before reaching the Nordic Seas and finally the Arctic basin[9]. On its way north, most of the AW entering the BS is carried by the Norwegian Atlantic Slope Current (NASC)[10–13]. From its entry point into the Norwegian Sea to Fram Strait, the NASC exhibits a quasi-simultaneous flow variability, implying that the volume transport variations are driven by the large-scale wind fields over the Nordic Seas domain[14]. In addition, the wind stress curl over the North Atlantic affects the interannual variability of the NASC volume transport from upstream[15].

The AW enters the BS as a multi-core current through the central Barents Sea Opening (BSO). The northern part of the BSO is dominated by cold and relatively fresh Polar Water on the Svalbard shelf and a strong and confined westward-directed current south of Bear Island at ~74.3°N, transporting Polar Water and modified AW out of the BS[16]. Along the Norwegian coast, the Norwegian Coastal Current carries low-salinity water into the BS. The observational estimate of the net BSO volume transport is 2.3 Sv[17]. Concerning the individual components, the Norwegian Coastal Current inflow is estimated to be 1.2 Sv, the central BSO inflow is about 2 Sv, and the westward-directed current at the Bear Island slope roughly balances the Norwegian Coastal Current volume transport, transporting about 1.2 Sv out of the BS[17,18]. The magnitude of the outflow is linked to the wind stress curl over the Svalbard shelf and the flow direction, on daily timescales, can reverse in the presence of strong cyclonic wind anomalies[16,19]. The main AW pathways toward the Arctic and the main currents in the BSO are shown in Fig. 1. Although long-term in situ ocean current measurements are sparse in the BSO, observations and model studies agree that strong variability in the ocean volume transport through the BSO is linked to both local[18–22] and remote[20,22,23] wind forcing. For the latter, the North Atlantic Oscillation (NAO), as a leading mode of sea level pressure (SLP) variability over the North Atlantic, is suggested to play a dominant role[15,20].

The NAO pattern can be characterized as an air pressure dipole of the Icelandic Low and the Azores High. It is usually computed as the first empirical orthogonal function of the SLP in the North Atlantic sector, and the associated principal component time-series is taken as the NAO index[24–26]. The NAO is associated with a certain wind anomaly pattern, whose sign and strength influence ocean heat content and gyre circulation in the North Atlantic and Nordic Seas[26]. Increased northward winds along the Norwegian coast associated with a positive NAO cause a narrowing and strengthening of the NASC and enhanced BSO inflow[21,27]. Thus, a narrower and strengthened NASC results in (i) less surface heat loss in the Norwegian Sea and consequently warmer AW temperature, and (ii) increased volume transport through the BSO because the NASC resides closer to the coast so that a larger portion of AW enters the BS[22].

After being predominantly negative in the 1970s and 1980s, the winter NAO shifted to a positive state in the early 1990s[24] with a related increase in AW transport toward the Arctic Ocean[28]. From the mid-1990s onward, the NAO index has been neither predominantly positive nor negative but strongly fluctuates from

year to year. There was a high correlation between NAO and BSO AW volume transport as well as BS sea ice cover before 2000, but the correlation broke down around the year 2000[18]. The cause for the breakdown is yet unknown and represents a major focus of this study.

In addition to the large-scale forcing, local SLP anomalies, e.g., associated with synoptic cyclones, can also have a significant impact on the transport through the BSO[16,19]. In general, the frequency and the path of cyclones in high latitudes are influenced by large-scale atmospheric conditions. Particularly the NAO has a strong influence on the winter storm tracks, with a positive (negative) NAO phase tending to increase (decrease) the frequency of cyclones in the vicinity of the climatological mean position of the Icelandic Low as well as in the Norwegian Sea[29,30]. In addition, the occurrence of atmospheric blocking and local baroclinicity, mainly influenced by upper-level winds and the jet stream, are important drivers of the variability of cyclone tracks in higher latitudes[29].

In this study, we disentangle the local and upstream forced contributions to transport anomalies through the BSO and evaluate their individual dependence on the NAO. We show that transport anomalies forced upstream at the Norwegian Atlantic coast are strongly bound to the NAO. This dependence, however, is not constant but varies in time. We further attribute a pronounced temporary breakdown of the co-variability between the BSO transport anomalies and the NAO in the 1995–2005 period to the anomalous occurrence of synoptic cyclones, affecting key regions relevant to the forcing of the BSO transport.
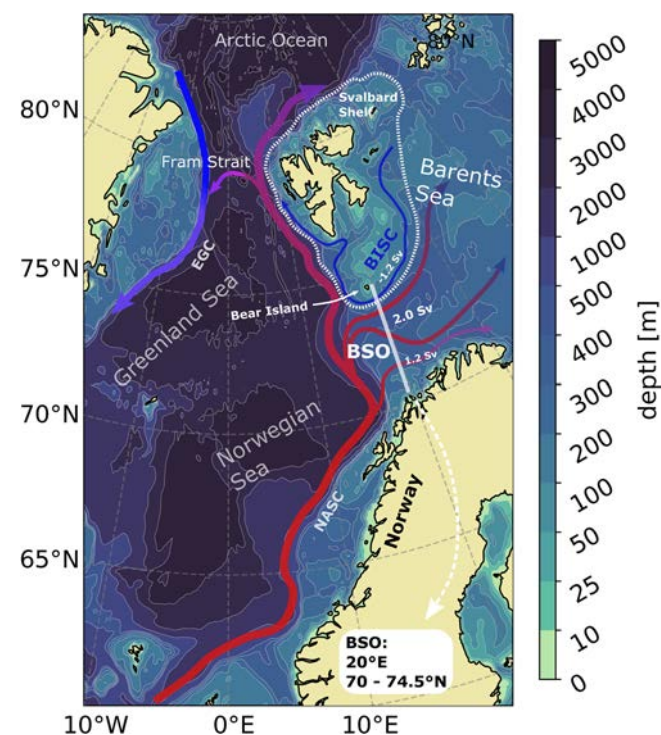
Fig. 1 Atlantic Water pathway through the Nordic Seas into the Barents Sea and Arctic Ocean. Overview of bathymetry, main currents transporting Atlantic Water towards the Arctic Ocean, and names of important islands, seas and currents. The BSO section where transports are evaluated in the model is highlighted by a white line. The wider shelf of Svalbard is encircled by a dashed white line. EGC East Greenland Current, NASC Norwegian Atlantic Slope Current, BSO Barents Sea Opening, BISC Bear Island Slope Current.

Results

(Co-)variability of local/upstream forced Barents Sea Opening transport and the North Atlantic Oscillation. The NAO, as the leading climate pattern in the North Atlantic sector, has a major impact on the transports through the BSO. Composite maps of 850 hPa geopotential height anomalies during winters with extraordinarily strong/weak net transports through the BSO (in CTRL, see "Methods") reveal a spatial structure that well resembles the air pressure dipole and wind anomalies associated with the NAO (Fig. 2 and Supplementary Fig. S1). For assessing the impact of the NAO on different components of the transport variability in the BSO, however, a separation of the transport components is needed. In order to separate the upstream and locally forced contributions to the interannual variability of the transport through the BSO, we carried out three dedicated model simulations with the global sea ice and ocean model FESOM2.1[31]: one control simulation, with the same reanalysis forcing everywhere (CTRL), one where a normal year forcing (similar to atmosphere climatology, see "Methods") replaces the reanalysis forcing in the Arctic (ArcClim), and one where the reanalysis

forcing outside the Arctic is replaced with the normal year forcing (ArcVari, see "Methods" for details).

By combining reanalysis and normal year forcing in ArcVari and ArcClim we are able to split the total transport anomalies in CTRL into their upstream (outside Arctic domain) and locally (inside Arctic domain) forced components. We found that the results of the ArcVari and ArcClim simulations are linearly additive to reproduce the CTRL variability[22] (Fig. 3a). The standard deviations of the winter BSO net transport anomalies (1970–2019) are 0.35 Sv in ArcVari, 0.31 Sv in ArcClim, and 0.58 Sv in CTRL. The comparable magnitudes of the variations indicate a similar contribution from the locally and upstream forced variability to the total transport variability in the BSO (Fig. 3a). In addition, we split the net transport anomalies into those arising from inflowing water (eastward flow) and from outflowing (westward flow) water (Fig. 3c, e). The BSO inflow variability (standard deviation of the eastward transport) is 0.55 Sv in CTRL, which evenly splits into one part forced locally (ArcVari: 0.24 Sv), and another part forced upstream (ArcClim: 0.28 Sv). Hence, the inflow is to a similar degree controlled by local and upstream forcing. In contrast, the outflow variability (standard deviation of the westward transport) is reduced by about half when the Arctic atmospheric variability is removed (ArcClim: 0.12 Sv, CTRL: 0.26 Sv). However, when there is only variability in the Arctic atmospheric forcing, the outflow standard deviation is the same as in the control run (ArcVari: 0.26 Sv). This implies the outflow is mainly locally driven.

The separation into local and upstream forced transport anomalies further reveals strong year-to-year variability as well as decadal variations in both ArcVari and ArcClim. The variations of the net transport and inflow are well aligned with the NAO index (Fig. 3a, c), confirming the results of the composite analysis (Fig. 2). For the full 1970–2019 period, the Pearson correlation between the detrended net (inflow, outflow) BSO transport and the detrended NAO index is 0.73 (0.70, 0.39) in CTRL, 0.51 (0.50, 0.23) in ArcVari, and 0.79 (0.71, 0.53) in ArcClim. All standard deviations, correlations, and statistical significance are summarized in the Supplementary Table S1. Our simulations reveal an overall high dependence of net transport variability in CTRL and ArcClim on the NAO state, and the high dependence is mainly attributed to the inflow variability. In contrast, neither locally forced (ArcVari) inflow variability nor outflow variability is as strongly linked to the NAO (Fig. 3a, c, e). Nevertheless, the simulations suggest that during the pronounced negative NAO from the mid-1970s to the end of the 1980s, locally forced transport anomalies (net and inflow) are well aligned with the NAO index (Fig. 3a, c). The correlation seemingly decreases with the shift towards positive NAO in the 1990s. The co-variability of the NAO and the locally and upstream forced transport anomalies thus seems to be subject to decadal variations.

In order to investigate potential decadal changes in the co-variability of different transport components and the NAO, we proceed with computing the Pearson correlation within a moving 11-year window of the timeseries, to capture decadal (co-)variability (Fig. 3b, d, f). The results demonstrate that the co-variabilities of the NAO and CTRL/ArcVari/ArcClim transports are not constant in time (Fig. 3b, d, f). For the net transport, the moving correlations between NAO/CTRL and NAO/ArcClim depict a pronounced minimum during the 1995–2005 period (Fig. 3b). Moreover, locally forced net transport anomalies strongly co-vary with the NAO in the mid-1970s to late 1980s before losing the co-variability at the beginning of the 1990s (Fig. 3b). Similar dependencies are found when considering the inflow (Fig. 3d). The minimum correlation in the 1995–2005 period is even more pronounced and suggests that the NAO loses control especially on the upstream forced inflow in these years.
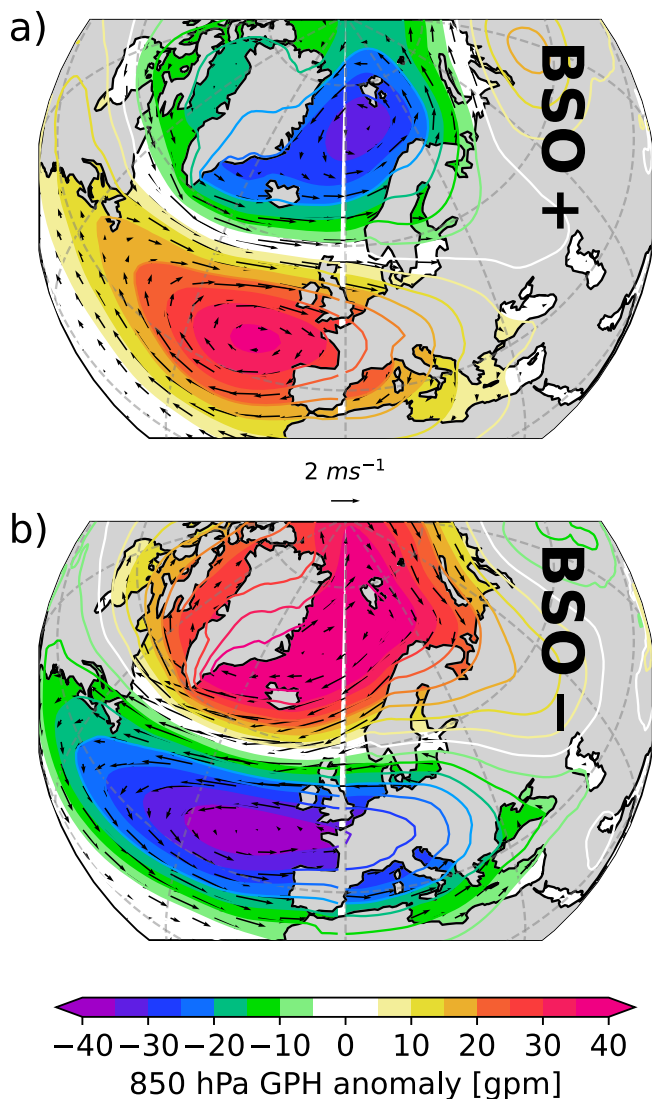

Fig. 2 Large-scale wind and pressure pattern associated with strong and weak Barents Sea Opening transport. Composite maps of 850 hPa geopotential height anomalies and associated wind anomalies (DJFM) during strong (**a**) and weak (**b**) net transport through BSO based on JRA55.
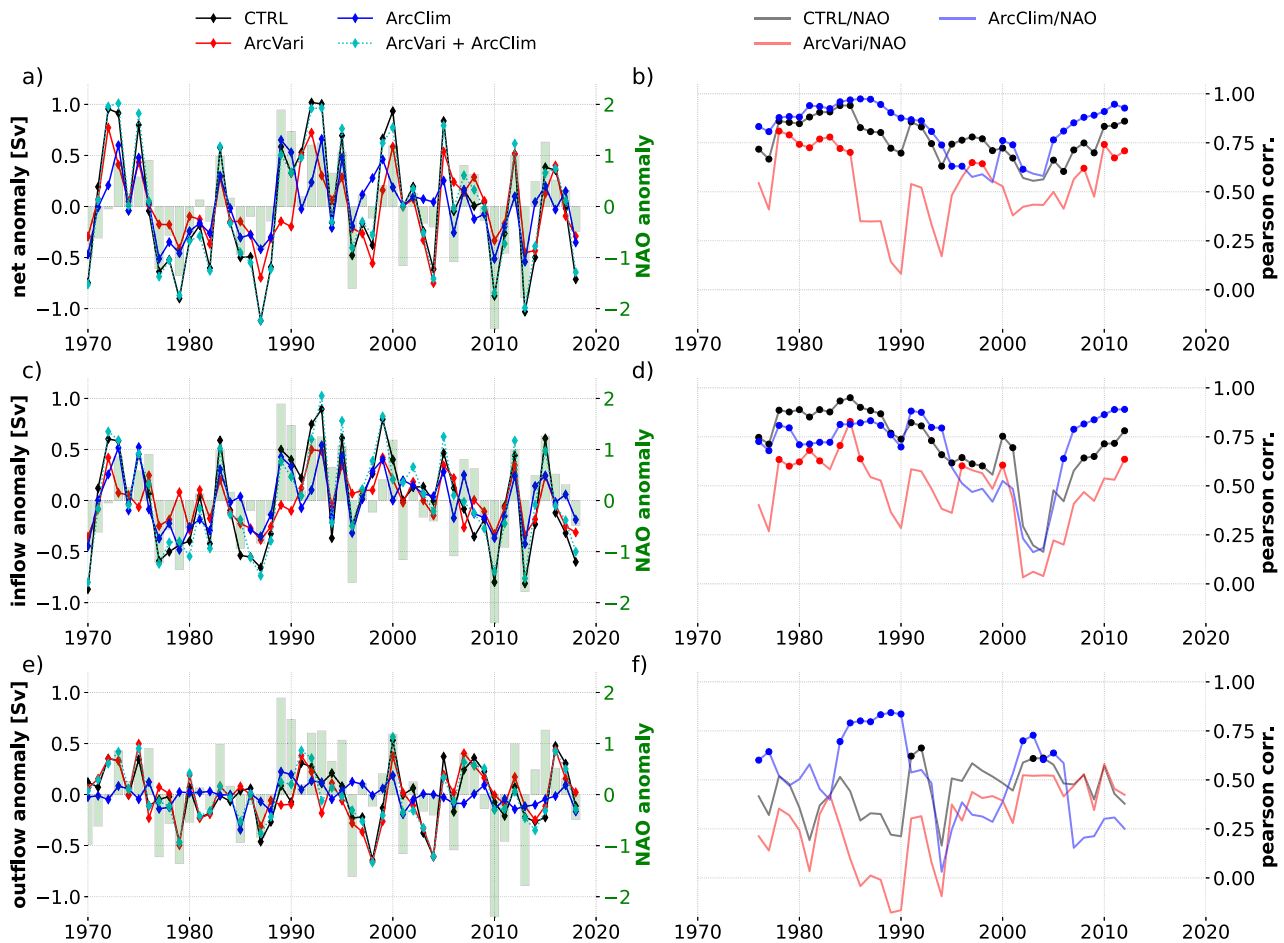
Fig. 3 Changing impact of the North Atlantic Oscillation on transports through the Barents Sea Opening. Net BSO transport anomalies in CTRL, ArcVari (non-Arctic variability removed), ArcClim (Arctic variability removed), and NAO index (**a**). Moving correlation (11-year window) between CTRL/NAO, ArcVari/NAO, ArcClim/NAO (**b**). Markers in (**b**, **d**, **f**) highlight statistically significant correlations. Years depict the center of the respective 11-year period. (**c**–**f**) Same as in (**a**, **b**) but for BSO inflow (eastward transport only) and outflow (westward transport only) only. In all timeseries presented in (**a**, **c**, **e**), the mean and the linear trend were removed. Note that negative outflow anomalies denote increased (westward) outflow.

In general, inflow variability is comparably weak in the 1995–2005 period. The variability strength (standard deviation) of the inflow reduces to 0.29 Sv in CTRL (−50%, compared to the 1970–2019 period), 0.16 Sv in ArcVari (−34%), and 0.20 Sv in ArcClim (−29%) when only considering the 1995–2005 period. In this period, extraordinary anomalies in the outflow (exceeding 2 standard deviations) occur in two winters (1998: −0.65 Sv, 2004: −0.60 Sv) (Fig. 3e). As already presented, outflow anomalies are forced locally and do not exhibit any statistically significant link to the NAO (95% confidence level). Reduced co-variability between the net BSO transports and the NAO in this time period might thus arise from a combination of a general decrease in the NAO's ability to control the upstream forced inflow and a simultaneous dominance of the non-NAO related outflow. The interim loss of the NAOs' ability to control the upstream forced inflow variability suggests a change in the large-scale wind forcing. The concurrent phenomena of the extraordinary outflow anomalies and the breakdown of the NAO control on the upstream forced inflow between 1995 and 2005 could share a common forcing mechanism, which will be explored below.

Interim change of large-scale and local wind patterns controlling the Barents Sea Opening transport variability. Despite that the composite analysis revealed a dominant control of the

NAO on the BSO volume transport (Fig. 2), the analysis of co-variability rather indicates that such a control does not function all the time (Fig. 3). To more precisely identify spatial patterns in the large-scale winds associated with the BSO transport variability and to monitor their robustness in space and time we further perform multivariate regression analysis with the zonal and meridional wind fields used to force the model as predictors of the net transport anomalies ("Methods"). The obtained regression coefficients are used to reconstruct the transport anomalies based on the local wind at every grid cell. Correlating the initial and reconstructed transport anomalies for each grid cell highlights areas most likely to impact the BSO transport. The coefficients of the regression fit at each grid point can further be interpreted as the local preferred wind direction to create anomalies in the BSO transport ("Methods"). As our simulations revealed strong decadal changes in the transport components and especially in their co-variability with the NAO (Fig. 3), we conducted the regressions for the periods 1970–1995, 1995–2005, and 2005–2018 separately.

From 1970 to 1995, the region most important for controlling the BSO net transport anomalies in CTRL is the Norwegian Sea coastal area, where correlations exceed 0.8 (Fig. 4a). The preferred wind direction in this area is along-coast, yielding onshore Ekman transport, an increased sea surface height (SSH) gradient perpendicular to the coast, and thus an acceleration of the NASC, finally leading to increased BSO inflow downstream. The area of most pronounced correlation at the Norwegian coast extends far
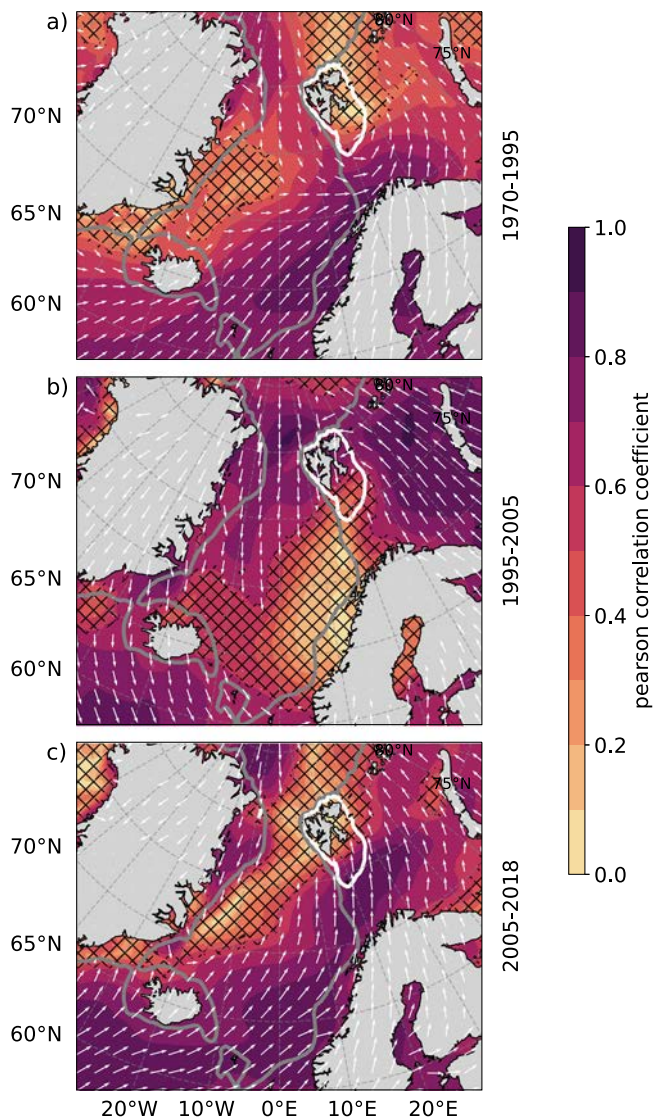
Fig. 4 Areas and wind patterns that can explain transport variability in the Barents Sea Opening. Correlation maps of modeled and reconstructed BSO net transport anomalies in CTRL. The analysis is performed for (**a**) 1970–1995, (**b**) 1995–2005, and (**c**) 2005–2018 separately. Arrows denote preferred wind direction and are scaled by the underlying correlation field. The gray (white) line depicts the 500 m (180 m) isobath. Non-significant correlations are covered by black hatching.

north into the BSO, where the same dynamical mechanism (alongshore winds producing an increased SSH gradient which sets up increased geostrophic flow) locally enhances transport in this period (Fig. 4a). In addition to local and remote alongshore winds perturbing the geostrophic inflow, our regression analysis identifies cyclonic winds centered over the Svalbard shelf as a third driver of BSO net transport variability on interannual timescales (Fig. 4a). Cyclonic wind anomalies over the northern BS shelf/southern Svalbard Bank cause divergent Ekman transport and thus a local reduction in SSH[16,19]. The negative SSH anomaly weakens the SSH gradient south of Bear Island, thus reducing the outflow and resulting in a positive net transport anomaly. Hence, while alongshore winds control the (both local and upstream forced portion) inflow variability, winds over the Svalbard shelf steer the variability of the outflow. Similar spatial patterns are found in the 2005–2018 period (Fig. 4c). Except for non-significant correlations west of Svalbard, the same forcing

mechanisms as in the 1970–1995 period are dominant. In both periods, the general wind pattern closely resembles the wind pattern associated with the NAO (Supplementary Fig. S1), namely westerly winds south of Iceland that turn southwesterly at the Norwegian coast, and northerly and northeasterly winds along the east Greenland coast.

During the 1995–2005 period when transports through the BSO and the NAO seemingly lose their strong correlation, the spatial pattern of the regression/correlation analysis reveals remarkable differences to the previous and subsequent periods and does not resemble the NAO pattern (Fig. 4b). Instead of the highly correlated areas along the Norwegian coastline, southerly winds in the BS turning westward north of Svalbard and northerly winds in Fram Strait form a cyclonic pattern and seem to be more important for shaping the net transport anomalies in the BSO. This is consistent with the dominance of the outflow variability in this period (Fig. 3a, e).

The wind variability in the Nordic Seas and BS in winter is heavily influenced by synoptic-scale atmosphere variability, especially synoptic cyclones affecting the SLP and wind field[32,33]. While propagating along the North Atlantic storm track into the Arctic region, cyclones affect the intensity of the alongshore winds driving the NASC. As already pointed out, the westward-directed Bear Island Slope current is also sensitive to cyclones passing over the northern BS shelf[16]. In order to understand the observed changes in the large-scale flow affecting the transports through the BSO, we thus further turn our attention to the propagation of cyclones towards the BS.

Anomalous atmospheric blocking and deflection of cyclones weakening the NAO control on BSO transport in the 1995–2005 period. Based on the timeseries presented in Fig. 3c, e, we have identified six anomalous years in this period, when the NAO state and the transport anomalies mismatch: two in terms of extraordinarily strong outflow (1998, 2004; exceeding 2 standard deviations of the locally forced (ArcVari) outflow) and four non-NAO driven inflow anomalies (1994, 2000, 2001, 2005; when the NAO does not relate to the upstream forced transport anomaly (ArcClim), i.e., when the NAO index has the opposite sign to the inflow anomaly) which seemingly contributed to the breakdown of the NAO influence on the transport through the BSO observed in the 1995–2005 period.

In the winters of 1998 and 2004, the net transport anomaly in the BSO is dominated by the extraordinarily strong outflow, which does not reveal any dependence on the NAO (Fig. 3a, e), but is known to be sensitive to local cyclone activity[16,19]. Considering the anomaly of the SLP and the anomalous surface winds in the winters 1998 and 2004 based on JRA55-do, it becomes evident that both winters are dominated by positive SLP anomalies associated with anomalous anticyclonic winds in the northern BS (Fig. 5a, b). Farther south, close to the Norwegian coast, a negative SLP anomaly associated with anomalous cyclonic winds is found. The wind anomaly patterns are thus similar to those obtained from the regression/correlation analysis for the 1995–2005 period (Fig. 4b), indicating that pronounced local wind anomalies are found in the BS and winds at the Norwegian coast are deflected (not relevant for the inflow anymore). In order to reveal the contribution of synoptic cyclones to the SLP and wind anomalies, and ultimately to the ocean transports, we further conduct analysis of trajectories of cyclones that reach the surrounding of the BS in the winters 1998 and 2004 based on a cyclone tracking algorithm[34]. We compute cyclone occurrence anomalies by counting the days per winter in which the respective grid cell is within the outermost closed isobar of the cyclones detected by the algorithm.
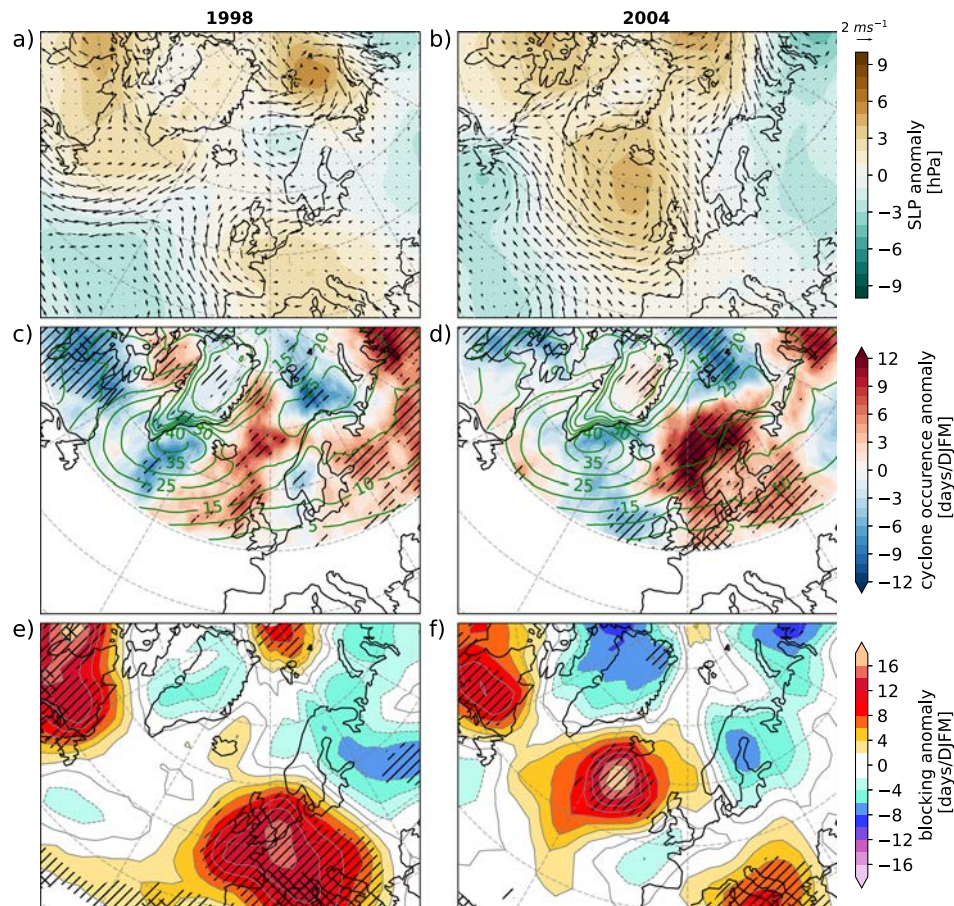
Fig. 5 Anomalous atmospheric circulation and cyclone occurrence in 1998 and 2004. Sea level pressure and wind anomalies of the winters (DJFM) 1998 and 2004 relative to the 1970–2019 winter mean from JRA55-do (**a**, **b**). Mean (1970–2019, green contours) and anomalous cyclone occurrence (color shading) of the respective winters (**c**, **d**). Note: Our cyclone database does not cover the region south of 50°N. Anomalous atmospheric blocking (**e**, **f**). Anomalies that exceed one standard deviation are highlighted with black stripes, crisscrossed areas depict areas, where the anomaly exceeds two standard deviations of the respective quantity (**c**–**f**).

For the respective winters, cyclones show a tendency to move rather zonally towards the northern Norwegian coast instead of traveling along the regular winter storm track through the Norwegian Sea into the BS (Fig. 5c, d). In 2004, 12 additional days per winter under strong cyclonic activity (+60% compared to long-term mean) are counted near the Norwegian coast (Fig. 5d). The more zonal trajectories of the cyclones lead to less persistent alongshore wind anomalies at the Norwegian coast that would adjust the inflow. In addition, fewer days under cyclone influence (−9 days per winter in both 1998 and 2004, ca. −40%) are detected in the northern BS (Fig. 5c, d). This most likely contributes to the observed anticyclonic wind anomalies in the region in these winters. As a result of the cyclone deficit, the more anticyclonic flow over the northern BS shelf causes an acceleration of the outflow south of Bear Island, dominating the net transport anomalies in these years. The unusually zonal trajectories of synoptic cyclones in these particular years can be related to anomalous atmospheric blocking in the vicinity of Iceland and Great Britain (Fig. 5e, f). In 2004 (1998), +16 (+14) days per winter of anomalous atmospheric blocking seemingly forced cyclones on a more zonally route towards the Norwegian coast, thus resulting in a cyclone deficit in the BS.

In 2000 (2005), the NAO is in a pronounced positive (neutral) phase, but the upstream forced inflow anomalies (0.0 Sv in 2000, 0.28 Sv in 2005) do not follow the NAO forcing (Fig. 3c). In 2000, an increased pressure dipole between the Azores High (+9 hPa) and the Icelandic Low (−11 hPa) is present, which is in

accordance with the positive NAO phase. However, compared to the NAO pattern, the low pressure is located to the east of the Icelandic Low location and resides over the White Sea. Based on our analysis, we find the displacement of the low-pressure anomaly to be aligned with reduced blocking over Scandinavia, increased blocking over the northern North Atlantic, and anomalously high occurrence of cyclones in this winter (Fig. 6c, e). In the center of the low-pressure anomaly, a doubling of days under cyclone impact is detected (+20 days/winter) in both 2000 and 2005. Consequently, the surface wind anomalies resulting from the low-pressure anomaly in 2000 are directed perpendicular to the coastline (Fig. 6a) instead of being parallel to the coastline as in a normal case of positive NAO conditions. Despite the positive NAO in this winter, the anomalous surface winds do not affect the geostrophic flow of the NASC and thus do not significantly increase the BSO inflow. In 2005, a neutral NAO winter, no NAO-like pattern is found in the SLP anomaly (Fig. 6b). Instead, massively increased blocking (exceeding 2 standard deviations) in the North Atlantic sector forms a persistent anticyclonic circulation anomaly that, as in 2000, strongly deflects synoptic cyclones. The increased cyclone occurrence in the Nordic Seas in this winter results in the cyclonic alongshore wind anomaly, which further increases the BSO inflow despite the neutral NAO (Figs. 3c and 6b, d, f).

The winters 1994 (positive NAO, slightly negative upstream forced inflow anomaly) and 2001 (negative NAO, slightly positive upstream forced transport anomaly) further illustrate a
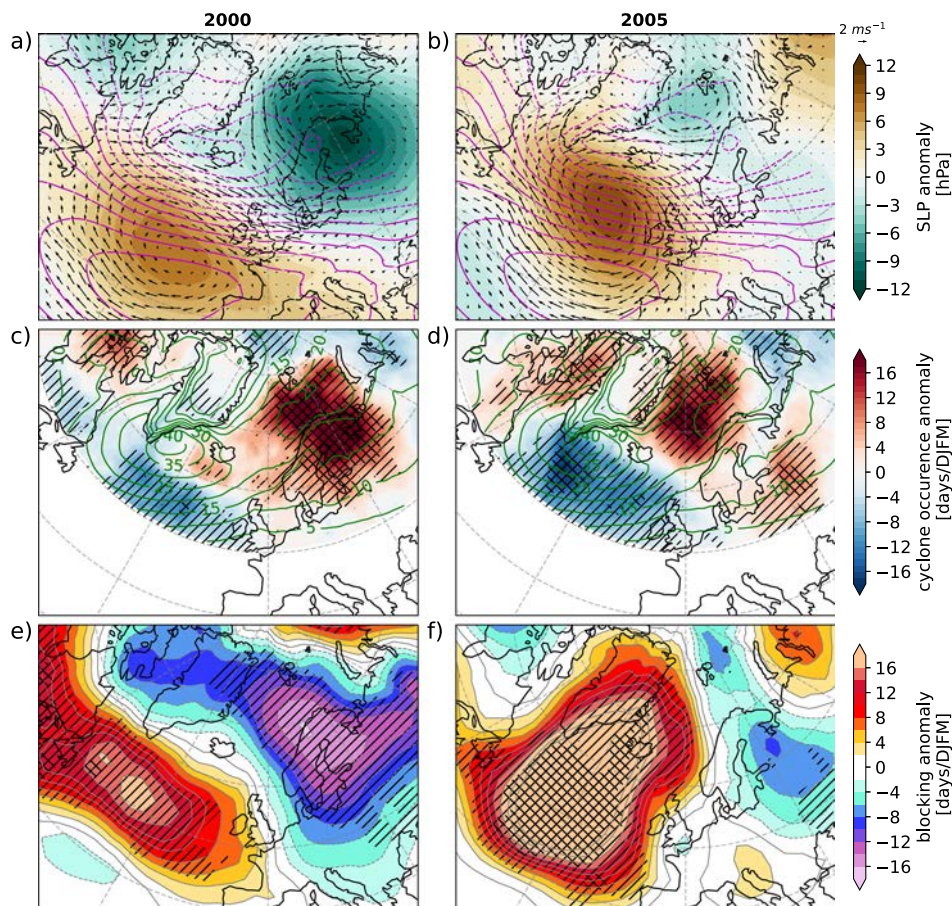
Fig. 6 Anomalous atmospheric circulation and cyclone occurrence in 2000 and 2005. All panels (**a**–**f**) as in Fig. 5a–f, but for the winters 2000 and 2005. In addition, the magenta lines in (**a**, **b**) depict the NAO pattern-related SLP anomaly as obtained from the EOF analysis. Note the modified color range in (**a**-**d**).

decoupling of the upstream forced BSO inflow from the NAO. Though the anomalous SLP in these winters matches the respective NAO state, winds at the Norwegian Atlantic coast do not represent the classical NAO pattern. In 2001, a strongly negative NAO would cause a strong northeast wind component at the Norwegian Atlantic coast, which would reduce the BSO inflow (Supplementary Fig. 1). However, the modification of the anomalously low cyclone occurrence on the SLP causes the along-coast component of the wind anomaly to be weak in this year (Fig. 7b, d). In 1994, the wind anomalies at the Norwegian coast are directed perpendicular to the coast, despite the positive NAO state which would suggest a more southwesterly wind anomaly in this area. The anomalously high cyclone occurrence modifies the low SLP pattern so that the anomalous wind is not directed along the coast (Fig. 7a, c). Extraordinary blocking anomalies (partly exceeding 2 standard deviations) are found in the North Atlantic sector in 1994 (−16 days/winter) and 2001 (−12 days/winter). In 1994, the low blocking increases the cyclone occurrence in the Norwegian Sea. In 2001, pronounced blocking occurred west of Greenland so the cyclone occurrence is reduced in the area around Greenland, including the Nordic Seas.

In summary, all 6 years support our hypothesis that anomalous regional atmosphere circulation patterns can heavily impact ocean transport through the BSO. Especially the loss of the NAO control on the BSO transport in the 1995–2005 period can specifically be attributed to anomalous atmospheric blocking which reshapes the North Atlantic storm track and the related synoptic cyclone activity in the Nordic Seas/BS domain affecting the ocean transport.

Discussion and conclusions

In this study, we disentangled locally and upstream forced contributions to ocean volume transport variability in the BSO and investigated their individual dependence on the NAO, the leading mode of climate variability in the North Atlantic sector. We found that the NAO cannot always explain the BSO transport variability, mainly due to changes in the spatial distribution of cyclones/NAO center of action associated with storm tracks in the Nordic Seas and the BS.

Wind variability associated with the NAO has been known to be a key factor controlling the ocean volume transport through the BSO[18,21,27]. However, the high correlation between the NAO and the BSO inflow broke down around the year 2000[18]. We discovered that the loss of NAO control on the BSO inflow is only temporary. Our analysis further illustrates that the loss of NAO control in the 1995–2005 period can be related to six winters exhibiting anomalous propagation of cyclones causing (i) a temporary dominance of the outflow anomalies over the inflow anomalies in 1998 and 2004 due to significantly fewer cyclones reaching the northern BS and (ii) a shift of cyclone trajectories during pronounced NAO conditions in 1994, 2000, 2001, and 2005 resulting in strong deviations from the normal NAO related wind anomalies at the Norwegian Atlantic coast. Our results confirm a previous study on cyclone statistics in the vicinity of the BS, that found a temporary deficit in the number of cyclones on a northerly path affecting the BS in the 1995–2005 period[32].

The exact fate of the NAO in a warmer future climate is yet unclear[35–38]. By the end of the twenty-first century, it is
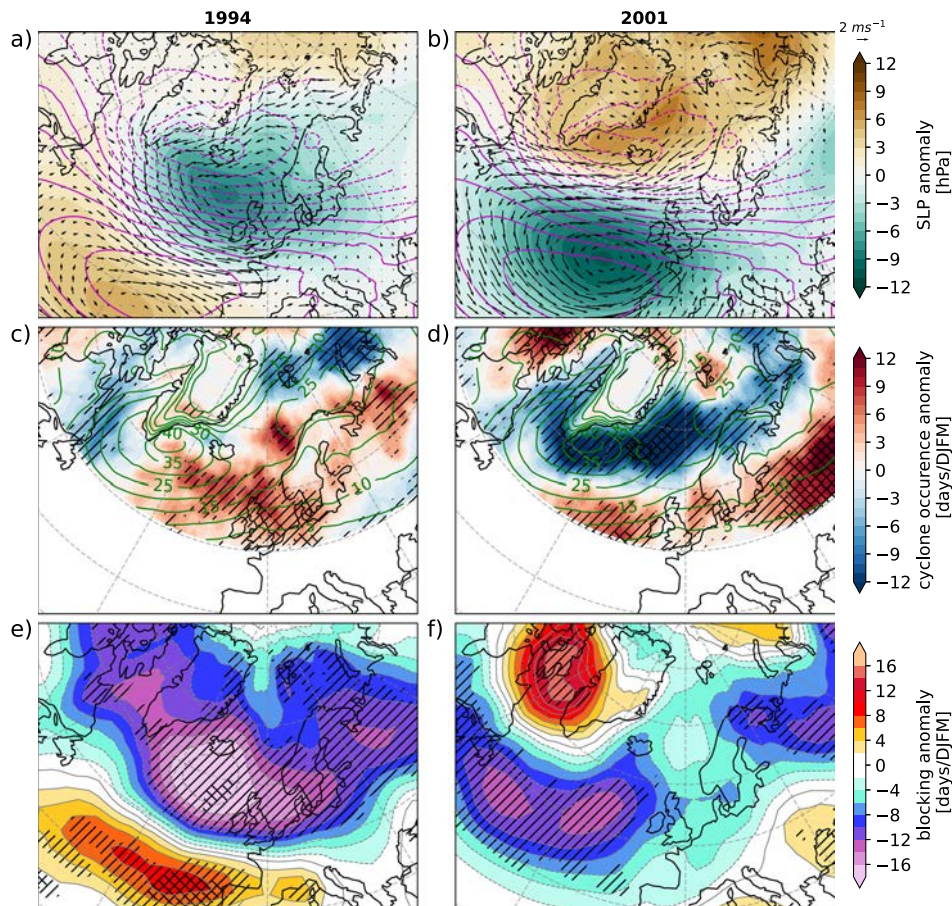
Fig. 7 Anomalous atmospheric circulation and cyclone occurrence in 1994 and 2001. All panels (**a**–**f**) as in Fig. 6a–f, but for the winters 1994 and 2001. Note the modified color range in (**c**, **d**).

projected that the characteristics of the NAO may be altered by anthropogenic forcing. Specifically, there may be a slight positive shift in the probability distribution of the NAO phase and a small northeastward displacement of its centers of action[39–42]. As presented in this study, both, the NAO trend and displacement of the centers of action are relevant for the transports in the BSO. Opposingly, no NAO trend[38] or even a trend toward more negative NAO by an equatorward jet shift caused by Arctic warming[37] is also projected. Especially in wintertime, there is in general a lack of model agreement on the future NAO trend. In addition, El Niño and La Niña events can impact the state of the NAO, thus influencing the BSO transport[43].

The NAO state can also influence cyclone paths. A positive NAO leads to a northward shift in the storm tracks possibly resulting in fewer cyclones passing through BSO[33,44]. Hence, along-coast winds in the BSO are less likely. In negative NAO conditions, storm tracks are at more southern locations. This observed co-variability of locally forced transport anomalies and the NAO during pronounced negative NAO conditions could become less relevant in a warmer future climate. For example, a more positive wintertime NAO as a result of increased CO_2 concentrations and a generally warmer climate would cause a more northerly storm track[45] and according to our findings a reduced impact of local forcing on the BSO transport anomalies. As the correlation between remotely forced transport anomalies in the BSO and the NAO is independent of the NAO state, anomalies forced remotely might become more dominant in the future. In addition, a shift of the NAOs' centers of action could impact cyclone propagation in

the North Atlantic sector and thus lead to a future change in the NAOs' control on BSO transports. However, no significant trends in the trajectories of synoptic cyclones reaching the vicinity of the Nordic Seas/BS in the 1979–2018 period were found[32]. In general, there is uncertainty regarding estimates of trends in cyclone occurrence and intensity in the Arctic over the past 40 years. Although some studies indicate an increase in cyclone depth and the occurrence of deep cyclones during winter[33], others report no significant changes[46] or a dependency on the period[47]. Future projections in global and regional climate models have shown an increase of cyclone frequency in the Arctic in winter (DJF) and a decrease in summer (JJA) to the end of the twenty-first century under the Representative Concentration Pathway 8.5 scenario. About half of these projections further predicts winter cyclones to become weaker and smaller[46], which could affect transports in the BSO based on the results of this study.

The current absence of a trend in cyclone occurrence and the observed recovery of the NAO/BSO transport correlation after 2005 suggests internal variability as the main cause for the deflection of the cyclones and not the ongoing global warming. The importance of the NAO, cyclone activity, and their interaction with the BSO ocean volume transport indicates that climate models must adequately resolve the related atmospheric processes to better predict future Arctic climate change.

In addition, the ocean volume and heat transports into the BS are one of the major drivers of sea ice variability in the Barents and Kara Seas[48,49]. An improved understanding of the volume and heat transports into the BS thus also leads to further advances

in our understanding of the sea ice variability as another large component of the Arctic climate system.

Methods

Model setup, experiment design, and evaluation. In this study, we use the Finite volumE Sea Ice and Ocean Model (FESOM2.1)[31]. FESOM2.1 is formulated on a triangular mesh, allowing for regional refinement in a global ocean setup. FESOM2.1 and its precursor FESOM have been extensively applied for simulating the Arctic Ocean[19,22,50–53]. In our experiments, we use a mesh with about 4.5 km grid size in the whole Arctic Ocean domain, including the Nordic Seas, and about 25 km in the adjacent seas. South of approximately 40°N, the horizontal resolution is set to nominal one degree (Supplementary Fig. S3a). Vertically the model is split into 46 z-layers with a thickness of 10 m close to the surface, increasing to 250 m in the deep ocean. All experiments are started from rest and initialized using the PHC3 hydrography[54].

In our model experiments, one part of the ocean domain is forced by atmospheric reanalysis forcing containing interannual variability, while the other is forced by a normal year atmospheric forcing without interannual variability. The choice of the two domains separates the Arctic from the rest of the globe. The boundaries separating the two domains are Fram Strait (76.5°N), BSO (17.5°E), Davis Strait (69°N), and Bering Strait (62°N) (Supplementary Fig. S3a). In the following, we refer to our three model simulations as CTRL, ArcVari, and ArcClim. In CTRL, the entire global model domain is forced with the Japanese 55-year Reanalysis of the atmosphere for driving ocean-sea-ice models[55] (JRA55-do) yielding a global hindcast simulation from 1958 until 2019. In ArcVari, atmospheric forcing outside the Arctic domain is replaced by NCEP-CORE1[56] (CORE1) normal year forcing that is repeated every year in the simulation. The normal year forcing is composed of a one-year annual cycle of 6-hourly atmospheric forcing fields, which represent the climatology of the atmosphere. In ArcClim, the CORE1 forcing is used in the Arctic domain and JRA55 elsewhere. These experiments allow us to separate the impact of inter-annually varying atmospheric processes inside and outside the Arctic domain on the BSO transport.

After a full 62-year cycle is performed as a spin-up for each experiment, the model runs are restarted from their respective final 2019 conditions for a second full cycle. The last 50 years of the second cycle (1970–2019) are evaluated in this study. The model yields monthly mean fields as output. In all experiments, hydrographic properties, sea ice area, as well as major currents in the BSO are well represented in the model (Supplementary Figs. S3 and S4). The model yields an annual mean BSO volume transport of 2.6 Sv, which is within the observational interannual range of 0.8 Sv to 2.9 Sv[13] and further matches the synthesized estimate of 2.3 Sv[18]. Further, the BSO net transport shares the same seasonal variability as in the observations with increased transport during winter and minimum transport in early summer[48]. All results in this study are based on winter (1st of December to 31st of March) means.

By combining forcing datasets, we create discontinuities along the border of the defined areas, which in the case of BSO section is close to BSO. The net transport anomalies as well as inflow anomalies and outflow anomalies in ArcVari and ArcClim almost perfectly add up to those of CTRL (Fig. 3a, c, e) proving the consistency of the transports when combining the forcing datasets even if the region of interest (BSO) is close to the forcing boundary. The small deviations of the transport anomalies between the sum of ArcClim and ArcVari and those of CTRL might be the result of discontinuities in the combined

forcing. As these are very small compared to the general magnitude of the transport variability, we consider the unwanted effect negligible. In addition, we investigated modifications of the velocity field of the BSO, such as the location of the main currents entering and leaving the BSO as well as the overall transport magnitude, in all simulations. The results are presented in Supplementary Fig. S4 and prove that neither the general velocity field across the BSO nor average net, inflow or outflow transports are strongly affected by the combining-forcing approach. In addition, mean temperature and salinity fields are not affected by the forcing approach, providing further evidence for the validity of the method.

Forcing interpolation. Using bilinear remapping, we spatially interpolated CORE1 to the JRA55 grid, applying the climate data operators (cdo remapbil). Temporally, nearest-neighbor interpolation was applied to interpolate the 6-hourly CORE1 forcing data to the 3-hourly JRA55 time axis.

Definition of winter means and anomalies. We define the winter mean as the average of the December-March period for each year in the 1970–2019 period. E.g., the winter 2000 relates to the average of 12/1999, 01/2000, 02/2000, and 03/2000. Anomalies are computed by removing the 1970–2019 mean and linearly detrending the data.

Definition of strong/weak transport events. Strong/weak BSO transport events used for composite analysis are defined as winters in which the detrended net transport anomalies are exceeding ±1 standard deviation.

North Atlantic Oscillation definition. We compute the NAO pattern as the first empirical orthogonal function (EOF) of winter SLP (DJFM, 1958-2019) in the North Atlantic sector (20°–70°N; 90°W–40°E)[26] in the model forcing (JRA55-do). The associated timeseries of principal components (PC) is taken as the NAO index. NAO± events are defined as winters, in which the detrended winter NAO index exceeds ±1 standard deviation.

Composite analysis. Composites are computed by averaging the linearly detrended atmospheric forcing data (DJFM means) during winters when a respective quantity exceeds ±1 standard deviation.

Moving correlation. The correlation between the NAO and the transport anomalies is computed as the Pearson correlation coefficient in a moving window of 11 years in length to capture interannual to decadal co-variability. The results are largely independent of the window length (Supplementary Fig. S2). The associated year provides the center of the respective 11-year period (e.g., 2000 relates to the 1995–2005 period). Correlations are considered significant when they differ from 0 on a 95% confidence level based on a two-sided hypothesis test (Fisher transformation). Both the NAO and the respective transport component (11-year periods) are detrended before computing the correlation.

Regression/correlation analysis. We perform multivariate linear regression analysis:

$$V' = \alpha_j u_j + \beta_j v_j + c + \epsilon \qquad (1)$$

where V' is the timeseries of detrended net transport anomalies, u_j and v_j are the detrended wind component anomalies at each

grid cell j, c is a constant, and ϵ the residual error term. We then reconstruct the transport anomalies at each grid point j based on the wind components u_j and v_j and the received regression coefficients α_j and β_j:

$$V_j^{rec} = \alpha_j u_j + \beta_j v_j \qquad (2)$$

By correlating V' and V_j^{rec} at each grid cell, we finally receive maps highlighting regions where the wind variability can reasonably reproduce the variability of the transport through BSO and thus is likely to affect the BSO volume transport. Correlations are regarded as significant when they are different from 0 at a 95% confidence level (two-sided hypothesis test).

In addition, the regression coefficients α_j and β_j can be interpreted as a vector property

$$w_j = |\alpha_j, \beta_j|^{-1} \cdot (\alpha_j, \beta_j) \qquad (3)$$

indicating the preferred wind direction of the regression fit.

Cyclone tracking algorithm. We make use of a cyclone detection and tracking algorithm[34] to analyze cyclone occurrence anomalies for specific winters. Cyclone occurrence is computed as days per winter that a specific grid cell is within the outermost closed isobar of a cyclone detected by the algorithm based on the sea level pressure of the JRA55-do reanalysis data[55] that is used to force the simulations. The anomaly is computed relative to the 1970–2019 winter (DJFM) mean. We only consider cyclones with a pressure difference of at least 10 hPa between the cyclone center and the outermost closed isobar.

2D atmospheric blocking. A two-dimensional (2D) atmospheric blocking index is used in this study[57]. To compute the 2D blocking index, we have used the daily geopotential height at 500 mb extracted from the JRA55 reanalysis[58]. The 2D blocking index is an extension of the one-dimensional (1D) Tibaldi-Molteni[59] (TM) to a two-dimensional map of blocking frequencies at every grid point. The southern geopotential height gradient (GHGS) and the northern geopotential height gradient (GHGN) for each grid point are evaluated as follows:

$$GHGS = \frac{Z(\Phi_0) - Z(\Phi_0 - 15^0)}{15^0} \qquad (4)$$

$$GHGN = \frac{Z(\Phi_0 + 15^0) - Z(\Phi_0)}{15^0} \qquad (5)$$

where ϕ_0 is the latitude of the considered grid point varying from 35°N to 75°N. For each month, we have calculated the ratio between the number of days when a certain grid point was blocked, i.e., the conditions GHGS > 0 and GHGN < (-10 m per °lat) are simultaneously satisfied for at least 5 consecutive days.

Data availability
BSO temperature data are available at https://ocean.ices.dk/core/iroc. NCEP-CORE1 forcing data can be accessed at https://data1.gfdl.noaa.gov/nomads/forms/mom4/CORE.html, JRA55-do-v1.4 and JRA55 are stored at https://climate.mri-jma.go.jp/pub/ocean/JRA55-do/ and https://rda.ucar.edu/datasets/ds628-0/, respectively. NSIDC sea ice concentration is available at https://nsidc.org/data/g10010. Data presented in this study are stored at https://doi.org/10.5281/zenodo.8249639.

Code availability
FESOM2.1 source code can be found at https://github.com/FESOM/fesom2. Analysis of FESOM2.1 model data was done with pyfesom2 (https://github.com/FESOM/pyfesom2). The specific model settings for the simulations, as well as the versions of the Python modules (anaconda environment) used for analyzing and visualizing the data, are stored at https://doi.org/10.5281/zenodo.8249639.

References
1. Skagseth, Ø. et al. Reduced efficiency of the Barents Sea cooling machine. *Nat. Clim. Change* **10**, 661–666 (2020).
2. Shu, Q., Wang, Q., Song, Z. & Qiao, F. The poleward enhanced Arctic Ocean cooling machine in a warming climate. *Nat. Commun.* **12**, 1–9 (2021).
3. Fossheim, M. et al. Recent warming leads to a rapid borealization of fish communities in the Arctic. *Nat. Clim. Change* **5**, 673–677 (2015).
4. Sandø, A. B. et al. Barents Sea plankton production and controlling factors in a fluctuating climate. *ICES J. Mar. Sci.* **78**, 1999–2016 (2021).
5. Wu, B., Handorf, D., Detloff, K., Rinke, A. & Hu, A. Winter weather patterns over Northern Eurasia and Arctic Sea ice loss. *Mon. Weather Rev.* **141**, 3786–3800 (2013).
6. Lo, Y. T. E., Mitchell, D. M., Watson, P. A. G. & Screen, J. A. Changes in winter temperature extremes from future Arctic Sea-Ice loss and ocean warming. *Geophys. Res. Lett.* **50**, e2022GL102542 (2023).
7. Lawrence, D. M., Slater, A. G., Tomas, R. A., Holland, M. M. & Deser, C. Accelerated Arctic land warming and permafrost degradation during rapid sea ice loss. *Geophys. Res. Lett.* **35**, 11506 (2008).
8. Melia, N., Haines, K. & Hawkins, E. Sea ice decline and 21st century trans-Arctic shipping routes. *Geophys. Res. Lett.* **43**, 9720–9728 (2016).
9. Buckley, M. W. & Marshall, J. Observations, inferences, and mechanisms of the Atlantic meridional overturning circulation: a review. *Rev. Geophys.* **54**, 5–63 (2016).
10. Furevik, T. Annual and interannual variability of Atlantic Water temperatures in the Norwegian and Barents Seas: 1980–1996. *Deep Sea Res. Part I Oceanographic Res. Papers* **48**, 383–404 (2001).
11. Ingvaldsen, R., Loeng, H. & Asplin, L. Variability in the Atlantic inflow to the Barents Sea based on a one-year time series from moored current meters. *Cont. Shelf Res.* **22**, 505–519 (2002).
12. Orvik, K. A. & Skagseth, Ø. Heat flux variations in the eastern Norwegian Atlantic Current toward the Arctic from moored instruments, 1995–2005. *Geophys. Res. Lett.* **32**, 1–5 (2005).
13. Skagseth, Ø. et al. Volume and heat transports to the Arctic Ocean via the Norwegian and Barents seas. *Arctic-Subarctic Ocean Fluxes: Defining the Role of the Northern Seas in Climate* 45–64. https://doi.org/10.1007/978-1-4020-6774-7_3/COVER (2008).
14. Skagseth, Ø., Orvik, K. A. & Furevik, T. Coherent variability of the Norwegian Atlantic Slope Current derived from TOPEX/ERS altimeter data. *Geophys. Res. Lett.* **31**. https://doi.org/10.1029/2004GL020057 (2004).
15. Orvik, K. A. & Skagseth, Ø. The impact of the wind stress curl in the North Atlantic on the Atlantic inflow to the Norwegian Sea toward the Arctic. *Geophys. Res. Lett.* **30**. https://doi.org/10.1029/2003GL017932 (2003).
16. Lien, V. S., Vikebø, F. B. & Skagseth, O. One mechanism contributing to co-variability of the Atlantic inflow branches to the Arctic. *Nat. Commun.* **4**, 1–6 (2013).
17. Smedsrud, L. H., Ingvaldsen, R., Nilsen, J. E. Ø. & Skagseth, Ø. Heat in the Barents Sea: transport, storage, and surface fluxes. *Ocean Sci.* **6**, 219–234 (2010).
18. Smedsrud, L. H. et al. The role of the Barents Sea in the Arctic climate system. *Rev. Geophys.* **51**, 415–449 (2013).
19. Heukamp, F. O., Kanzow, T., Wang, Q., Wekerle, C. & Gerdes, R. Impact of cyclonic wind anomalies caused by massive winter sea ice retreat in the Barents Sea on Atlantic water transport toward the Arctic: a model study. *J. Geophys. Res. Oceans* **128**, e2022JC019045 (2023).
20. Ingvaldsen, R. B., Asplin, L. & Loeng, H. The seasonal cycle in the Atlantic transport to the Barents Sea during the years 1997–2001. *Cont. Shelf Res.* **24**, 1015–1032 (2004).
21. Ingvaldsen, R. B., Asplin, L. & Loeng, H. Velocity field of the western entrance to the Barents Sea. *J. Geophys. Res. Oceans* **109**. https://doi.org/10.1029/2003JC001811 (2004).
22. Wang, Q. et al. Ocean heat transport into the Barents Sea: distinct controls on the upward trend and interannual variability. *Geophys. Res. Lett.* **46**, 13180–13190 (2019).
23. Blindheim, J. et al. Upper layer cooling and freshening in the Norwegian Sea in relation to atmospheric forcing. *Deep Sea Res. Part I Oceanographic Res. Papers* **47**, 655–680 (2000).
24. Hurrell, J. W., Kushnir, Y. & Visbeck, M. The North Atlantic oscillation. *Science* **291**, 603–605 (2001).
25. Hurrell, J. W. & Deser, C. North Atlantic climate variability: the role of the North Atlantic Oscillation. *J. Mar. Syst.* **79**, 231–244 (2010).
26. Hurrell, J. W. et al. Decadal trends in the North Atlantic Oscillation: regional temperatures and precipitation. *Science* **269**, 676–679 (1995).

27. Ingvaldsen, R., Loeng, H., Ottersen, G. & Ådlandsvik Ingvaldsen, B. Climate variability in the Barents Sea during the 20th century with a focus on the 1990s. *ICES Mar. Sci. Symp.* **219**, 160–168 (2003).

28. Dickson, R. R. et al. The Arctic Ocean response to the North Atlantic Oscillation. *J. Clim.* **13**, 2671–2696 (2000).

29. Serreze, M. C., Carse, F., Barry, R. G. & Rogers, J. C. Icelandic low cyclone activity: climatological features, linkages with the NAO, and relationships with recent changes in the northern hemisphere circulation. *J. Clim.* **10**, 453–464 (1997).

30. Deser, C., Walsh, J. E. & Timlin, M. S. Arctic sea ice variability in the context of recent atmospheric circulation trends. *J. Clim.* **13**, 617–633 (2000).

31. Danilov, S., Sidorenko, D., Wang, Q. & Jung, T. The finite-volume sea ice–ocean model (FESOM2). *Geosci. Model Dev.* **10**, 765–789 (2017).

32. Madonna, E., Hes, G., Li, C., Michel, C. & Siew, P. Y. F. Control of Barents Sea wintertime cyclone variability by large-scale atmospheric flow. *Geophys. Res. Lett.* **47**. https://doi.org/10.1029/2020GL090322 (2020).

33. Zahn, M., Akperov, M., Rinke, A., Feser, F. & Mokhov, I. I. Trends of cyclone characteristics in the Arctic and their patterns from different reanalysis data. *J. Geophys. Res. Atmos.* **123**, 2737–2751 (2018).

34. Akperov, M., Semenov, V. A., Mokhov, I. I., Dorn, W. & Rinke, A. Impact of Atlantic water inflow on winter cyclone activity in the Barents Sea: insights from coupled regional climate model simulations. *Environ. Res. Lett.* **15**, 024009 (2020).

35. Deser, C., Hurrell, J. W. & Phillips, A. S. The role of the North Atlantic Oscillation in European climate projections. *Clim. Dyn.* **49**, 3141–3157 (2017).

36. Deser, C., Magnusdottir, G., Saravanan, R. & Phillips, A. The effects of North Atlantic SST and sea ice anomalies on the winter circulation in CCM3. Part II: direct and indirect components of the response. *J. Clim.* **17**, 877–889 (2004).

37. Screen, J. A., Simmonds, I., Deser, C. & Tomas, R. The atmospheric response to three decades of observed Arctic sea ice loss. *J. Clim.* **26**, 1230–1248 (2013).

38. Cusinato, E., Rubino, A. & Zanchettin, D. Winter Euro-Atlantic climate modes: future scenarios from a CMIP6 multi-model ensemble. *Geophys. Res. Lett.* **48**. https://doi.org/10.1029/2021GL094532 (2021).

39. Ulbrich, U. & Christoph, M. A shift of the NAO and increasing storm track activity over Europe due to anthropogenic greenhouse gas forcing. *Clim. Dyn.* **15**, 551–559 (1999).

40. Branstator, G. & Selten, F. "Modes of variability" and climate change. *J. Clim.* **22**, 2639–2658 (2009).

41. Deser, C., Phillips, A., Bourdette, V. & Teng, H. Uncertainty in climate change projections: the role of internal variability. *Clim. Dyn.* **38**, 527–546 (2012).

42. Barnes, E. A. & Polvani, L. M. CMIP5 projections of Arctic amplification, of the North American/North Atlantic circulation, and of their relationship. *J. Clim.* **28**, 5254–5271 (2015).

43. Luo, B. et al. Origins of Barents-Kara sea-ice interannual variability modulated by the Atlantic pathway of El Niño–Southern Oscillation. *Nat. Commun.* **14**, 1–13 (2023).

44. Vessey, A. F., Hodges, K. I., Shaffrey, L. C. & Day, J. J. An inter-comparison of Arctic synoptic scale storms between four global reanalysis datasets. *Clim. Dyn.* **54**, 2777–2795 (2020).

45. Stephenson, D. B., Pavan, V., Collins, M., Junge, M. M. & Quadrelli, R. North Atlantic Oscillation response to transient greenhouse gas forcing and the impact on European winter climate: a CMIP2 multi-model assessment. *Clim. Dyn.* **27**, 401–420 (2006).

46. Akperov, M. et al. Future projections of cyclone activity in the Arctic for the 21st century from regional climate models (Arctic-CORDEX). *Glob. Planet Change* **182**, 103005 (2019).

47. Valkonen, E., Cassano, J. & Cassano, E. Arctic cyclones and their interactions with the declining sea ice: a recent climatology. *J. Geophys. Res. Atmos.* **126**, e2020JD034366 (2021).

48. Årthun, M., Eldevik, T., Smedsrud, L. H., Skagseth, Ø. & Ingvaldsen, R. B. Quantifying the influence of Atlantic heat on Barents sea ice variability and retreat. *J. Clim.* **25**, 4736–4743 (2012).

49. Lien, V. S., Schlichtholz, P., Skagseth, Ø. & Vikebø, F. B. Wind-driven Atlantic water flow as a direct mode for reduced Barents Sea ice cover. *J. Clim.* **30**, 803–812 (2017).

50. Wang, Q. et al. Intensification of the Atlantic water supply to the Arctic Ocean through Fram Strait induced by Arctic Sea ice decline. *Geophys. Res. Lett.* **47**. https://doi.org/10.1029/2019GL086682 (2020).

51. Wekerle, C., Wang, Q., Danilov, S., Jung, T. & Schröter, J. The Canadian Arctic Archipelago throughflow in a multiresolution global model: model assessment and the driving mechanism of interannual variability. *J. Geophys. Res. Oceans* **118**, 4525–4541 (2013).

52. Wekerle, C. et al. Eddy-resolving simulation of the Atlantic Water circulation in the Fram Strait with focus on the seasonal cycle. *J. Geophys. Res. Oceans* **122**, 8385–8405 (2017).

53. Wang, Q. et al. Eddy kinetic energy in the Arctic Ocean from a global simulation with a 1-km Arctic. *Geophys. Res. Lett.* **47**. https://doi.org/10.1029/2020GL088550 (2020).

54. Steele, M., Morley, R. & Ermold, W. PHC: a global ocean hydrography with a high-quality Arctic ocean. *J. Clim.* **14**, 2079–2087 (2001).

55. Tsujino, H. et al. JRA-55 based surface dataset for driving ocean–sea-ice models (JRA55-do). *Ocean Model* **130**, 79–139 (2018).

56. Yeager, S. G. Diurnal to decadal global forcing for ocean and sea-ice models: the data sets and flux climatologies coordinated ocean-ice reference experiments view project. https://doi.org/10.5065/D6KK98Q6 (2004).

57. Scherrer, S. C., Croci-Maspoli, M., Schwierz, C. & Appenzeller, C. Two-dimensional indices of atmospheric blocking and their statistical relationship with winter climate patterns in the Euro-Atlantic region. *Int. J. Climatol.* **26**, 233–249 (2006).

58. KOBAYASHI, S. et al. The JRA-55 reanalysis: general specifications and basic characteristics. *J. Meteorol. Soc. Japn. Ser. II* **93**, 5–48 (2015).

59. TIBALDI, S. & MOLTENI, F. On the operational predictability of blocking. *Tellus A* **42**, 343–365 (1990).

Acknowledgements

Author contributions

F.O.H. designed the study, carried out the model experiments, and wrote the paper draft. L.A. analyzed the cyclone data. Q.W. and C.W. assisted in setting up and executing the model simulations. M.I. carried out the atmospheric blocking analysis. T.K. and A.R., as well as all other coauthors, assisted in interpreting and contextualizing the results. All coauthors were involved in reviewing and finalizing the manuscript.

Funding

Competing interests

The authors declare no competing interests.

Additional information

Supplementary information The online version contains supplementary material available at https://doi.org/10.1038/s43247-023-00985-1.

Correspondence and requests for materials should be addressed to Finn Ole Heukamp.

Peer review information *Communications Earth & Environment* thanks Vidar Lien and the other, anonymous, reviewer(s) for their contribution to the peer review of this work. Primary Handling Editors: Jennifer Veitch, Heike Langenberg. A peer review file is available.

Reprints and permission information is available at http://www.nature.com/reprints

Publisher's note Springer Nature remains neutral with regard to jurisdictional claims in published maps and institutional affiliations.

Bibliography

Achatz, U. (2022), *Atmosphärendynamik*, Springer Berlin Heidelberg, Berlin, Heidelberg.

Akperov, M., I. Mokhov, A. Rinke, K. Dethloff, and H. Matthes (2015), Cyclones and their possible changes in the arctic by the end of the twenty first century from regional climate model simulations, *Theoretical and Applied Climatology*, *122*, 85–96, `https://doi.org/10.1007/s00704-014-1272-2`.

Akperov, M., V. A. Semenov, I. I. Mokhov, W. Dorn, and A. Rinke (2020), Impact of atlantic water inflow on winter cyclone activity in the barents sea: insights from coupled regional climate model simulations, *Environmental Research Letters*, *15*(2), 024009, `https://doi.org/10.1088/1748-9326/ab6399`.

Akperov, M. G., M. Y. Bardin, E. M. Volodin, G. S. Golitsyn, and I. I. Mokhov (2007), Probability distributions for cyclones and anticyclones from the ncep/ncar reanalysis data and the inm ras climate model, *Izvestiya, Atmospheric and Oceanic Physics*, *43*, 705–712, `https://doi.org/10.1134/S0001433807060047`.

Årthun, M., T. Eldevik, L. H. Smedsrud, Skagseth, and R. B. Ingvaldsen (2012), Quantifying the influence of atlantic heat on barents sea ice variability and retreat, *Journal of Climate*, *25*(13), 4736 – 4743, `https://doi.org/10.1175/JCLI-D-11-00466.1`.

Aue, L., and A. Rinke (2023), Cyclone impacts on sea ice concentration in the atlantic arctic ocean: Annual cycle and recent changes, *Geophysical Research Letters*, *50*(17), e2023GL104657, `https://doi.org/10.1029/2023GL104657`.

Aue, L., T. Vihma, P. Uotila, and A. Rinke (2022), New insights into cyclone impacts on sea ice concentration in the Atlantic part of the Arctic Ocean in winter, *Geophysical Research Letters*, *49*(22), e2022GL100051, `https://doi.org/10.1029/2022GL100051`.

Aue, L., L. Röntgen, W. Dorn, P. Uotila, T. Vihma, G. Spreen, and A. Rinke (2023), Impact of three intense winter cyclones on the sea ice cover in the barents sea: A case study with a coupled regional climate model, *Frontiers in Earth Science*, *11*, `https://doi.org/10.3389/feart.2023.1112467`.

Bardin, M. Y., and A. B. Polonsky (2005), North atlantic oscillation and synoptic variability in the european-atlantic region in winter, *Izvestiya, Atmospheric and Oceanic Physics*, *41*, 127–136.

Blanchard-Wrigglesworth, E., M. Webster, L. Boisvert, C. Parker, and C. Horvat (2022), Record Arctic cyclone of January 2022: Characteristics, impacts, and predictability, *Journal of Geophysical Research: Atmospheres*, *127*(21), e2022JD037161, `https://doi.org/10.1029/2022JD037161`.

Block, K., F. A. Schneider, J. Mülmenstädt, M. Salzmann, and J. Quaas (2020), Climate models disagree on the sign of total radiative feedback in the arctic, *Tellus A: Dynamic Meteorology and Oceanography*, *72*(1), 1–14, `https://doi.org/10.1080/16000870.2019.1696139`.

Boisvert, L., A. Petty, and J. Stroeve (2016), The impact of the extreme winter 2015/16 arctic cyclone on the barents-kara seas, *Monthly Weather Review*, *144*, 4279–4287, `https://doi.org/10.1175/MWR-D-16-0234.1`.

Bott, A. (2016), *Synoptische Meteorologie: Methoden der Wetteranalyse und -prognose*, Springer Berlin Heidelberg, Berlin, Heidelberg.

Buschmann, M., N. M. Deutscher, M. Palm, T. Warneke, C. Weinzierl, and J. Notholt (2017), The arctic seasonal cycle of total column CO_2 and CH_4 from ground-based solar and lunar FTIR absorption spectrometry, *Atmospheric Measurement Techniques*, *10*, 2397–2411, `https://doi.org/10.5194/amt-10-2397-2017`.

Buschmann, M., C. Petri, M. Palm, T. Warneke, and J. Notholt (2022), TCCON data from Ny-Ålesund, Svalbard (NO), Release GGG2020.R0 (Version R0), CaltechDATA, `https://doi.org/10.14291/tccon.ggg2020.nyalesund01.R0`.

Cai, L., V. A. Alexeev, and J. E. Walsh (2020), Arctic sea ice growth in response to synoptic- and large-scale atmospheric forcing from cmip5 models, *Journal of Climate*, *33*(14), 6083–6099, `https://doi.org/10.1175/JCLI-D-19-0326.1`.

Cao, Y., S. Liang, L. Sun, J. Liu, X. Cheng, D. Wang, Y. Chen, M. Yu, and K. Feng (2022), Trans-arctic shipping routes expanding faster than the model projections, *Global Environmental Change*, *73*, 102488, `https://doi.org/10.1016/j.gloenvcha.2022.102488`.

Capute, P. K., and R. D. Torn (2021), A comparison of arctic and atlantic cyclone predictability, *Monthly Weather Review*, *149*(11), 3837–3849, `https://doi.org/10.1175/MWR-D-20-0350.1`.

Cherry-Garrard, A. (1922), *The worst journey in the world - Antarctic 1910-1913*, p. 17, Constable & Company Ltd., London.

Chikhar, K., J.-F. Lemieux, F. Dupont, F. Roy, G. C. Smith, M. Brady, S. E. L. Howell, and R. Beaini (2019), Sensitivity of ice drift to form drag and ice strength parameterization in a coupled ice–ocean model, *Atmosphere-Ocean*, *57*(5), 329–349, `https://doi.org/10.1080/07055900.2019.1694859`.

Choi, Y.-S., J. Hwang, J. Ok, D.-S. R. Park, H. Su, J. H. Jiang, L. Huang, and T. Limpasuvan (2020), Effect of arctic clouds on the ice-albedo feedback in midsummer, *International Journal of Climatology*, *40*(10), 4707–4714, `https://doi.org/10.1002/joc.6469`.

Clancy, R., C. M. Bitz, E. Blanchard-Wrigglesworth, M. C. McGraw, and S. M. Cavallo (2022), A cyclone-centered perspective on the drivers of asymmetric patterns in the atmosphere and sea ice during arctic cyclones, *Journal of Climate*, *35*(1), 73–89, `https://doi.org/10.1175/JCLI-D-21-0093.1`.

Colony, R., and A. S. Thorndike (1984), An estimate of the mean field of arctic sea ice motion, *Journal of Geophysical Research: Oceans*, *89*(C6), 10623–10629, `https://doi.org/10.1029/JC089iC06p10623`.

Cornish, S. B., H. L. Johnson, R. D. C. Mallett, J. Dörr, Y. Kostov, and A. E. Richards (2022), Rise and fall of sea ice production in the arctic oceans ice factories, *Nature Communications*, *13*, 7800, `https://doi.org/10.1038/s41467-022-34785-6`.

Cox, C., M. Gallagher, M. Shupe, O. Persson, A. Solomon, et al. (2021a), 10-meter (m) meteorological flux tower measurements (Level 1 Raw), Multidisciplinary Drifting Observatory for the Study of Arctic Climate (MOSAiC), central Arctic, October 2019 – September 2020., Arctic Data Center, `https://doi.org/10.18739/A2VM42Z5F`.

Cox, C., M. Gallagher, M. Shupe, O. Persson, A. Solomon, et al. (2021b), Atmospheric Surface Flux Station #30 measurements (Level 1 Raw), Multidisciplinary Drifting Observatory for the Study of Arctic Climate (MOSAiC), central Arctic, October 2019 – September 2020., Arctic Data Center, `https://doi.org/10.18739/A20C4SM1J`.

Cox, C., M. Gallagher, M. Shupe, O. Persson, A. Solomon, et al. (2021c), Atmospheric Surface Flux Station #40 measurements (Level 1 Raw), Multidisciplinary Drifting Observatory for the Study of Arctic Climate (MOSAiC), central Arctic, October 2019 – September 2020., Arctic Data Center, `https://doi.org/10.18739/A2CJ87M7G`.

Cox, C., M. Gallagher, M. Shupe, O. Persson, A. Solomon, et al. (2021d), Atmospheric Surface Flux Station #50 measurements (Level 1 Raw), Multidisciplinary Drifting Observatory for the Study of Arctic Climate (MOSAiC), central Arctic, October 2019 – September 2020., Arctic Data Center, `https://doi.org/10.18739/A2445HD46`.

Crawford, A. D., J. V. Lukovich, M. R. McCrystall, J. C. Stroeve, and D. G. Barber (2022), Reduced sea ice enhances intensification of winter storms over the arctic ocean, *Journal of Climate*, *35*(11), 3353–3370, `https://doi.org/10.1175/JCLI-D-21-0747.1`.

Curry, J. A., J. L. Schramm, and E. E. Ebert (1995), Sea ice-albedo climate feedback mechanism, *Journal of Climate*, *8*(2), 240–247, `https://doi.org/10.1175/1520-0442(1995)008<0240:SIACFM>2.0.CO;2`.

Deardorff, J. W. (1968), Dependence of air-sea transfer coefficients on bulk stability, *Journal of Geophysical Research (1896-1977)*, *73*(8), 2549–2557, `https://doi.org/10.1029/JB073i008p02549`.

Deser, C., J. E. Walsh, and M. S. Timlin (2000), Arctic sea ice variability in the context of recent atmospheric circulation trends, *Journal of Climate*, *13*(3), 617–633, `https://doi.org/10.1175/1520-0442(2000)013<0617:ASIVIT>2.0.CO;2`.

Docquier, D., R. Fuentes-Franco, T. Koenigk, and T. Fichefet (2020), Sea ice—ocean interactions in the barents sea modeled at different resolutions, *Frontiers in Earth Science*, *8*, `https://doi.org/10.3389/feart.2020.00172`.

Dorn, W., K. Dethloff, and A. Rinke (2009), Improved simulation of feedbacks between atmosphere and sea ice over the Arctic Ocean in a coupled regional climate model, *Ocean Modelling*, *29*, 103–114, `https://doi.org/10.1016/j.ocemod.2009.03.010`.

Dorn, W., A. Rinke, C. Köberle, K. Dethloff, and R. Gerdes (2019), Evaluation of the sea-ice simulation in the upgraded version of the coupled regional atmosphere-ocean-sea ice model HIRHAM–NAOSIM 2.0, *Atmosphere*, *10*, 431, `https://doi.org/10.3390/atmos10080431`.

Duarte, P., A. Sundfjord, A. Meyer, S. R. Hudson, G. Spreen, and L. H. Smedsrud (2020), Warm Atlantic water explains observed sea ice melt rates north of Svalbard, *Journal of Geophysical Research: Oceans*, *125*(8), e2019JC015662, `https://doi.org/10.1029/2019JC015662`.

Dörr, J., M. Årthun, T. Eldevik, and E. Madonna (2021), Mechanisms of regional winter sea-ice variability in a warming arctic, *Journal of Climate*, *34*(21), 8635–8653, `https://doi.org/10.1175/JCLI-D-21-0149.1`.

Eady, E. T. (1949), Long waves and cyclone waves, *Tellus*, *1*(3), 33–52, `https://doi.org/10.1111/j.2153-3490.1949.tb01265.x`.

Etling, D. (2008), *Theoretische Meteorologie: Eine Einführung*, Springer Berlin Heidelberg, Berlin, Heidelberg.

Fearon, M. G., J. D. Doyle, D. R. Ryglicki, P. M. Finocchio, and M. Sprenger (2021), The role of cyclones in moisture transport into the arctic, *Geophysical Research Letters*, *48*(4), e2020GL090353, `https://doi.org/10.1029/2020GL090353`.

Finocchio, P. M., and J. D. Doyle (2021), Summer cyclones and their association with short-term sea ice variability in the pacific sector of the arctic, *Frontiers in Earth Science*, *9*, `https://doi.org/10.3389/feart.2021.738497`.

Finocchio, P. M., J. D. Doyle, D. P. Stern, and M. G. Fearon (2020), Short-term impacts of arctic summer cyclones on sea ice extent in the marginal ice zone, *Geophysical Research Letters*, *47*(13), e2020GL088338, `https://doi.org/10.1029/2020GL088338`.

Finocchio, P. M., J. D. Doyle, and D. P. Stern (2022), Accelerated sea ice loss from late summer cyclones in the new arctic, *Journal of Climate*, *35*(23), 7751–7769, `https://doi.org/10.1175/JCLI-D-22-0315.1`.

Fitzroy, R. (1863), *The Weather Book: A Manual of Practical Meteorology*, Longman, Green, Longman, Roberts und Green, London.

Graham, R., et al. (2019), Winter storms accelerate the demise of sea ice in the atlantic sector of the arctic ocean, *Scientific Reports*, *9*, 9222, `https://doi.org/10.1038/s41598-019-45574-5`.

Gryanik, V. M., and C. Lüpkes (2018), An efficient non-iterative bulk parametrization of surface fluxes for stable atmospheric conditions over polar sea-ice, *Boundary-Layer Meteorology*, *166*, 301–325, `https://doi.org/10.1007/s10546-017-0302-x`.

Gultepe, I., et al. (2019), A review of high impact weather for aviation meteorology, *Pure and Applied Geophysics*, *176*, 1869–1921, `https://doi.org/10.1007/s00024-019-02168-6`.

Guo, Y., T. Shinoda, B. Guan, D. E. Waliser, and E. K. M. Chang (2020), Statistical relationship between atmospheric rivers and extratropical cyclones and anticyclones, *Journal of Climate*, *33*(18), 7817–7834, `https://doi.org/10.1175/JCLI-D-19-0126.1`.

Haas, C. (2017), Sea ice thickness distribution, in *Sea Ice*, edited by D. N. Thomas, chap. 2, pp. 42–64, John Wiley & Sons, Ltd., `https://doi.org/10.1002/9781118778371.ch2`.

Hegyi, B., and P. Taylor (2017), The arctic oscillation and arctic dipole regionally influence the wintertime arctic surface radiation budget and sea ice growth, *Geophysical Research Letters*, *44*, 4341—4350, `https://doi.org/10.1002/2017GL073281`.

Hersbach, H., et al. (2020), The era5 global reanalysis, *Quarterly Journal of the Royal Meteorological Society*, *146*(730), 1999–2049, `https://doi.org/10.1002/qj.3803`.

Heukamp, F. O., T. Kanzow, Q. Wang, C. Wekerle, and R. Gerdes (2023a), Impact of cyclonic wind anomalies caused by massive winter sea ice retreat in the barents sea on atlantic water transport toward the arctic: A model study, *Journal of Geophysical Research: Oceans*, *128*(3), e2022JC019045, `https://doi.org/10.1029/2022JC019045`.

Heukamp, F. O., L. Aue, Q. Wang, M. Ionita, T. Kanzow, C. Wekerle, and A. Rinke (2023b), Cyclones modulate the control of the north atlantic oscillation on transports into the barents sea, *Communications Earth & Environment*, *4*, 324, `https://doi.org/10.1038/s43247-023-00985-1`.

Hibler, W. D., III (1979), A dynamic thermodynamic sea ice model, *Journal of Physical Oceanography*, *9*, 815–846, `https://doi.org/10.1175/1520-0485(1979)009<0815:ADTSIM>2.0.CO;2`.

Hussain, M., and I. Mahmud (2019), pymannkendall: a python package for non parametric mann kendall family of trend tests., *Journal of Open Source Software*, *4*(39), 1556, `https://doi.org/10.21105/joss.01556`.

Inoue, J. (2021), Review of forecast skills for weather and sea ice in supporting Arctic navigation, *Polar Sci.*, *27*, 100523, `https://doi.org/10.1016/j.polar.2020.100523`.

IPCC (2021), Summary for policymakers, in *Climate Change 2021: The Physical Science Basis. Contribution of Working Group I to the Sixth Assessment Report of the Intergovernmental Panel on Climate Change*, pp. 3–32, Cambridge University Press, Cambridge, United Kingdom, `https://doi.org/10.1017/9781009157896.001`.

Isaksen, K., et al. (2022), Exceptional warming over the barents area, *Scientific Reports*, *12*, 9371, `https://doi.org/10.1038/s41598-022-13568-5`.

Itkin, P., et al. (2017), Thin ice and storms: Sea ice deformation from buoy arrays deployed during n-ice2015, *Journal of Geophysical Research: Oceans*, *122*(6), 4661–4674, `https://doi.org/10.1002/2016JC012403`.

Jäkel, E., J. Stapf, M. Wendisch, M. Nicolaus, W. Dorn, and A. Rinke (2019), Validation of the sea ice surface albedo scheme of the regional climate model HIRHAM–NAOSIM using aircraft measurements during the ACLOUD/PASCAL campaigns, *Cryosphere*, *13*, 1695–1708, `https://doi.org/10.5194/tc-13-1695-2019`.

Jakobson, L., T. Vihma, and E. Jakobson (2019), Relationships between sea ice concentration and wind speed over the arctic ocean during 1979–2015, *Journal of Climate*, *32*(22), 7783–7796, `https://doi.org/10.1175/JCLI-D-19-0271.1`.

Kay, J. E., and A. Gettelman (2009), Cloud influence on and response to seasonal arctic sea ice loss, *Journal of Geophysical Research: Atmospheres*, *114*, D18204, `https://doi.org/10.1029/2009JD011773`.

Kim, Y.-H., S.-K. Min, N. P. Gillett, D. Notz, and E. Malinina (2023), Observationally-constrained projections of an ice-free arctic even under a low emission scenario, *Nature Communications*, *14*, 3139, `https://doi.org/10.1038/s41467-023-38511-8`.

Koo, Y., R. Lei, Y. Cheng, B. Cheng, H. Xie, M. Hoppmann, N. T. Kurtz, S. F. Ackley, and A. M. Mestas-Nuñez (2021), Estimation of thermodynamic and dynamic contributions to sea ice growth in the central Arctic using ICESat-2 and MOSAiC SIMBA buoy data, *Remote Sensing of Environment*, *267*, 112730, `https://doi.org/10.1016/j.rse.2021.112730`.

Kovács, T., R. Gerdes, and J. Marshall (2020), Wind feedback mediated by sea ice in the nordic seas, *Journal of Climate*, *33*(15), 6621–6632, `https://doi.org/10.1175/JCLI-D-19-0632.1`.

Kraus, H. (2004), *Die Atmosphäre der Erde: Eine Einführung in die Meteorologie*, Springer Berlin Heidelberg, Berlin, Heidelberg.

Kriegsmann, A., and B. Brümmer (2014), Cyclone impact on sea ice in the central Arctic Ocean: a statistical study, *Cryosphere*, *8*(1), 303–317, `https://doi.org/10.5194/tc-8-303-2014`.

Kwok, R. (2018), Arctic sea ice thickness, volume, and multiyear ice coverage: losses and coupled variability (1958–2018), *Environmental Research Letters*, *13*(10), 105005, `https://doi.org/10.1088/1748-9326/aae3ec`.

Lindzen, R. S., and B. Farrell (1980), A simple approximate result for the maximum growth rate of baroclinic instabilities, *Journal of Atmospheric Sciences*, *37*(7), 1648–1654, `https://doi.org/10.1175/1520-0469(1980)037<1648:ASARFT>2.0.CO;2`.

Liu, Z., et al. (2022), Atmospheric forcing dominates winter Barents-Kara sea ice variability on interannual to decadal time scales, *Proceedings of the National Academy of Sciences of the United States of America*, *119*(36), e2120770119, `https://doi.org/10.1073/pnas.2120770119`.

Lukovich, J. V., J. C. Stroeve, A. Crawford, L. Hamilton, M. Tsamados, H. Heorton, and F. Massonnet (2021), Summer extreme cyclone impacts on Arctic sea ice, *Journal of Climate*, *34*(12), 4817–4834, `https://doi.org/10.1175/JCLI-D-19-0925.1`.

Lüpkes, C., and V. M. Gryanik (2015), A stability-dependent parametrization of transfer coefficients for momentum and heat over polar sea ice to be used in climate models, *J. Geophys. Res. Atmos.*, *120*, 552–581, `https://doi.org/10.1002/2014JD022418`.

Lüpkes, C., T. Vihma, G. Birnbaum, and U. Wacker (2008), Influence of leads in sea ice on the temperature of the atmospheric boundary layer during polar night, *Geophysical Research Letters*, *35*(3), L03805, `https://doi.org/10.1029/2007GL032461`.

Madonna, E., G. Hes, C. Li, C. Michel, and P. Y. F. Siew (2020), Control of barents sea wintertime cyclone variability by large-scale atmospheric flow, *Geophysical Research Letters*, *47*(19), e2020GL090322, `https://doi.org/10.1029/2020GL090322`.

Manucharyan, G. E., and A. F. Thompson (2017), Submesoscale sea ice-ocean interactions in marginal ice zones, *Journal of Geophysical Research: Oceans*, *122*(12), 9455–9475, `https://doi.org/10.1002/2017JC012895`.

Martin, T., M. Tsamados, D. Schroeder, and D. L. Feltham (2016), The impact of variable sea ice roughness on changes in Arctic Ocean surface stress: A model study, *J. Geophys. Res. Oceans*, *121*, 1931–1952, `https://doi.org/10.1002/2015JC011186`.

Maykut, G. A. (1986), The surface heat and mass balance, in *The Geophysics of Sea Ice*, edited by N. Untersteiner, chap. 5, pp. 395–463, Springer US, Boston, MA, `https://doi.org/10.1007/978-1-4899-5352-0_6`.

McPhee, M. G. (1992), Turbulent heat flux in the upper ocean under sea ice, *J. Geophys. Res.*, *97*(C4), 5365–5379, `https://doi.org/10.1029/92JC00239`.

McPhee, M. G. (2017), The sea ice–ocean boundary layer, in *Sea Ice*, edited by D. N. Thomas, chap. 5, pp. 138–159, John Wiley & Sons, Ltd., `https://doi.org/10.1002/9781118778371.ch5`.

Meier, W. N., and J. Stroeve (2022), An updated assessment of the changing Arctic sea ice cover, *Oceanography*, *35*(3-4), 10–19, `https://doi.org/10.5670/oceanog.2022.114`.

Moore, G. (2016), The december 2015 north pole warming event and the increasing occurrence of such events, *Scientific Reports*, *6*, `https://doi.org/10.1038/srep39084`.

Morrison, A. L., J. E. Kay, W. R. Frey, H. Chepfer, and R. Guzman (2019), Cloud response to arctic sea ice loss and implications for future feedback in the cesm1 climate model, *Journal of Geophysical Research: Atmospheres*, *124*(2), 1003–1020, `https://doi.org/10.1029/2018JD029142`.

Muilwijk, M., et al. (2019), Arctic ocean response to greenland sea wind anomalies in a suite of model simulations, *Journal of Geophysical Research: Oceans*, *124*(8), 6286–6322, `https://doi.org/10.1029/2019JC015101`.

Nansen, F. (1897), *Farthest North, Vol. II*, p. 708, Harper & brothers, New York.

Nansen, F. (1902), *Norwegian North Polar Expedition 1893-1896, Scientific Results, vol. 3, The Oceanography of the North Pole Basin*, p. 427, Longmans, Green, Toronto, Canada.

Neu, U., et al. (2013), Imilast: A community effort to intercompare extratropical cyclone detection and tracking algorithms:, *Bulletin of the American Meteorological Society*, *94*(4), 529–547, `https://doi.org/10.1175/BAMS-D-11-00154.1`.

Olbers, D., J. Willebrand, and C. Eden (2012), The meridional overturning of the oceans, in *Ocean Dynamics*, chap. 15, pp. 487–560, Springer Berlin Heidelberg, Berlin, Heidelberg, `https://doi.org/10.1007/978-3-642-23450-7_15`.

Omstedt, A., and J. S. Wettlaufer (1992), Ice growth and oceanic heat flux: Models and measurements, *J. Geophys. Res.*, *97*(C6), 9383–9390, `https://doi.org/10.1029/92JC00815`.

Park, H.-S., S. Lee, S.-W. Son, S. B. Feldstein, and Y. Kosaka (2015), The impact of poleward moisture and sensible heat flux on arctic winter sea ice variability, *Journal of Climate*, *28*(13), 5030–5040, `https://doi.org/10.1175/JCLI-D-15-0074.1`.

Parker, C. L., P. A. Mooney, M. A. Webster, and L. N. Boisvert (2022), The influence of recent and future climate change on spring Arctic cyclones, *Nature Communications*, *13*, 6514, `https://doi.org/10.1038/s41467-022-34126-7`.

Petrich, C., and H. Eicken (2017), Overview of sea ice growth and properties, in *Sea Ice*, edited by D. N. Thomas, chap. 1, pp. 1–41, John Wiley & Sons, Ltd., `https://doi.org/10.1002/9781118778371.ch1`.

Petty, A. A., M. M. Holland, D. A. Bailey, and N. T. Kurtz (2018), Warm Arctic, increased winter sea ice growth?, *Geophysical Research Letters*, *45*(23), 12,922–12,930, `https://doi.org/10.1029/2018GL079223`.

Pithan, F., and T. Mauritsen (2014), Arctic amplification dominated by temperature feedbacks in contemporary climate models, *Nature Geoscience*, *7*, 181–184, `https://doi.org/10.1038/ngeo2071`.

Previdi, M., K. L. Smith, and L. M. Polvani (2021), Arctic amplification of climate change: a review of underlying mechanisms, *Environmental Research Letters*, *16*(9), 093003, `https://doi.org/10.1088/1748-9326/ac1c29`.

Rampal, P., J. Weiss, and D. Marsan (2009), Positive trend in the mean speed and deformation rate of arctic sea ice, 1979–2007, *Journal of Geophysical Research: Oceans*, *114*(C5), `https://doi.org/10.1029/2008JC005066`.

Rantanen, M., A. Y. Karpechko, A. Lipponen, K. Nordling, O. Hyvärinen, K. Ruosteenoja, T. Vihma, and A. Laaksonen (2022), The arctic has warmed nearly four times faster than the globe since 1979, *Communications Earth & Environment*, *3*, 168, `https://doi.org/10.1038/s43247-022-00498-3`.

Reiser, F., S. Willmes, and G. Heinemann (2020), A new algorithm for daily sea ice lead identification in the arctic and antarctic winter from thermal-infrared satellite imagery, *Remote Sensing*, *12*(12), `https://doi.org/10.3390/rs12121957`.

Renfrew, I. A., et al. (2021), An evaluation of surface meteorology and fluxes over the Iceland and Greenland Seas in ERA5 reanalysis: The impact of sea ice distribution, *Q J R Meteorol Soc.*, *147*(734), 691–712, `https://doi.org/10.1002/qj.3941`.

Rheinlænder, J. W., R. Davy, E. Ólason, P. Rampal, C. Spensberger, T. D. Williams, A. Korosov, and T. Spengler (2022), Driving mechanisms of an extreme winter sea ice breakup event in the beaufort sea, *Geophysical Research Letters*, *49*(12), e2022GL099024, `https://doi.org/10.1029/2022GL099024`.

Ricker, R., S. Hendricks, F. Girard-Ardhuin, L. Kaleschke, C. Lique, X. Tian-Kunze, M. Nicolaus, and T. Krumpen (2017a), Satellite-observed drop of Arctic sea ice growth in winter 2015–2016, *Geophysical Research Letters*, *44*(7), 3236–3245, `https://doi.org/10.1002/2016GL072244`.

Ricker, R., S. Hendricks, L. Kaleschke, X. Tian-Kunze, J. King, and C. Haas (2017b), A weekly Arctic sea-ice thickness data record from merged CryoSat-2 and SMOS satellite data, *Cryosphere*, *11*(4), 1607–1623, `https://doi.org/10.5194/tc-11-1607-2017`.

Riebold, J., A. Richling, U. Ulbrich, H. Rust, T. Semmler, and D. Handorf (2023), On the linkage between future arctic sea ice retreat, euro-atlantic circulation regimes and

temperature extremes over europe, *Weather and Climate Dynamics*, *4*(3), 663–682, `https://doi.org/10.5194/wcd-4-663-2023`.

Rieke, O., M. Årthun, and J. S. Dörr (2023), Rapid sea ice changes in the future barents sea, *Cryosphere*, *17*(4), 1445–1456, `https://doi.org/10.5194/tc-17-1445-2023`.

Rigor, I. G., J. M. Wallace, and R. L. Colony (2002), Response of sea ice to the arctic oscillation, *Journal of Climate*, *15*(18), 2648–2663, `https://doi.org/10.1175/1520-0442(2002)015<2648:ROSITT>2.0.CO;2`.

Rinke, A., M. Maturilli, R. Graham, H. Matthes, D. Handorf, L. Cohen, S. Hudson, and J. Moore (2017), Extreme cyclone events in the arctic: Wintertime variability and trends, *Environmental Research Letters*, *12*, 094006, `https://doi.org/10.1088/1748-9326/aa7def`.

Rinke, A., J. J. Cassano, E. N. Cassano, R. Jaiser, and D. Handorf (2021), Meteorological conditions during the MOSAiC expedition: Normal or anomalous?, *Elementa: Science of the Anthropocene*, *9*(1), 00023, `https://doi.org/10.1525/elementa.2021.00023`.

Rudels, B., and D. Quadfasel (1991), Convection and deep water formation in the arctic ocean-greenland sea system, *Journal of Marine Systems*, *2*(3), 435–450, `https://doi.org/10.1016/0924-7963(91)90045-V`.

Schneider, T., C. Lüpkes, W. Dorn, D. Chechin, D. Handorf, S. Khosravi, V. M. Gryanik, I. Makhotina, and A. Rinke (2022), Sensitivity to changes in the surface-layer turbulence parameterization for stable conditions in winter: A case study with a regional climate model over the Arctic, *Atmospheric Science Letters*, *23*, e1066, `https://doi.org/10.1002/asl.1066`.

Schreiber, E., and M. Serreze (2020), Impacts of synoptic-scale cyclones on arctic sea-ice concentration: a systematic analysis, *Annals of Glaciology*, *61*, 1–15, `https://doi.org/10.1017/aog.2020.23`.

Screen, J. A., I. Simmonds, and K. Keay (2011), Dramatic interannual changes of perennial arctic sea ice linked to abnormal summer storm activity, *Journal of Geophysical Research: Atmospheres*, *116*(D15), `https://doi.org/10.1029/2011JD015847`.

Serreze, M. C. (1995), Climatological aspects of cyclone development and decay in the arctic, *Atmosphere-Ocean*, *33*(1), 1–23, `https://doi.org/10.1080/07055900.1995.9649522`.

Serreze, M. C., and A. P. Barrett (2008), The summer cyclone maximum over the central arctic ocean, *Journal of Climate*, *21*(5), 1048–1065, `https://doi.org/10.1175/2007JCLI1810.1`.

Serreze, M. C., and R. G. Barry (2005), *The Arctic Climate System*, 1 ed., Cambridge University Press, Cambridge.

Serreze, M. C., and W. N. Meier (2019), The arctic's sea ice cover: trends, variability, predictability, and comparisons to the antarctic, *Annals of the New York Academy of Sciences*, *1436*(1), 36–53, `https://doi.org/10.1111/nyas.13856`.

Serreze, M. C., and J. Stroeve (2015), Arctic sea ice trends, variability and implications for seasonal ice forecasting, *Phil. Trans. R. Soc. A.*, *373*, 20140159, `https://doi.org/10.1098/rsta.2014.0159`.

Shu, Q., Q. Wang, Z. Song, and F. Qiao (2021), The poleward enhanced arctic ocean cooling machine in a warming climate, *Nature Communications*, *12*, `https://doi.org/10.1038/s41467-021-23321-7`.

Shupe, M. D., et al. (2020), The MOSAiC expedition: A year drifting with the Arctic sea ice, *Arctic Report Card*, `https://doi.org/10.25923/9g3v-xh92`.

Shupe, M. D., et al. (2022), Overview of the MOSAiC expedition: Atmosphere, *Elementa: Science of the Anthropocene*, *10*(1), 00060, `https://doi.org/10.1525/elementa.2021.00060`.

Smedsrud, L. H., et al. (2013), The role of the barents sea in the arctic climate system, *Reviews of Geophysics*, *51*(3), 415–449, `https://doi.org/10.1002/rog.20017`.

Sorteberg, A., and B. Kvingedal (2006), Atmospheric forcing on the Barents Sea winter ice extent, *Journal of Climate*, *19*(19), 4772–4784, `https://doi.org/10.1175/JCLI3885.1`.

Spreen, G., R. Kwok, and D. Menemenlis (2011), Trends in Arctic sea ice drift and role of wind forcing: 1992–2009, *Geophysical Research Letters*, *38*(19), L19501, `https://doi.org/10.1029/2011GL048970`.

Stern, D. P., J. D. Doyle, N. P. Barton, P. M. Finocchio, W. A. Komaromi, and E. J. Metzger (2020), The impact of an intense cyclone on short-term sea ice loss in a fully coupled atmosphere-ocean-ice model, *Geophysical Research Letters*, *47*(4), e2019GL085580, `https://doi.org/10.1029/2019GL085580`.

Stroeve, J. C., J. Maslanik, M. C. Serreze, I. Rigor, W. Meier, and C. Fowler (2011), Sea ice response to an extreme negative phase of the arctic oscillation during winter 2009/2010, *Geophysical Research Letters*, *38*(2), `https://doi.org/10.1029/2010GL045662`.

Stuecker, M., et al. (2018), Polar amplification dominated by local forcing and feedbacks, *Nature Climate Change*, *8*, 1076–1081, `https://doi.org/10.1038/s41558-018-0339-y`.

Sumata, H., L. de Steur, D. V. Divine, M. A. Granskog, and S. Gerland (2023), Regime shift in arctic ocean sea ice thickness, *Nature*, *615*, 443–449, `https://doi.org/10.1038/s41586-022-05686-x`.

Thompson, D. W. J., and J. M. Wallace (1998), The arctic oscillation signature in the wintertime geopotential height and temperature fields, *Geophysical Research Letters*, *25*(9), 1297–1300, `https://doi.org/10.1029/98GL00950`.

Thomson, A. M., et al. (2011), RCP4.5: a pathway for stabilization of radiative forcing by 2100, *Climatic Change*, *109*, 77, `https://doi.org/10.1007/s10584-011-0151-4`.

Thorndike, A. S., and R. Colony (1982), Sea ice motion in response to geostrophic winds, *Journal of Geophysical Research: Oceans*, *87*(C8), 5845–5852, `https://doi.org/10.1029/JC087iC08p05845`.

Tian, Z., X. Liang, J. Zhang, H. Bi, F. Zhao, and C. Li (2022), Thermodynamical and dynamical impacts of an intense cyclone on arctic sea ice, *Journal of Geophysical Research: Oceans*, *127*(12), e2022JC018436, `https://doi.org/10.1029/2022JC018436`.

Tietsche, S., M. Alonso-Balmaseda, P. Rosnay, H. Zuo, X. Tian-Kunze, and L. Kaleschke (2018), Thin arctic sea ice in l-band observations and an ocean reanalysis, *Cryosphere*, *12*(6), 2051–2072, `https://doi.org/10.5194/tc-12-2051-2018`.

Trenberth, K. E., and J. M. Caron (2001), Estimates of meridional atmosphere and ocean heat transports, *Journal of Climate*, *14*(16), 3433–3443, `https://doi.org/10.1175/1520-0442(2001)014<3433:EOMAAO>2.0.CO;2`.

Valkonen, E., J. Cassano, and E. Cassano (2021), Arctic cyclones and their interactions with the declining sea ice: A recent climatology, *Journal of Geophysical Research: Atmospheres*, *126*(12), e2020JD034366, `https://doi.org/10.1029/2020JD034366`.

Valkonen, E., J. Cassano, E. Cassano, and M. Seefeldt (2023), Declining sea ice and its relationship with arctic cyclones in current and future climate part i: Current climatology

in cmip6 models, *Weather and Climate Dynamics Discussions*, *2023*, 1–40, `https://doi.org/10.5194/wcd-2023-2`.

Vessey, A., K. Hodges, L. Shaffrey, and J. Day (2020), An inter-comparison of arctic synoptic scale storms between four global reanalysis datasets, *Climate Dynamics*, *54*, `https://doi.org/10.1007/s00382-020-05142-4`.

von Albedyll, L. (2022), Sea ice deformation and sea ice thickness change, Phd thesis, University of Bremen, `https://doi.org/10.26092/elib/1868`.

von Albedyll, L., et al. (2022), Thermodynamic and dynamic contributions to seasonal Arctic sea ice thickness distributions from airborne observations, *Elementa: Science of the Anthropocene*, *10*(1), 00074, `https://doi.org/10.1525/elementa.2021.00074`.

Walbröl, A., et al. (2022), Atmospheric temperature, water vapour and liquid water path from two microwave radiometers during MOSAiC, *9*, 534, `https://doi.org/10.1038/s41597-022-01504-1`.

Wang, J., J. Zhang, E. Watanabe, M. Ikeda, K. Mizobata, J. E. Walsh, X. Bai, and B. Wu (2009), Is the dipole anomaly a major driver to record lows in arctic summer sea ice extent?, *Geophysical Research Letters*, *36*(5), `https://doi.org/10.1029/2008GL036706`.

Wayand, N. E., C. M. Bitz, and E. Blanchard-Wrigglesworth (2019), A year-round subseasonal-to-seasonal sea ice prediction portal, *Geophysical Research Letters*, *46*(6), 3298–3307, `https://doi.org/10.1029/2018GL081565`.

Weeks, W. F., and S. F. Ackley (1986), The growth, structure, and properties of sea ice, in *The Geophysics of Sea Ice*, edited by N. Untersteiner, chap. 1, pp. 9–164, Springer US, Boston, MA, `https://doi.org/10.1007/978-1-4899-5352-0_2`.

Wendisch, M., et al. (2023), Atmospheric and surface processes, and feedback mechanisms determining arctic amplification: A review of first results and prospects of the (ac)3 project, *Bulletin of the American Meteorological Society*, *104*(1), E208–E242, `https://doi.org/10.1175/BAMS-D-21-0218.1`.

Wernli, H., and L. Papritz (2018), Role of polar anticyclones and mid-latitude cyclones for arctic summertime sea-ice melting, *Nature Geoscience*, *13*(3), 108–113, `https://doi.org/10.1175/1520-0442(2000)013<0617:ASIVIT>2.0.CO;2`.

Willmes, S., G. Heinemann, and F. Schnaase (2023), Patterns of wintertime arctic sea-ice leads and their relation to winds and ocean currents, *The Cryosphere*, *17*(8), 3291–3308, `https://doi.org/10.5194/tc-17-3291-2023`.

Woodgate, R. A., T. Weingartner, and R. Lindsay (2010), The 2007 bering strait oceanic heat flux and anomalous arctic sea-ice retreat, *Geophysical Research Letters*, *37*(1), `https://doi.org/10.1029/2009GL041621`.

Woods, C., and R. Caballero (2016), The role of moist intrusions in winter arctic warming and sea ice decline, *Journal of Climate*, *29*(12), 4473–4485, `https://doi.org/10.1175/JCLI-D-15-0773.1`.

Yu, X., A. Rinke, W. Dorn, G. Spreen, C. Lüpkes, H. Sumata, and V. M. Gryanik (2020), Evaluation of Arctic sea ice drift and its dependency on near-surface wind and sea ice conditions in the coupled regional climate model HIRHAM–NAOSIM, *Cryosphere*, *14*, 1727–1746, `https://doi.org/10.5194/tc-14-1727-2020`.

Zahn, M., M. Akperov, A. Rinke, F. Feser, and I. Mokhov (2018), Trends of cyclone characteristics in the arctic and their patterns from different reanalysis data, *Journal of Geophysical Research: Atmospheres*, *123*, `https://doi.org/10.1002/2017jd027439`.

Zhang, F., X. Pang, R. Lei, M. Zhai, X. Zhao, and Q. Cai (2022), Arctic sea ice motion change and response to atmospheric forcing between 1979 and 2019, *International Journal of Climatology*, *42*(3), 1854–1876, `https://doi.org/10.1002/joc.7340`.

Zhang, J., R. Lindsay, A. Schweiger, and I. Rigor (2012), Recent changes in the dynamic properties of declining arctic sea ice: A model study, *Geophysical Research Letters*, *39*(20), `https://doi.org/10.1029/2012GL053545`.

Zhang, J., R. Lindsay, A. Schweiger, and M. Steele (2013), The impact of an intense summer cyclone on 2012 arctic sea ice retreat, *Geophysical Research Letters*, *40*(4), 720–726, `https://doi.org/10.1002/grl.50190`.

Zhang, P., G. Chen, M. Ting, L. Ruby Leung, B. Guan, and L. Li (2023), More frequent atmospheric rivers slow the seasonal recovery of Arctic sea ice, *Nature Climate Change*, *13*, 266–273, `https://doi.org/10.1038/s41558-023-01599-3`.

Zuo, H., M. A. Balmaseda, S. Tietsche, K. Mogensen, and M. Mayer (2019), The ecmwf operational ensemble reanalysis–analysis system for ocean and sea ice: a description of the system and assessment, *Ocean Science*, *15*(3), 779–808, `https://doi.org/10.5194/os-15-779-2019`.

Acknowledgements

First and foremost, I would like to thank Annette Rinke for giving me the opportunity to work on this exciting topic and for the continuous support throughout the last 3 years. This thesis would not have been possible without your great supervision and your scientific advice, which has been constructive and encouraging at all times. I further would like to express my gratitude to my main supervisor Markus Rex and to all members of my thesis advisory committee, Günther Heinemann, Gunnar Spreen, Dörthe Handorf and Wolfgang Dorn. Your academic guidance has been a great help in all stages of my PhD project. I would like to thank Timo Vihma and Petteri Uotila for the fruitful scientific collaboration during my PhD and for hosting me during my visit in Helsinki. And, I would like to thank Markus Rex, Torsten Kanzow and Thomas Spengler for agreeing to review this thesis.

A big thank you goes to all the fellow early career researchers from AWI and the AC3 project who accompanied me on the road during the last years: Going through the ups and downs of a PhD together was a large help to stay motivated. Specifically, I would like to thank the Potsdam-AC3 crew, Nils, Sofie and Ines for their comradeship, and Finn for reminding me that not only the atmosphere, but also the ocean is a quite interesting research topic.

I would like to thank all my colleagues from the atmo section in Potsdam. It has been a pleasure working with all of you during the last years! Particular thanks go to Sandro, but also to Benjamin, Johannes and Raphael, for welcoming me to Potsdam and for a number of entertaining evenings. We'll see each other at the Joy!

Finally, I would like to thank my parents, my brothers, my fiancée Johanna and all my friends for their support throughout the last three years and beyond.

Eidesstattliche Erklärung

Hiermit versichere ich, dass ich die vorliegende Arbeit selbstständig verfasst und keine anderen als die angegebenen Quellen und Hilfsmittel verwendet habe. Alle Stellen, die wörtlich oder sinngemäß aus anderen Veröffentlichungen entnommen wurden, sind als solche kenntlich gemacht. Ich versichere weiterhin, dass diese Arbeit in gleicher oder ähnlicher Form noch nicht in einem anderen Prüfungsverfahren eingereicht wurde.

Potsdam, den 23. Oktober 2023

_____

Lars Aue